UNIVERSITEIT VAN PRETORIA
UNIVERSITY OF PRETORIA
YUNIBESITHI YA PRETORIA

Investigating the intracellular trafficking of mature African horse sickness virus particles

By Ané Oosthuizen

Submitted in fulfilment of the requirements for the degree

Magister Scientiae

In the Faculty of Natural & Agricultural Science

University of Pretoria

Pretoria

January 2019

Under the supervision of Dr. V. van Staden

DECLARATION

I, Ané Oosthuizen declare that this dissertation, which I hereby submit for the degree *Magister Scientiae* at the University of Pretoria, is my own work and has not previously been submitted by me for a degree at this or any other tertiary institution.

Signature:  Date: 26/03/2019

TABLE OF CONTENTS

DECLARATION 2

TABLE OF CONTENTS 3

ACKNOWLEDGEMENTS 5

SUMMARY 6

CHAPTER 1 7

1.1. Introduction 8

1.2. Historical background 9

1.3. Geographic distribution, vector-borne transmission cycle and economic consequences of AHSV 9

1.4. Pathogenesis of AHS 11

1.5. Prevention and control 12

1.6. Molecular Biology 13

1.6.1. Virus Structure 13

1.7. Viral life cycle 15

1.7.1. Adsorption, penetration and the outer capsid proteins 15

1.7.2. Uncoating, formation of replicative complexes and the composition of virus inclusion bodies 16

1.7.3. Viral genome transcription 17

1.7.4. Expression of viral proteins 17

1.7.5. Viral morphogenesis 19

1.7.5. Virus trafficking to and release from the cell surface 20

1.8. Intracellular trafficking pathways prone to viral exploitation 24

1.9. Concluding remarks 27

1.10. Aim and objectives 27

CHAPTER 2 28

2.1. Introduction 29

2.2. Materials and Methods 31

2.2.1. Cell lines 31

2.2.2. Virus strain 31

2.2.3. Cell culture infections 31

2.2.4. Transmission electron microscopy 31

2.2.4.1. High-pressure freezing and freeze substitution reactions of cells 31

2.2.4.2. Chemical fixation and dehydration reaction of cells 32
2.2.4.3. Resin embedding and ultrathin sectioning of cell pellets 32
2.2.4.4. Staining and electron microscopy of cell sections 32
2.2.5. Inhibition assays 32
2.2.6. Cell viability assays 33
2.2.7. Virus titration 34
2.2.8. Protein resolution by polyacrylamide gel electrophoresis 34
2.2.9. Western blot analysis and antibodies 34
2.3. Results 36
2.3.1 Ultrastructural investigation of AHSV particle localisation in mammalian and insect cell culture 36
2.3.1.1. Ultrastructural characterisation of AHSV particle localisation in BSR cells 36
2.3.1.2 Ultrastructural characterisation of AHSV particle localisation in KC cells 52
2.3.2. Investigating the role of cellular transport pathways in AHSV trafficking 68
2.3.2.1. AHSV replication in mammalian and insect cell systems 68
2.3.2.2. Effect of inhibited cellular pathways on AHSV replication 70
2.4. Discussion 88
2.5. Concluding Remarks 98
RESEARCH OUTPUTS 99
LIST OF ABBREVIATIONS 100
LIST OF BUFFERS 104
LIST OF FIGURES 105
LIST OF REFERENCES 106

ACKNOWLEDGEMENTS

Thank you to the National Research Foundation (grant: SFH150729132408 and AEMD170626244817), the University of Pretoria, and the Poliomyelitis Research Foundation for the continuous financial support. Many thanks to the Department of Genetics and the Laboratory for Microscopy and Microanalysis at UP for the use of their facilities and technical assistance.

Thank you, Vida. It has been a privilege to complete this project under your supervision, I have learnt so much from you. You helped shape the scientist I am, and I could not have asked for a better mentor. Your passion for science and life will always inspire me. You always make time for your students, and your efforts to educate are always sincere. Thank you.

To Linda and Eudri, I am grateful for your encouragement, troubleshooting expertise, and technical advice. Especially thank you to Eudri for all your patience and expert input with TEM. To Shareen, Gayle, and Litia thank you for the laughs, advice and support. Thank you, Wilma, for encouraging me and your willingness to help. To Prof J. Theron and Andelé Conradie, thank you for providing some of the embedded cell pellets.

Thank you, God, for the ability, strength, and perseverance. Thank you to my dear husband who always exhorts, believes and empowers me to be the best I can be. Thank you to my sister and brother-in-law for their continuous loving support, and to my family-in-law who always make an effort to listen to how my research is going. To my Mother, you inspire, support and motivate me. You have formed so much of the person I am. Thank you. To my Father who passed away during my MSc studies, I miss you every day. We shared a passion for science and knowledge, I dedicate this dissertation to your memory.

SUMMARY

African horse sickness virus (AHSV) is an arbovirus in the genus *Orbivirus* and the family *Reoviridae* known to successfully propagate in different species, such as mammalian hosts and insect vectors. In mammalian cells, infection by AHSV results in cell lysis and release of progeny virions, while insect cells establish persistent infection with no visible cytopathic effect and progeny virions escape infected cells by non-lytic processes. The events leading to AHSV release from infected cells, mammalian or insect, is unknown and is thought to contribute to the cytopathic effect observed in mammalian cells and absence thereof in insect cells. This study aimed to investigate and compare AHSV trafficking in mammalian and insect cells, with the hope of detecting underlying differences between mammalian and insect cells.

Transmission electron microscopy revealed that particles distributed either to inside the lumen of vesicles, were associated with the cytoplasmic face of vesicles, or were present in the cytoplasm without close proximity to any intracellular structures or organelles. In mammalian cells, the majority of particles distributed inside the lumen of vesicles at early times post infection and to the cytoplasm at later times post infection. In insect cells, the majority of particles distributed to the cytoplasm throughout the course of infection. The presence of mature AHSV particles in the lumen of small smooth-surfaced membrane-bound structures in both mammalian cells and insect cells implicated a role for membrane trafficking pathways in virus transport. We subsequently targeted cellular factors involved in membrane trafficking in cells to elucidate cellular pathways involved in AHSV replication. The targets were: vesicle formation along the secretory route, the ubiquitin-proteasome system regulating the levels of free ubiquitin, and lipid kinases involved in multivesicular body (MVB) biogenesis.

Inhibition of vesicle-dependent transport along the secretory route significantly decreased virus release in mammalian but not insect cells. Together with TEM findings these results suggest AHSV transport in mammalian cells occurs by vesicle-dependent mechanisms early after infection, and support NS3-mediated transport models for the non-lytic release of particles. From our TEM analysis, AHSV transport later after infection in mammalian cells seem not to predominantly involve membrane trafficking. The mechanism of transport and non-lytic release in insect cells does not involve the secretory pathway and remains to be elucidated. Other components of the exocytic and MVB pathways are involved in AHSV replication in mammalian and insect cells, but not directly involved in AHSV transport to the cell surface. Our findings demonstrate the involvement of membrane trafficking pathways in events leading to AHSV release. Inhibition of cellular factors affected virus replication differently in mammalian and insect cells, and shows a difference in the cell-mediated events leading to release from infected mammalian cells versus infected insect cells. These results demonstrate the relevance of elucidating cell-mediated events leading to AHSV release in understanding viral pathogenesis, and describe the involvement of additional host proteins/pathways in AHSV egress which provide new insights to understand orbivirus interactions with their hosts.

CHAPTER 1

Overview of the epidemiology, molecular biology and life cycle of African horse sickness virus

1.1. Introduction

African horse sickness virus (AHSV) is an arthropod-borne vertebrate pathogen, classified within the family *Reoviridae* and the genus *Orbivirus* (BORDEN *et al.* 1971). AHSV infection in equids causes the disease African horse sickness (AHS) (THEILER 1902). AHS is considered to be the most lethal viral disease of horses with a mortality rate of up to 95% in fully susceptible naïve horses (HENNING 1956). AHSV is enzootic in sub-Saharan Africa and has caused several outbreaks outside this geographical range (ERASMUS 1972; GUTHRIE *et al.* 2009; GUTHRIE *et al.* 2013; ZIENTARA AND LECOLLINET 2015).

As a consequence of its severity in horses and history of epizootics, AHS is listed as an Office International des Epizooties (OIE) notifiable disease (OIE 2019). Other orbiviruses such as bluetongue virus (BTV) and epizootic haemorrhagic disease virus (EHDV) are also OIE-listed pathogens, and have inspired research into orbivirus architecture and replication. Twelve serogroups comprise the *Orbivirus* genus and each serogroup is further divided into serotypes, AHSV for example has nine serotypes (HOWELL 1962). BTV is the model orbivirus of the genus, and is the best understood orbivirus at molecular level [reviewed in (PATEL AND ROY 2014)]. Even though BTV architecture, molecular constituents, replicative strategy and cytopathogenicity are comparable to that of AHSV, a lot remains unknown about the molecular mechanisms of the AHSV life cycle.

Replication, as with other viruses, proceeds via a series of highly specific consecutive processes dictated by the virus. The underlying dynamics of virus entry, uncoating and replicative complex formation has been characterised, while the dynamics of subsequent core maturation and egress remain to be fully elucidated and defined. In mammalian cells, infection by AHSV results in cell lysis and release of progeny virions, while insect cells establish persistent infection with no visible cytopathic effect (COETZER AND GUTHRIE 2004; STASSEN *et al.* 2012). Progeny virions escape infected insect cells by non-lytic processes; and prior to cell lysis, virions escape mammalian cells by budding and extrusion.

Full virus particles are therefore trafficked to the cell surface for release in both mammalian and insect cells. Cell processes are thought to underlie these events and elucidation thereof could improve our understanding of AHSV pathogenesis. In this regard, reports of the vesicular distribution of BTV (CELMA AND ROY 2011) and novel vesicle-like structures containing AHSV particles and proteins (VENTER *et al.* 2014) are of particular interest. Since it implicates cellular processes involving membrane traffic. Studies demonstrating the crucial role of the virus-encoded membrane protein NS3/3A in virus release (BEATON *et al.* 2002; WIRBLICH *et al.* 2006; CELMA AND ROY 2009; CELMA AND ROY 2011; BHATTACHARYA *et al.* 2015) also indicate the relevance of evaluating the role of membrane trafficking pathways in AHSV egress. This study therefore aims to investigate the role of membrane traffic events leading to AHSV release from infected cells. To give the necessary background to the aims of this study various aspects of AHSV will be reviewed. These include the transmission, pathogenicity, molecular biology and the viral replication cycle of AHSV. A detailed review of intracellular pathways prone to exploitation by viruses bearing some similarity to AHSV will also be included, as very little is known about these mechanisms in orbiviruses.

1.2. Historical background

The first recorded reference of AHS was from 1327 in Yemen (MOULE 1896). Evident by the species name, the disease causing agent almost certainly originated in Africa where the zebra, the natural vertebrate host and reservoir of AHSV, occurs (BARNARD 1998). First reports of the disease in Africa only appeared in 1569, following the introduction of horses during the exploration of central and east Africa (THEAL 1900). In southern Africa the disease has probably been present from early times but AHS was not recognised until around 60 years after the first introduction of horses, with the first well-recorded AHS epidemic occurring in 1719 when approximately 1 700 animals died (HENNING 1956).

Since then several severe outbreaks have been recorded in southern Africa, with the largest being in South Africa in 1854-1855 when over 70 000 horses died (COETZER AND ERASMUS 1994; BARNARD 1998). Throughout the last century, the frequency, extent and severity of outbreaks in southern Africa have declined significantly, coinciding with major decrease in the horse and zebra populations and the introduction of AHS vaccines (MELLOR AND HAMBLIN 2004). However, over the last decade outbreaks of AHS have increased in South Africa. For example, 24 cases were reported for 2014-2015, followed by 44 cases for 2015-2016, and 109 cases for 2016-2017 (AHS Trust 2019).

1.3. Geographic distribution, vector-borne transmission cycle and economic consequences of AHSV

AHSV is enzootic in tropical and sub-tropical areas of sub-Saharan Africa (MELLOR AND HAMBLIN 2004). All nine serotypes of AHSV occur in eastern and southern Africa (MACLACHLAN AND GUTHRIE 2010). The virus may also occur in Yemen in the Arabian Peninsula (SAILLEAU *et al.* 2000), but is not considered endemic due to its uncertain long-term status in this area. Studies are still being done to improve the understanding of AHSV epidemiology and control [reviewed by (CARPENTER *et al.* 2017)], but occasional outbreaks have been reported in the Middle East, Spain and Portugal (ERASMUS 1972; GUTHRIE *et al.* 2009; GUTHRIE *et al.* 2013; ZIENTARA AND LECOLLINET 2015).

AHSV is predominantly transmitted via the bites of competent *Culicoides* midges (Diptera: *Ceratopogonidae*) to all equids (MELLOR *et al.* 1990; CALISHER AND MERTENS 1998). Competent midge species include *C. imicola*, common throughout Africa and South-East Asia, *C. bolitinos* in cooler highland areas in southern Africa, and *C. obsoletus* and *C. pulicaris* in Europe (MELLOR AND HAMBLIN 2004; WILSON *et al.* 2009). These species are competent AHSV vectors, due to the capacity of the virus to surpass the three main barriers to infection in *Culicoides* species, namely the midgut infection barrier, the midgut escape barrier and the dissemination barrier (PURSE AND ROGERS 2009). Other hematophagous arthropods capable of AHSV infection and transmission include some species of mosquitoes (OZAWA AND NAKATA 1965; BRAVERMAN AND BOORMAN 1978; MELLOR 1993) and *Hyalomma dromadarii* ticks (ANWAR AND QURESHI 1972). These species are however generally considered to be of minor epidemiological significance in the field. Secondary host species of AHSV

include camels, goats and buffalo (AWAD *et al.* 1981). Antibodies to different serotypes of AHSV have even been detected in African carnivores such as dogs (VAN RENSBERG *et al.* 1981; ALEXANDER *et al.* 1995) and elephants (BINEPAL *et al.* 1992). These species are regarded as dead-end hosts rather than reservoirs for infection, as it is not known how frequently *Culicoides* vectors of AHSV bite them, if at all (VAN RENSBERG *et al.* 1981; ALEXANDER *et al.* 1995). Recent research however suggests that this is not the case for South African domestic dogs, and that AHS is much more prevalent in dogs than previously expected (VAN SITTERT *et al.* 2013; O'DELL *et al.* 2018).

Biological transmission between vector and host species follows a cyclical trend. The virus must be present in the peripheral blood vessels or skin tissues of the equid, making it accessible to *Culicodes* vectors. The time between ingestion and the insect being able to transmit AHSV to another vertebrate host is termed the extrinsic incubation period (WILSON *et al.* 2009). During this period AHSV penetrates, infects and replicates in the gut cells of the midge, which leads to the dissemination of the virus to the haemocoel, and salivary glands. Once here, transmission of the virus becomes possible during subsequent blood-feeding events (WILSON *et al.* 2009). The time from inoculation via vector to host transmission and systemic AHSV infection in the equid is termed the intrinsic incubation period (MELLOR *et al.* 2000; WILSON *et al.* 2009). Hereafter the host serves as a reservoir for subsequent host to vector transmission events.

The geographical distribution of AHSV depend not only on the presence of the virus and equids but also on the abundance of competent vectors (MELLOR *et al.* 2000). *C. imicola* breeds in damp organically enriched soil and adult females feed on equids, ruminants and pigs as a protein source for egg production (DU TOIT 1944; NEVILL AND ANDERSON 1972; WILSON *et al.* 2009). Outbreaks of AHS therefore occur during summer in areas with warm weather and high rainfall (MEISWINKEL *et al.* 1994). Major outbreaks of AHS in South Africa have coincided with periods of heavy rainfall that are preceded by drought, an occurrence that also encourages susceptible hosts to congregate at watering holes, amplifying even further transmission (WILSON *et al.* 2009). AHS is typically not prevalent in the greater part of South Africa (THOMPSON *et al.* 2012), only in the northeast parts in the Lowveld of the Mpumalanga Province.

Recently, cases of AHS have been reported earlier than usual and in areas beyond this region in South Africa (AHS Trust 2019). There has also been an increase in the number of serotypes present within the northern limits of AHSV's range in sub-Saharan Africa (MACLACHLAN AND GUTHRIE 2010). Climate change may be creating new breeding grounds in regions not previously favourable for *Culicoides* species. Since 2007 AHSV has unexpectedly spread northward to several African countries such as Senegal, Ghana, Nigeria and Ethiopia where it caused numerous outbreaks (DIOUF *et al.* 2012; OIE 2019). From past experiences with BTV's incursion into Europe (MACLACHLAN 2010), once *Culicoides* vectored viruses reach North Africa they readily spread to countries in Europe and the Middle East - many of which are extensively involved in the international trade and movement of horses. The incursion of AHSV into such areas would be economically devastating. The cost should major outbreaks of AHS occur in Great Britain have been estimated at

approximately £-35 000 000 (GOSLING *et al.* 2012). Thus, there is substantial concern regarding the potential northward spread of AHSV's enzootic region to include North Africa and Europe.

1.4. Pathogenesis of AHS

Following inoculation of the vertebrate host, AHSV rapidly replicates in the regional lymph nodes followed by dissemination throughout the body via the blood (LAEGREID *et al.* 1992) and subsequent infection of target organs and cells. Target organs include the spleen, lungs, caecum, pharynx, choroid plexus and most lymph nodes (MELLOR AND HAMBLIN 2004). Vascular and lymphatic endothelial cells are considered the primary cellular targets of all AHSV serotypes, while large cells of the red pulp of the spleen are the ancillary targets (BARRATT-BOYES AND MACLACHLAN 1994; MELLOR AND HAMBLIN 2004). Other minor cellular targets include mononuclear cells, resembling phagocytic cells, and their surrounding lymphoid follicles (BARRATT-BOYES AND MACLACHLAN 1994; WOHLSEIN *et al.* 1997).

Preferential replication and dissemination from these sites give rise to secondary viremia of variable duration depending on the viral virulence and host susceptibility (LAEGREID *et al.* 1993; COETZER AND ERASMUS 1994; MELLOR AND HAMBLIN 2004). A more virulent virus strain and a larger dose of the virus have been reported to shorten the incubation period (COETZER AND ERASMUS 1994). Under natural conditions, the time from initial infection to the commencement of secondary viremia usually occurs within nine days, although experimentally it has been shown to vary between two and 21 days (MELLOR 1994). In horses AHSV titres of up to $10^{5.0}$ $TCID_{50}$/mL have been recorded, but viremia may last four to eight days and has not been detected beyond 21 days (COETZER AND ERASMUS 1994). Levels of viremia in zebras and donkeys are lower ($<10^{3.0}$ $TCID_{50}$ /mL) and extended, lasting for up to four weeks in some instances even in the presence of circulating antibodies (COETZER AND ERASMUS 1994).

The onset of secondary viremia usually coincides with the time the host has sustained sufficient cell damage to perturb homeostasis, apparent by the presence of macro- and/or microlesions. Once this occurs AHS manifests as pyrexia, and clinical signs compatible with impaired respiratory and circulatory function due to serous effusion and haemorrhage in lymphatic, pulmonary and cardiac tissue are observed (HOWELL 1963; CLIFT AND PENRITH 2010). Four clinicopathological forms of AHS exist (THEILER 1921), each with different severities. In ascending severity these forms are the horse sickness fever form, subacute or cardiac form, mixed or cardiopulmonary form, and the peracute or pulmonary form (MAURER 1963; ERASMUS 1972). Other *Equidae* species such as donkeys and mules are considerably less susceptible than horses and generally only develop horse sickness fever with infection (COETZER AND ERASMUS 1994). Zebra have long been considered the natural vertebrate host and reservoir of AHSV and rarely exhibit clinical signs of infection (BARNARD 1998; MELLOR AND HAMBLIN 2004).

Macro- and/or microlesions vary in accordance to each disease form. With the pulmonary form (~95% fatal) macrolesions in interlobular and sub-pleural tissues are the most conspicuous and result in pulmonary

oedema and hydrothorax (COETZER AND ERASMUS 1994; MELLOR AND HAMBLIN 2004). In the subacute form (~50% fatal) the most prominent macrolesions are in the subacutaneous, sub-fascial and intramuscular tissue and lymph nodes, and typically result in hydropericardium and haemorrhages on epicardial and/or endocardial surfaces (SAILLEAU *et al.* 2000; MELLOR AND HAMBLIN 2004). In the mixed form (~70% fatal), macrolesions common to both the pulmonary and subacute from of AHS occur (WOHLSEIN *et al.* 1997; MELLOR AND HAMBLIN 2004). The prevalence and extent of microlesions correspond with disease severity and result in the impairment of several organ systems, including the muscular, circulatory, respiratory and excretory and digestive systems (MELLOR AND HAMBLIN 2004). Horse sickness fever is invariably mild, typically involving only mild to moderate pyrexia and oedema of the supraorbital fossae, with no mortality (MELLOR AND HAMBLIN 2004). The form of AHS seen in infected horses is the result of several factors, such as the route of infection and/or the tropism of subpopulations of virus particles (ERASMUS 1973).

1.5. Prevention and control

There is no specific treatment for equids suffering from AHS. Rest and good husbandry is usually advised. AHSV is non-contagious and can only be spread via bites of infected *Culicoides* species. Zebra are long-term reservoirs of AHSV and play a central role in the persistence of the virus in Africa. AHS prevention and control therefore depends on vaccination, isolation or slaughter of infected animals, restrictions on movements of equids and vector control (MELLOR AND HAMBLIN 2004).

Live-attenuated strains have been used for the past few decades for vaccination purposes (MIRCHAMSY AND TASLIMI 1964). Commercially available vaccines are either mono- or polyvalent variants of AHSV attenuated through passage in cell culture and as such have several drawbacks (MELLOR AND HAMBLIN 2004). The first being the potential production of viruses with novel antigenic properties due to reassortment between live vaccine viruses and wild-type viruses in either invertebrate or vertebrate hosts (MELLOR AND HAMBLIN 2004). Three or more courses of prophylactic immunization per annum is needed before a horse is considered well protected against the disease (COETZER AND ERASMUS 1994). Exerted and/or immunocompromised animals usually develop the disease upon immunization (COETZER AND ERASMUS 1994), which defeats the purpose of such preventative measures. Lastly, the use of these vaccines in gestating females are also prohibited due to reported teratogenic effects (MELLOR AND HAMBLIN 2004).

In order to find a way around these drawbacks and produce inherently safe, efficacious vaccines past research has been focused on inactivated and sub-unit vaccines. Assurance of complete inactivation was subsequently found to be very difficult (DUBOURGET *et al.* 1992) and production too costly for commercial use. Sub-unit vaccines, comprising only synthetic core-like (CLP) or virus-like particles (VLP) have been promising but protective immunity in horses is yet to be achieved (MELLOR AND HAMBLIN 2004).

It is impossible to completely eliminate populations of vector *Culicoides*. Vector control strategies therefore mainly aim to reduce the number of infecting bites that susceptible animals receive. A combination of

approaches is usually used, namely habitat alterations and application of insecticides and repellents (MELLOR AND HAMBLIN 2004). The collective power of these strategies however relies on the identification of all *Culicoides* species involved in transmission, and is limited due to a lack of knowledge of their bio-ecology and efficient operational methods (CARPENTER *et al.* 2008).

In light of these impediments there is a need for improved vector control measures, surveillance systems and vaccines to replace the commercially available live-attenuated vaccines if we are to prevent AHS outbreaks in the future (MELLOR AND HAMBLIN 2004). A greater insight into the molecular biology and life cycle of AHSV and role of specific viral proteins in AHSV virulence and pathogenicity in vertebrate and invertebrate is needed if we are to attain such intervention strategies.

1.6. Molecular Biology

The first molecular characterisation of AHSV was performed by Verwoerd and Huismans in the late 1960s (VERWOERD AND HUISMANS 1969). Since then, over the last 40 years, detailed molecular and genetic analyses of the virion and virus life cycle have been and continue to be undertaken.

1.6.1. Virus Structure

AHSV is classified in the genus *Orbivirus* in the family *Reoviridae.* As such its morphology has been described as essentially identical to BTV (ROY *et al.* 1994), and comparable to other orbiviruses such as equine encephalosis virus (EEV) (SPENCE *et al.* 1984). The AHS virion is a non-enveloped particle composed of an icosahedral core and an outer capsid (Fig 1 A) (VERWOERD *et al.* 1972).

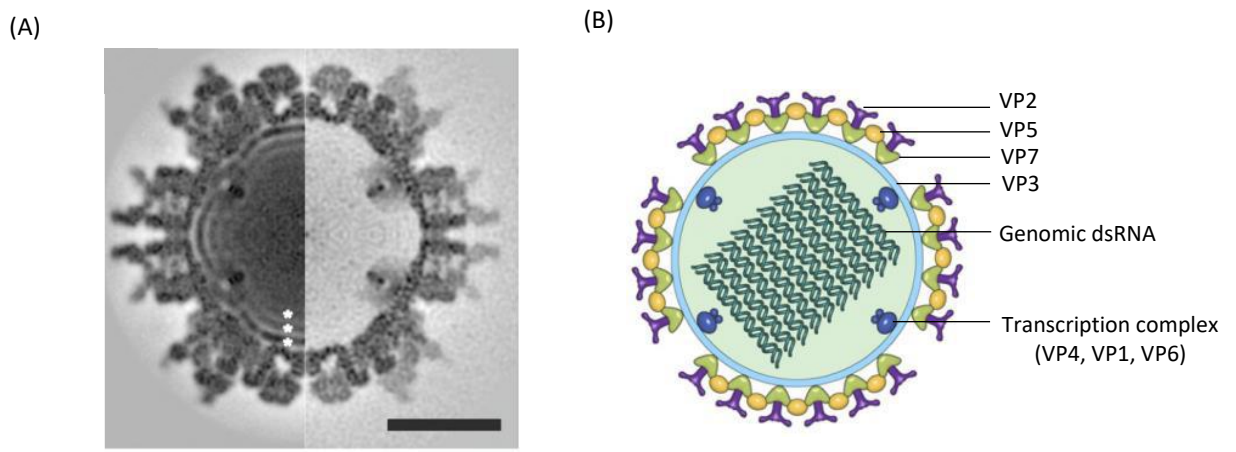

Figure 1. Overall organization of AHSV virion. (A) Central cross section through AHSV reconstructions from filled (left; 0.18 nm thick) and empty (right; 0.28 nm thick) virus particles. Three well-ordered layers of genomic dsRNA (white asterisks) are indicated. Bar 25 nm. All proteins are in black. (B) Schematic representation of AHSV reconstructions (from Manole *et al.* 2012).

The virus is approximately 70 nm in diameter and the core approximately 50 nm (MARTIN AND ZWEERINK 1972). The outer capsid of AHSV, like BTV, has been described as fibrillar (Fig 1 A). Structural proteins VP2 and VP5 form the outer capsid (Fig 1 B). The core consists of VP3 which forms the subcore upon which VP7 capsomeres are located (Fig 1 B) (HUISMANS *et al.* 1987b; HYATT AND EATON 1988; GRIMES *et al.* 1998). Cryo-EM studies have shown that VP1 and VP4 directly underlie the VP3 layer (NASON *et al.* 2004). Channels transverse the subcore where the minor structural proteins VP1, VP4 and VP6 are located, possibly for the passage of metabolites and nucleoside triphosphates (NTP) into and from the core (Fig 1 B) (OELLERMANN *et al.* 1970; BREMER *et al.* 1990; ROY *et al.* 1991). These minor structural proteins form the transcription complex required for the replication and transcription of viral RNA (ROY 2005; ROY 2008)

The triple-layered icosahedral capsid contains the viral genome comprised of ten double-stranded RNA (dsRNA) segments, numbered according to size from largest to smallest (Seg-1 to Seg-10) (Table 1) (OELLERMANN *et al.* 1970; BREMER 1976; ZWART *et al.* 2015). Each segment encodes at least one of the seven structural (VP1-7) or one of the four non-structural (NS1, NS2, NS3/3A and NS4) proteins (Table 1) (OELLERMANN *et al.* 1970; BREMER 1976; BELHOUCHET *et al.* 2011). Non-structural proteins involved in virus replication, morphogenesis and release are present after viral transcription and translation have occurred (VAN STADEN AND HUISMANS 1991; VAN STADEN *et al.* 1991; ROY *et al.* 1994; BELHOUCHET *et al.* 2011).

Table 1. Size of AHSV-4 genome segments and encoded proteins

Segment (sequence size in base pairs)	Protein/s encoded (size in kilodaltons)
Seg-1 (3 965)	**VP1** (150.35)
Seg-2 (3 229)	**VP2** (124.08)
Seg-3 (2 792)	**VP3** (103.26)
Seg-4 (1 978)	**VP4** (75.73)
Seg-5 (1 748)	**NS1** (63.23)
Seg-6 (1 566)	**VP5** (56.73)
Seg-7 (1 167)	**VP7** (37.84)
Seg-8 (1 166)	**NS2** (41.08)
Seg-9 (1 169)	**VP6** (38.29) **NS4** (20.00)
Seg-10 (756)	**NS3** (23.68) **NS3A** (22.37)

Courtesy of the National Centre for Biotechnology Information (NCBI)
GenBank and RefSeq databases.

Nine different AHSV serotypes exist with little cross-neutralization between serotypes (McIntosh 1958; Howell 1962). The outer capsid protein VP2 is highly variable between serotypes and is the main determinant of serotype specificity and the neutralization-specific immune response (Burrage *et al.* 1993; Vreede and Huismans 1994). The physiochemical properties of AHSV is well known. Virions are acid sensitive and readily inactivated at a pH below 6.0, but remains relatively stable to pH changes on the alkaline side of neutrality with the optimal range being 7.0 – 8.5 (Cybinski and St George 1982). It is relatively heat resistant, and resistant to ether and other lipid solvents (Coetzer and Erasmus 1994). Virus derived from cell culture in a medium containing foetal calf serum is stable for 3 months at 4°C, and the virus can be stored for at least six months at 4°C in saline containing 10% foetal calf serum (Coetzer and Erasmus 1994). Even so, AHSV is best stored in a lyophilised state or frozen at -70°C (Coetzer and Erasmus 1994).

1.7. Viral life cycle

Evident from its vector-borne transmission cycle, orbiviruses successfully propagate in both mammalian hosts and insect vectors. The outcomes of virus infection on these species are however distinct, with hosts exhibiting a range of clinical signs, while vectors remain unaffected (Mellor *et al.* 2000; Mellor *et al.* 2009). Infection induces dramatic changes in the morphology and physiology of mammalian cells, termed cytopathic effect (CPE) that ultimately ends in cell death (Coetzer and Guthrie 2004; Stassen *et al.* 2012). Within 12 hours, cells infected with AHSV display increased cell rounding and detachment visible by light and electron microscopy (Laegreid *et al.* 1992; Coetzer and Guthrie 2004; Meiring *et al.* 2009). Infection in insect tissue culture has very little, if any, effect on cell morphology and physiology (Coetzer and Guthrie 2004; Stassen *et al.* 2012).

This difference in outcome could be attributed to the AHSV-induced apoptotic response in mammalian cells and the absence thereof in insect cells (Stassen *et al.* 2012), or the result of different mechanisms of virus release as with BTV (Hyatt *et al.* 1989; Beaton *et al.* 2002; Wirblich *et al.* 2006). The factors contributing to each outcome is probably the result of complex and multifactorial molecular interactions between orbivirus proteins and host factors, and most likely involve every stage of the virus life cycle (Huismans *et al.* 2004). The major events in orbivirus replication will be reviewed in the following section. The molecular determinants of BTV and AHSV virulence will also be discussed at various viral life cycle stages.

1.7.1. Adsorption, penetration and the outer capsid proteins

AHSV binds rapidly to the cell surface receptors facilitated by VP2 (Manole *et al.* 2012). Little is known of the identity of the receptors involved in orbivirus entry except that its distributed all over the cell surface and are associated with the cytoskeleton (Brookes *et al.* 1993) Following adsorption, particles penetrate the cell surface and underlying cortical matrix by clathrin-dependent endocytosis (Forzan *et al.* 2007) and/or macropinocytosis (Vermaak *et al.* 2016). Following up take, endocytic vesicles are transported to a juxta-nuclear position presumably by components of the cytoskeleton (Gould and Hyatt 1994). During this process

vesicles fuse and particles are delivered to acidic components of the endocytic route, namely early endosomes.

Virus adsorption and penetration may be different in host and vector species. The outermost core protein, VP7, has been shown to exhibit *Culicoides* cell binding activity and may participate in vector cell entry (XU *et al.* 1997; TAN *et al.* 2001). The outer capsid protein, VP2 may thus not be essential for infection in insect cells. In support, particles lacking VP2 show enhanced infection capabilities in insect cells compared to full particles and cores (MERTENS *et al.* 1996; WILSON *et al.* 2009). The proteases responsible for outer capsid digestion, chymotrypsin and trypsin, have been found in the saliva of competent *Culicoides* vector species in significantly higher quantities than non-vector species (WILSON *et al.* 2009; DARPEL *et al.* 2011). VP2 is however essential for AHSV release from insect cells but not mammalian cells and VP5 for *in vitro* replication (VAN GENNIP *et al.* 2017). These characteristics and their inherent high level of inter-serotype variation has led to the identification of VP2 and VP5 as principal AHSV virulence determinants (HUISMANS *et al.* 2004). Subsequent studies have confirmed this characterisation in BTV and AHSV, as the exchange of one of the capsid proteins between serotypes or even strains were found to affect the growth kinetics of the virus and in some instances even leading to partial attenuation (JANOWICZ *et al.* 2015; VAN DE WATER *et al.* 2015).

Further support for VP2 and VP5 as virulence factors was given when the combined expression of the outer capsid proteins was found to induce apoptosis in mammalian cells but not insect cells (MORTOLA *et al.* 2004; VERMAAK AND THERON 2015). Mammalian cells infected with AHSV or BTV exhibit membrane blebbing, DNA fragmentation and the formation of apoptotic bodies, all of which are characteristics of apoptotic induction (MORTOLA *et al.* 2004; UMESHAPPA *et al.* 2010; STASSEN *et al.* 2012). The extrinsic apoptotic pathway was recently shown to be active in AHSV infected cells (VERMAAK AND THERON 2015) along with the already established intrinsic apoptotic pathway (STASSEN *et al.* 2012) as in the case of BTV infection (NAGALEEKAR *et al.* 2007; STEWART AND ROY 2010).

1.7.2. Uncoating, formation of replicative complexes and the composition of virus inclusion bodies

Endosomal acidification along the endocytic route causes the degradation of VP2 and exposure of VP5 trimers. This destabilizes the endosomal membrane and initiates membrane permeabilization by VP5 and membrane fusion (HASSAN *et al.* 2001; FORZAN *et al.* 2004; FORZAN *et al.* 2007; ZHANG *et al.* 2010b; STASSEN *et al.* 2011), allowing for the release of the core particle lacking VP5 and VP2 into the cytoplasm (HUISMANS *et al.* 1987a). *In vitro* studies have shown a pH of 5.0 is sufficient to remove VP2 (HUISMANS *et al.* 1987b) and that within one hour of infection VP2 and VP5 are removed (HUISMANS *et al.* 1987c).

The release of core particles which does not disassemble into the surrounding cytoplasm is followed by the formation of a matrix around the core particles. Channels present in the VP7/VP3 core layer (refer to section 1.6.1.) facilitate the supply of substrates and metal ions, the removal of waste and the release of transcripts from the transcriptionally active core (VAN DIJK AND HUISMANS 1980; BASAK *et al.* 1997; DIPROSE *et al.* 2001;

MERTENS AND DIPROSE 2004). The matrix around cores, known as viral inclusion bodies (VIBs), consist of viral RNA and proteins. *In-situ* hybridization show that the single-strand RNA (ssRNA) content of VIBs are virus-specific messenger RNA (mRNA) (GOULD AND HYATT 1994). Structural proteins (VP3, 7 and 5) are contained in VIBs as well as non-structural proteins (NS1 and 2) of which NS2 is the major constituent (EATON *et al.* 1987; THOMAS *et al.* 1990). Inclusion bodies are characteristic of orbivirus infection and grow in size and complexity with the progression of infection. VIBs form from parental virus particles, but as more viruses enter the cell and are uncoated the number of VIBs increase (HYATT *et al.* 1989; BROOKES *et al.* 1993).

1.7.3. Viral genome transcription

The genome remains sequestered within the core in the cytoplasm of cells, possibly to abrogate an innate immune response. Transcription takes places inside the core via the virus-encoded transcription machinery (GOUET *et al.* 1999). The ten segments are templates for simultaneous and repeated transcription of each of the segments. Ten to twelve transcription complexes are contained within a core (NASON *et al.* 2004). These complexes are responsible for the simultaneous and repeated synthesis of positive sense-strand mRNAs from each genomic segment (DIPROSE *et al.* 2002; MERTENS AND DIPROSE 2004). The RNA helicase VP6 unwinds blunt-ended dsRNA and 3' and 5' overhang templates through the use of its RNA-binding and ATPase activity (ROY *et al.* 1990; STÄUBER *et al.* 1997; DE WAAL AND HUISMANS 2005), RNA-dependent RNA polymerase VP1 facilitate the production of protein-coding mRNAs (URAKAWA *et al.* 1989; BOYCE *et al.* 2004), and the VP4 capping enzyme caps transcripts as they dissociate from the genomic template (RAMADEVI *et al.* 1998).

The formation of the methylated 5'-cap structure is achieved before the transcripts are extruded through core channels to the cytoplasm (DIPROSE *et al.* 2001). This cap1 structure (^{7}mGppGm) is identical to cellular mRNAs (MARTINEZ-COSTAS *et al.* 1998), making these viral mRNAs suitable substrates for translation via host machinery (SACHS *et al.* 1997). From their function, core proteins are expected to affect virus growth. For BTV, VP1, VP4, VP6 (transcription complex subunits) and VP7 (outermost core protein) contribute to viral growth and are virulence determinants (JANOWICZ *et al.* 2015). The extent of their contribution is yet to be determined.

1.7.4. Expression of viral proteins

Following infection BTV proteins rapidly accumulate and become the most abundant cytoplasmic proteins. BTV protein synthesis is highest 10 to 26 hours post infection (hpi) (HUISMANS 1979). The ten viral mRNAs synthesised by the viral RNA-dependent RNA polymerase are translated by host machinery into eleven viral proteins (VP1-7, NS1-4) (SANGAR AND MERTENS 1983; MERTENS *et al.* 1984; BELHOUCHET *et al.* 2011). Each genome segment encodes a single protein, except for Seg-9 which encodes two proteins (VP6 and NS4) in two different reading frames (BELHOUCHET *et al.* 2011), and Seg-10 which encodes the two isoforms, NS3 and NS3A through alternative initiation codons in the same reading frame (VAN STADEN AND HUISMANS 1991).

The first ultrastructural evidence of virus gene expression is the formation of cytoplasmic hollow tubules in insect and mammalian cells (HUISMANS AND ELS 1979; EATON *et al.* 1990b). These tubules are comprised of a lattice of non-structural protein NS1, resulting from high levels of NS1 expression early in viral replication (HUISMANS *et al.* 1987a; ROY 1989) and are characteristic of orbivirus-infected cells (EATON *et al.* 1990b). Tubules are normally found at peri- or juxtanuclear locations, and have a fine rectangular appearance with smooth edges (HUISMANS AND ELS 1979; MAREE AND HUISMANS 1997; VAN STADEN *et al.* 1998). Viruses do not associate with tubules and these structures are thought of biologically inert storage forms of NS1. Whether tubules have a function is yet to be determined, but studies have linked BTV NS1 with cytopathogenicity (OWENS *et al.* 2004), the upregulation of viral mRNA translation (BOYCE *et al.* 2012) and the disruption of the centrosome (SHAW *et al.* 2013). Whether NS1 directly plays a role in cellular pathogenesis, and the role of AHSV NS1, needs to be investigated.

The formation of hexagonal crystals provides more ultrastructural evidence of virus gene expression in AHSV-infected mammalian and insect cells (BURROUGHS *et al.* 1994; BEKKER *et al.* 2014; VENTER *et al.* 2014). The crystalline lattice is made of insoluble VP7 aggregates that form via a self-assembly processes independent of intracellular trafficking and host defence pathways (BEKKER *et al.* 2014). The function of these VP7 crystals is yet to be determined, but their presence seems to be undesirable as such formations sequester the bulk of newly formed VP7, thereby preventing the incorporation of expressed VP7 into the AHSV particle (BEKKER *et al.* 2014).

VIBs visible by electron microscopy as granular perinuclear cytoplasmic densities also provide ultrastructural evidence of viral gene expression (BROOKES *et al.* 1993). Inclusion bodies are the site of viral core assembly, and recruit all the proteins required for core assembly (BROOKES *et al.* 1993; BOYCE *et al.* 2004). The expression of non-structural protein NS2 is both necessary and sufficient for VIB formation, but co-expression of VP1, VP3, VP4 and VP6 are necessary for the recruitment of VP7 to the VIB (UITENWEERDE *et al.* 1995; KAR *et al.* 2007). NS2 preferentially binds viral ssRNA over nonspecific RNAs, via cis-acting sequences distributed throughout the coding and non-coding regions of different genome segments (LYMPEROPOULOS *et al.* 2003). This binding affinity is essential for the recruitment and sequestration of viral ssRNA to VIBs. NS2 undergoes phosphorylation by protein kinase CK2 (HUISMANS *et al.* 1987a; THERON *et al.* 1994), and the phosphorylation status of NS2 influences VIB formation in infected cells (MODROF *et al.* 2005).

NS2 provides the matrix for viral core assembly, but also performs specific functions in this process. It has been shown that NS2 via secondary structure recognition differentially selects mRNAs for incorporation into assembling virions (LYMPEROPOULOS *et al.* 2003). NS2 assembles into multimers that associate with VIBs (UITENWEERDE *et al.* 1995). These homomultimers possess nucleotidyl phosphatase activity and hydrolyse the α, β and γ phosphodiester bonds of all NTPs (TARAPOREWALA *et al.* 2001). It has been suggested that this activity provides the energy required for secondary replication i.e. the conversion of the ssRNA segments into the dsRNA genome (BUTAN AND TUCKER 2010). Evidence of NS2 interacting with microtubules and

condensed chromosomes suggests that NS2 also functions to disrupt the microtubule organising centre (MTOC) and thereby the cell division process (SHAW *et al.* 2013).

The expression of the other two non-structural proteins is not essential for replication but confers a replicative advantage by functioning in supportive roles. For example, BTV and AHSV mutants lacking NS3 show reduced pathogenesis, replication and release in mammalian and insect cells, thereby confirming the replicative advantage of the protein (FEENSTRA *et al.* 2014; VAN GENNIP *et al.* 2014; VAN DE WATER *et al.* 2015). NS3 therefore functions as a virulence factor and its role in intracellular virus trafficking and subsequent release will be discussed in the following section.

NS4 is the most recently identified non-structural protein and also not essential for replication. Studies of BTV NS4 found it in the cytoplasm, but distinctly in the nucleoli of cells (BELHOUCHET *et al.* 2011; RATINIER *et al.* 2011). It has been proposed to counteract the antiviral interferon (IFN) response (RATINIER *et al.* 2011) by modulating the activity of a wide range of IFN stimulated promoters *in vitro* in IFN competent cells and *in vivo* in sheep (RATINIER *et al.* 2016). The protein has also been shown to protect DNA from DNase activity (BELHOUCHET *et al.* 2011). Although none of these replicative advantages have been shown for AHSV NS4 and the intracellular localisation is different to BTV in infected cells, nucleic acid binding assays have illustrated its dsDNA binding ability which might be suggestive of comparable functions (ZWART *et al.* 2015).

1.7.5. Viral morphogenesis

Subcores (VP1, VP4, VP6 and VP3) develop into cores (VP1, VP4, VP6, VP3 and VP7) and then into full particles (VP1, VP4, VP6, VP3, VP7, VP5, VP2) which, in turn, are released into the surrounding environment (BROOKES *et al.* 1993). Functional core assembly is driven by ssRNAs and the recruitment thereof initiates subcore formation (LOURENCO AND ROY 2011). The transcription complex assembles first and VP4 plays a central role in this process and interacts with all subcore proteins (LOURENCO AND ROY 2011). VP6 act as a RNA translocator during the assembly of the transcriptase complex (MATSUO AND ROY 2013). Newly synthesised ssRNA associates with the transcription complex prior to encapsidation by VP3 and VP7. This requires a VP1-VP4-VP6 interaction before the interaction with VP3 to stabilize the transcription complex (LOUDON AND ROY 1991; LOURENCO AND ROY 2011). The binding of this complex to VP3 decamer intermediates formed from newly synthesised VP3 dimers induces the encapsidation of ssRNA, VP1, VP4 and VP6 and the complete assembly of the VP3 subcore *via* decamer-decamer interactions (GOUET *et al.* 1999).

Genomic packaging occurs during nascent core assembly and is a highly coordinated reaction in which Seg-10 plays a key role (LOURENCO AND ROY 2011). BTV Seg-10 initiates genome packaging and triggers RNA-RNA interactions with other smaller genome segments forming a complex network. Medium to larger segments are subsequently recruited until the complete genome is packaged. The untranslated regions of Seg-10 is critical for sequential genomic packaging (SUNG AND ROY 2014). Conserved structural signals contained in the 5’ and 3’ ends of ssRNAs serve as packaging signals and ensure the encapsidation of the entire segmented

genome (BURKHARDT *et al.* 2014). The encapsidated ssRNA recruited before assembly are used as templates for dsRNA synthesis during the assembly pathway, leading to the generation of complete cores (LOURENCO AND ROY 2011).

VP7 forms trimers in solution (BASAK *et al.* 1992) that assemble onto the VP3 subcore (LIMN *et al.* 2000). The completion of the outer VP7 layer of the core contributes to viral yield by strengthening the overall structure (LOUDON AND ROY 1991) and mitigating subcore RNase sensitivity (LOURENCO AND ROY 2011). Once assembled, newly constructed cores can continue to transcribing mRNA for the production of progeny virions, or they can receive their outer capsid proteins that will supress their transcriptional activity (FRENCH AND ROY 1990). The latter involves the final stage in viral morphogenesis which does not occur within the VIB. Neither VP2 nor VP5 are recruited by VIBs (KAR *et al.* 2007), instead each interacts independently with host cell machinery. For example, VP5 interacts with SNARE regulatory protein synaptotagmin I of the exocytosis pathway (BHATTACHARYA AND ROY 2008) and VP2 with vimentin, a major component of intermediate filaments and cell cytoskeleton (BHATTACHARYA *et al.* 2007). Exactly how these proteins locate to the VIB periphery is not known, but outer capsid proteins are added at this site (GOULD *et al.* 1988). Upon addition of these proteins the BTV virions associate with the cell cytoskeleton (EATON *et al.* 1987). Failure of developing virions to receive the correct complement of outer capsid proteins presumably results in their incorporation into the matrix of VIBs (GOULD *et al.* 1988)

1.7.5. Virus trafficking to and release from the cell surface

Studies have shown that NS3 is ultimately responsible for the trafficking and subsequent release of progeny virions in mammalian cells (HYATT *et al.* 1991; HYATT *et al.* 1993; STOLTZ *et al.* 1996). NS3 is one of the smallest AHSV proteins, and possess several functional domains (Fig 2) that confer a replicative advantage by performing specific roles in facilitating intracellular trafficking and mediating the subsequent release of viruses (FEENSTRA *et al.* 2014; VAN GENNIP *et al.* 2014; VAN DE WATER *et al.* 2015). The roles of the domains shown in Fig 2 will be discussed in the section to follow.

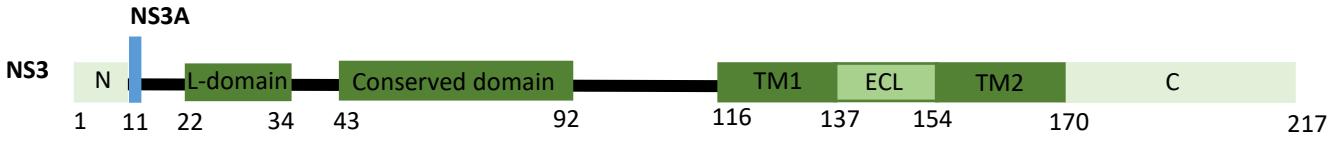

Figure 2. Schematic representation of the functional domains (green) of AHSV NS3 protein (adapted from van Staden *et al.* 1995 and van Niekerk *et al.* 2001). The NS3A initiation codon is indicated in blue. TM refers to the hydrophobic transmembrane domains and ECL to the hydrophilic extracellular loop. The numbers refer to amino acid residues in NS3. The 50 residues from residue 43 to 92 represents the conserved domain found in four different orbiviruses. N and C refers to the N-terminal domain and C-terminal domain.

The Seg-10 gene of AHSV encodes two proteins, NS3 and NS3A, through alternative initiation codons in the same reading frame (VAN STADEN AND HUISMANS 1991). The two proteins are isoforms. NS3A lacks the 13 N-terminal residues present in NS3 that forms an amphiphatic α-helix and interacts with a member of the S100 family, called cellular protein p11 (calpactin light chain) (BEATON *et al.* 2002). In BTV this p11-binding motif of NS3 (Fig 2) is highly specific and competes with p36 (annexin II heavy chain) to form part of the annexin II complex involved in exocytosis (BEATON *et al.* 2002). This virus-host interaction is extremely important for efficient virus release in mammalian cells, suggesting the redundancy of NS3A in mammalian cells (CELMA AND ROY 2011). Expression analysis of N3/NS3A in BTV-infected cells, showed the proteins to accumulate in low levels in mammalian cells but to higher levels in insect cells (FRENCH *et al.* 1989; GUIRAKHOO *et al.* 1995), suggesting that it may act differently in different cell types for virus egress. The role of NS3/NS3A may also be different during AHSV and BTV infection as the isomers are expressed in equimolar amounts during AHSV infection but not BTV infection (WU *et al.* 1992; VAN STADEN *et al.* 1995).

Late domain motifs (L-domain) (Fig 2) have been identified in BTV NS3 that resemble the highly conserved L-domains of matrix proteins encoded by enveloped viruses (WIRBLICH *et al.* 2006; CELMA AND ROY 2009). Enveloped viruses acquire their surrounding membranes by budding. This occurs when matrix protein motifs interact with different members of the cellular endosomal sorting complex (ESCRT) pathway to facilitate viral budding (VOTTELER AND SUNDQUIST 2013). The ESCRT pathway is the key mediator of multivesicular body (MVB) biogenesis (STUFFERS *et al.* 2009), and ESCRTs are ubiquitin-dependent. As such these proteins, collectively recognise, sort and sequester ubiquitinated cargo by deforming the endosomal-limiting membrane of MVBs (KATZMANN *et al.* 2001; NICKERSON *et al.* 2007; HENNE *et al.* 2011).

If newly formed viruses bud through the plasma membrane, the virus is released without violating the integrity of the cell, and if it buds through the bounding membrane of an intracellular compartment such as the endoplasmic reticulum (ER), it exits the cell *via* conventional secretion. Three classes of L-domain motifs have been identified in NS3, which could explain the budding morphology exhibited by BTV at the cell surface (HYATT *et al.* 1991; CELMA AND ROY 2009). The PSAP motif, the first class, recruits the tumour susceptibility gene 101 protein (Tsg101) (WIRBLICH *et al.* 2006), a component of the ESCRT-I complex essential for normal membrane trafficking and membrane fission in endosomes (BABST *et al.* 2000; WILLIAMS AND URBE 2007). Recruitment of Tsg101 was shown to be essential to the release of BTV from mammalian cells *via* viral budding (WIRBLICH *et al.* 2006). The second class, YXPL and LXXLF motifs, bind to cellular AIP-1/Alix and facilitate bridging of ESCRT-I and ESCRT-III by acting just downstream of Tsg101 (CARPP *et al.* 2011). The PPXY motif, the third class, binds to NEDD4-like ubiquitin ligases, a family of ubiquitin ligases responsible for target-specific transfer of ubiquitin (MACIAS *et al.* 2002; WIRBLICH *et al.* 2006; VOTTELER AND SUNDQUIST 2013).

Ubiquitin is a highly conserved 76 amino acid peptide that can be covalently attached to lysine residues in a target protein to post-translationally modify the protein (HERSHKO AND CIECHANOVER 1998; PICKART AND EDDINS 2004). This occurs through a enzymatic conjugation reaction involving the ubiquitin-activating enzyme (E1),

ubiquitin carrier protein (E2) and ubiquitin-protein ligase (E3) (HERSHKO AND CIECHANOVER 1998). Ubiquitination is one of the signals transmembrane proteins, such as NS3 for example, can utilise to direct its intracellular distribution. The ubiquitin status of membrane-bound proteins has been shown to regulate endoplasmic reticulum (ER)-associated degradation (BONIFACINO AND WEISSMAN 1998; MCCRACKEN AND BRODSKY 2006), sorting in the *trans*-Golgi (HELLIWELL *et al.* 2001), endocytosis from the plasma membrane (HICKE AND RIEZMAN 1996), and entry into MVBs (KATZMANN *et al.* 2001).

In mammalian cells, the disruption of the PSAP motif in BTV NS3 seemed to not affect the trafficking of the virus to the plasma membrane, only the release (CELMA AND ROY 2009). The abrogation of the PPXY motif had an effect on the distribution of virus particles, which consequently affected virus release (BHATTACHARYA *et al.* 2015). Although none of these interactions have been demonstrated for AHSV NS3, it is expected to function in much the same manner as residues 22-34 of AHSV NS3 are comparable to the putative L-domain of BTV NS3 (VAN STADEN *et al.* 1995), and NS3 has been identified at sites of AHSV budding (STOLTZ *et al.* 1996).

NS3/NS3A of AHSV and BTV possess two large hydrophobic domains (Fig 2) that facilitate the transmembrane (TM) secondary structure of the protein (VAN STADEN *et al.* 1995; BANSAL *et al.* 1998). N-linked glycosylated and non-glycosylated forms of BTV NS3/NS3A exist in infected cells (WU *et al.* 1992). Two glycosylation sites exist in the protein (LEE AND ROY 1986; HWANG *et al.* 1992) but only asparagine 150, located between the two transmembrane domains in the extracellular loop (Fig 2), is glycosylated (BANSAL *et al.* 1998). The glycosylation status of the protein also influences the membrane organization of NS3. The incorporation of AHSV NS3/NS3 into membranes requires both TM domains and alters the membrane permeability of cells leading to cell death (VAN STADEN *et al.* 1995; VAN STADEN *et al.* 1998; VAN NIEKERK *et al.* 2001). This characteristic of NS3 is similar to the effect of viroporins (HAN AND HARTY 2004), which are proteins that induce the formation of hydrophilic pores in the lipid bilayer of the plasma membrane that disrupt a number of physiological properties of the cell to aid viral replication (NIEVA *et al.* 2012). Several of the physiological disruptions caused by viroporins, such as increased membrane permeability, virus-orientated cellular transport, altered cellular electrochemical gradients and CPE have been associated with NS3 and lytic release in tissue culture (VAN NIEKERK *et al.* 2001; HAN AND HARTY 2004; VAN DE WATER *et al.* 2015). The viroporin activity of NS3 could explain release from a locally disrupted mammalian plasma membrane of BTV (BHATTACHARYA *et al.* 2015) and AHSV (VENTER *et al.* 2014).

Collectively, NS3/3A has been implicated in virus budding and extrusion release mechanisms. Recent evidence indicates its involvement in the intracellular trafficking of progeny viruses and parental viruses during entry. BTV NS3, in addition other structural proteins (VP2, VP5 and VP6), interacts with lipid raft domains (BHATTACHARYA AND ROY 2010), suggesting that trafficking occurs on the lipid raft domains of vesicles leading to combined virion maturation and export (DOMITROVIC *et al.* 2013). Lipid raft domains are rich in cholesterol and sphingolipids, and the side chains of the phospholipids present are usually highly enriched in saturated fatty acids compared to the surrounding regions in the membrane (SIMONS AND IKONEN 1997; CALDER

AND YAQOOB 2007). They are generally found in the membranes of the endoplasmic reticulum, Golgi apparatus, endosomes, lysosomes and the plasma membrane, and act as platforms to co-localize proteins involved in intracellular signalling pathways, such as transmembrane proteins (SIMONS AND IKONEN 1997; HELMS AND ZURZOLO 2004).

Owing to the presence of specific kinases and phosphatases at these membrane bound organelles different phospholipid derivatives, called phosphoinositide phosphates (PIP), are present at these subcellular compartments (SASAKI *et al.* 2009). For example, phosphoinositol-4,5-bisphosphate [$PI(4,5)P_2$] and phosphoinositol-3,4,5-triphosphate [$PI(3,4,5)P_3$] are mostly contained in the plasma membrane, while phosphoinositol-3-phosphate [PI_3P] is found in membranes of the endocytic pathway (ALENQUER AND AMORIM 2015). PIP are important for vesicularisation and trafficking of vesicles by recruiting Rab GTPases, the primary regulator of vesicular trafficking in eukaryotes (CHAVRIER *et al.* 1990). Protein-raft co-localization on membranes are achieved either through covalent lipid modifications, or *via* transmembrane domains (KUNDU *et al.* 1996). In the case of BTV, lipid rafts seem to act to concentrate fusion proteins and transmembrane proteins to facilitate trafficking.

VP5 has fusiogenic properties, as it possesses a highly conserved WHXL membrane-docking domain that is also present in the SNARE regulatory protein synaptotagmin I (FUKUDA *et al.* 2000). This domain has been shown to be responsible for docking of cellular proteins in the plasma membrane through $PI(4,5)P_2$ interactions (JAMES *et al.* 2008). When the WHXL of VP5 was substituted with a series of alanines, the association of VP5 with lipid rafts was severely perturbed and it was no longer localized to the plasma membrane as normally seen in infected cells, but was visible as patches in the cytoplasm (BHATTACHARYA AND ROY 2008). This suggested that VP5 possesses an autonomous signal for membrane targeting, implicating its involvement in trafficking.

In comparison to VP5, VP2 does not contain any obvious lipid raft binding domains. The exact mechanism of interaction between lipid rafts and VP2 is still not clear, but the interaction between the N-terminal of VP2 and vimentin filaments, which are known to move along the microtubule network, is thought of as a key player in the intracellular trafficking of newly synthesised virus particles (BHATTACHARYA *et al.* 2007). The disruption of the microtubule network or the mutation of the N-terminal of VP2 results in a decrease of particle release and a corresponding increase in cell associated particles (BHATTACHARYA *et al.* 2007). The last functional domain of NS3/3A, the C-terminal (Fig 2), binds to VP2 (BEATON *et al.* 2002), suggesting that NS3 forms a bridging molecule that facilitate virus engagement with the cellular export machinery. This NS3/3A-VP2-mediated mechanism for virus release has been proposed as the major mechanism of release from insect cells (GUIRAKHOO *et al.* 1995), and recent evidence support this postulate (VAN GENNIP *et al.* 2017).

It is evident from these studies that orbiviruses exploit a variety of cellular proteins to complete their life cycles, but the underlying host pathways remain to be fully elucidated and defined.

1.8. Intracellular trafficking pathways prone to viral exploitation

Virions are transported in the cytoplasm during two stages of the life cycle: first, during viral entry and second, during virus egress. To overcome barriers of diffusion, many viruses use host intracellular trafficking pathways. Intracellular trafficking depends on a complex network of three cytosolic filaments, involving microtubules of α- and β-tubulin, intermediate filaments of heterogenous proteins such as keratin, and microfilaments of actin (SODEIK 2000). Transport of cargo along action or tubulin is mediated by motor protein complexes such as myosins, kinesins and dyneins. Direct interactions between these cytoskeleton components and viral components to facilitate entry or exit have been reported for herpes simplex virus (HSV) (SODEIK *et al.* 1997; BEARER *et al.* 2000), adenovirus (SUOMALAINEN *et al.* 1999; LEOPOLD *et al.* 2000), and ebola virus (RUTHEL *et al.* 2005). Other viruses like Semliki forest virus (HELENIUS *et al.* 1980), influenza virus (GOTTLIEB *et al.* 1993), vesicular stomatitis virus (GRIFFITHS AND ROTTIER 1992) and human immunodeficiency virus (HIV) (NYDEGGER *et al.* 2003) use membrane trafficking pathways for transport during entry and to the cell surface. As transport between membrane-bound organelles requires an intact cytoskeleton, viral entry and exit of these enveloped virus particles involve cytoskeleton exploitation (COLE AND LIPPINCOTT-SCHWARTZ 1995; BAYER *et al.* 1998; ALLAN AND SCHROERT 1999; SCHROER 2000).

Non-enveloped viruses are predominantly released into the medium with cell lysis and presumably do not require specific transport mechanisms. Yet complex intracellular trafficking and release strategies involving membrane trafficking pathways have been suggested for several non-enveloped viruses, including poliovirus (JACKSON *et al.* 2005; TAYLOR *et al.* 2009) coxsackievirus (ROBINSON *et al.* 2014), hepatitis C virus (SHRIVASTAVA *et al.* 2016), and members of *Reoviridae*, namely rotavirus (JOURDAN *et al.* 1997) and BTV (BHATTACHARYA *et al.* 2015). From recent transmission electron microscopic imaging performed by Venter *et al.* (2014), membrane-trafficking pathways also seem to be exploited by AHSV. From this study, the accumulation of AHSV into vesicle-like structures seemed non-random and such structures were usually in close proximity to the plasma membrane. This implicates the involvement of membrane-related events in the final stages of the AHSV life cycle. In support, BTV particles have also been occasionally observed within or budding into smooth membrane-limited vesicles, indicating the importance of membrane trafficking pathways in the final stages of BTV replication (HYATT *et al.* 1991). BTV NS3/NS3A associate with components of membrane trafficking pathways such as the plasma membrane at sites of virion budding or extrusion (HYATT *et al.* 1989; HYATT *et al.* 1991). AHSV NS3/3A have been observed at sites of viral extrusion (STOLTZ *et al.* 1996). Taken together, reports of the vesicular distribution of BTV and AHSV particles, reports of the intracellular distribution of BTV and AHSV NS3 and evidence of BTV NS3 host and viral protein interactions show the relevance of investigating the role of membrane trafficking pathways in the intracellular trafficking of AHSV.

Membrane trafficking in cells (Fig 3) involve a variety of endo- and exocytic routes of transport. Endo- and exocytosis consist of number of trafficking pathways that converge to perform specific and, in some cases, overlapping functions (TOKAREV *et al.* 2009). Membrane-bound vesicles comprise these pathways and are

formed using a multitude of mechanisms (ALENQUER AND AMORIM 2015). For the purpose of this study, membrane trafficking pathways prone to viral targeting that support the final stages of virus growth will be reviewed. There are two different secretory pathways (Fig 3), the regulated pathway and the constitutive pathway. In the regulated pathway, newly synthesised proteins and lipids are consolidated into vesicles that are secreted in response to a signal, whereas constitutive pathway vesicles continuously form and carry proteins and lipids from the Golgi to the cell surface (LODISH *et al.* 2000b; ALBERTS *et al.* 2002). Both of these pathways are targets for viral exploitation and several picornaviruses, coronaviruses and flaviviruses have been implicated in the manipulation of these pathways (HSU *et al.* 2010). For example, poliovirus hijack components of the secretory pathway, called guanine nucleotide exchange factors responsible for the recycling of ADP-ribosylation factor (ARF) necessary for the synthesis of secretory transport vesicles (SCHEKMAN AND ORCI 1996) to support virus growth (BELOV *et al.* 2007).

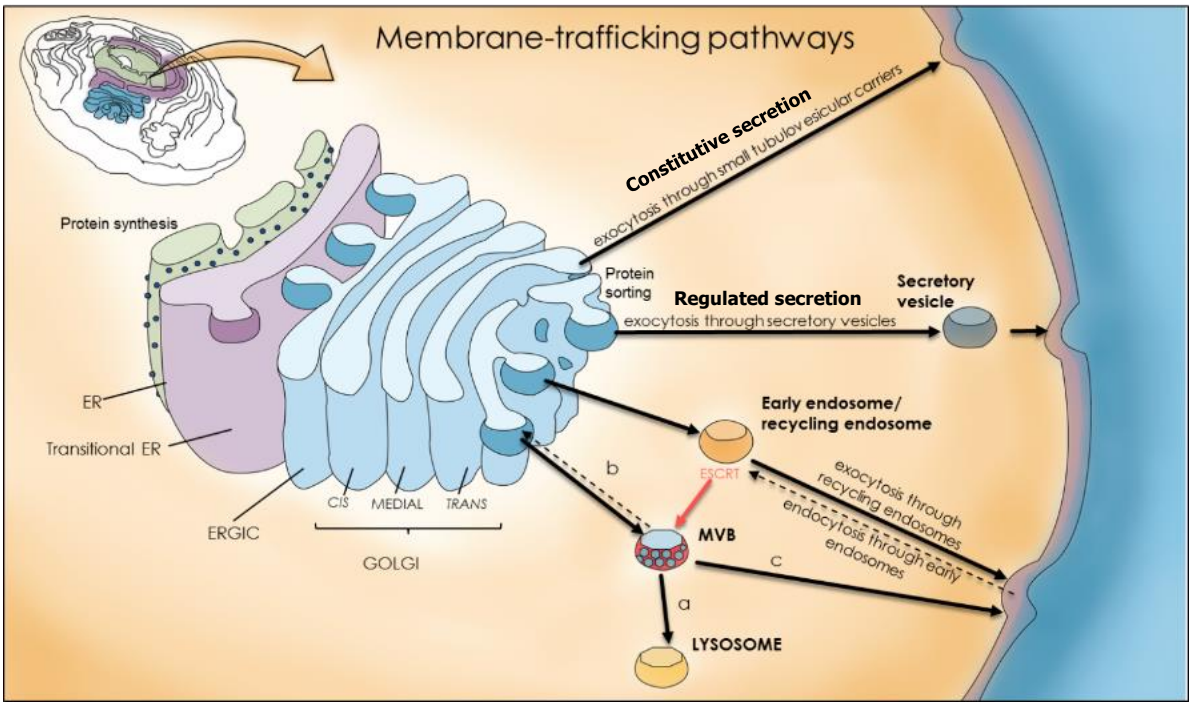

Figure 3. Schematic representation of membrane-trafficking pathways facilitating secretion at the cell surface. The biosynthetic secretory pathway facilitates constitutive and regulated secretion at the cell surface. The trans-Golgi network (TGN), Golgi apparatus secretory vesicles and plasma membrane comprise this pathway. Endocytic recycling compartments facilitate recycling of proteins and lipids to the cell surface. (a) Multivesicular body (MVB) can fuse with lysosomes for degradation, (b) be re-routed to the TGN, or (c) can fuse with the plasma membrane and secrete exosomes.

Endocytic recycling pathways involving sorting endosomes and endocytic recycling compartments (Fig 3) (reviewed in (MAXFIELD AND MCGRAW 2004) has recently been identified as targets for viral subversion during infection by influenza A virus among other for the trafficking, assembly and budding of these viruses (reviewed in (BRUCE *et al.* 2012)). Components integral to MVB biogenesis have also been implicated in the final stages of BTV growth (BHATTACHARYA *et al.* 2015). MVBs are late endosomal compartments displaying intraluminal vesicles (ILVs) (SOTELO AND PORTER 1959) which either fuse with lysosomes for degradation(Fig 3a), are re-routed to TGN (Fig 3b) or fuse with the plasma membrane (Fig 3c) in a exocytic manner (PAN AND JOHNSTONE 1983). The latter results in the release of the ILVs from the MVB lumen into the extracellular milieu, upon which the ILVs are referred to as exosomes (HARDING *et al.* 1983; PAN *et al.* 1985; VIDAL *et al.* 1989; RAPOSO *et al.* 1996). No underlying mechanism has yet been reported to differentiate MVB formation for degradation or fusion with the plasma membrane (ALENQUER AND AMORIM 2015). Interestingly, cells infected with viruses such as HIV release exosomes containing viral proteins and RNA (FANG *et al.* 2007) (reviewed in (SCHOREY *et al.* 2015)).

Cell membrane-associated proteins synthesised by the rough ER are co-translationally incorporated into the endoplasmic reticulum (ER) phospholipid bilayer (LODISH *et al.* 2000a). Proteins synthesised on the ER membrane or transported into the ER lumen have access to the secretory pathway (LODISH *et al.* 2000b). Consistently, BTV NS3, a membrane-associated protein (LEE AND ROY 1986; HWANG *et al.* 1992) is transported after synthesis by host machinery to the Golgi apparatus and then to the plasma membrane (WU *et al.* 1992). Given that AHSV NS3 is membrane-associated (VAN STADEN *et al.* 1995; VAN NIEKERK *et al.* 2001) and essential for virion trafficking and release implicate the potential of AHSV to exploit membrane-related events along the secretory pathway. Phospholipid signalling critical to MVB biogenesis (ODORIZZI *et al.* 1998; WURMSER AND EMR 1998) and the ubiquitin-proteasome system necessary for protein sorting in the Golgi (HELLIWELL *et al.* 2001) and delivery into MVBs (KATZMANN *et al.* 2001) has recently been implicated in BTV growth (BHATTACHARYA *et al.* 2015).

It has previously been shown for poliovirus that more than one viral transport mechanism can exist in a cell (TAYLOR *et al.* 2009). Studies of HIV and HSV transport during viral assembly and egress implicate that the mechanism of cytoplasmic transport and release depends on specific host factors present in only some cell types (reviewed by (SODEIK 2000)). A better understanding of AHSV trafficking could therefore provide valuable insight into the cellular pathogenicity of the virus in mammalian and insect tissue culture. Overall this project aimed to contribute to the understanding of one of the less understood stages of the orbivirus life cycle, virus release.

1.9. Concluding remarks

AHSV causes disease in equids of such international significance that it is allocated to the OIE notifiable disease list. The occurrence of disease is dependent on the prevalence of and seasonal incidence of the major vector of AHSV, the *Culicoides* biting midge. In mammalian cells AHSV infection induces severe CPE, while insect cells sustain asymptomatic infection. CPE manifests as cell rounding, apoptosis and the lytic release of virions into the culture medium. To better understand the cellular pathogenicity of AHSV, this project focused on providing preliminary insight into the intracellular trafficking of progeny virions.

The trafficking and subsequent release of virus from infected cells remains to be elucidated and defined. Interactions between the membrane-associated protein NS3, outer capsid proteins and components of the exocytic pathway suggests a role for host membrane traffic in the final stages of replication. Further, cellular components of the MVB and exocytic pathway have recently been shown to play a role in BTV growth. Many viruses use host transport machinery for transport to and release from the plasma membrane. The involvement of membrane trafficking pathways in AHSV transport is unknown, and will be addressed in this study. In doing this we hope to elucidate the role of cellular transport pathways in AHSV trafficking, and improve the understanding of AHSV trafficking and release.

1.10. Aim and objectives

The aim of this study was to investigate the viral usurpation of cellular trafficking pathways for the transport of mature AHSV particles to the plasma membrane in cell culture systems.

To address this aim, the following three objectives were identified:

i. Analyse and compare the cytosolic distribution of mature AHSV particles in mammalian and insect cell culture at different times post infection.
ii. Determine and compare virus yield and the percentage virus release in mammalian and insect cell culture at different times post infection.
iii. Investigate the role of cellular transport pathways in AHSV trafficking in mammalian and insect cell culture.

CHAPTER 2

Gaining insight into the transport of African horse sickness virus particles to the cell surface

2.1. Introduction

African horse sickness virus (AHSV) is a non-enveloped icosahedral symmetric virus consisting of a triple-layered protein capsid (MANOLE *et al.* 2012) containing ten double-stranded RNA segments (BREMER *et al.* 1990). It is classified in the genus *Orbivirus* and the family *Reoviridae* (BORDEN *et al.* 1971) and causes a disease called African horse sickness (AHS) spread by *Culicodes* biting midges (URBANO AND URBANO 1994). AHS has a mortality rate of up to 95% in naïve horses (HENNING 1956) and is monitored by the World Organisation of Animal Health (OIE 2019). The overall replicative strategy at a cellular level has been informed by BTV studies, the model orbivirus of the genus, but gaps in our understanding still remain, especially with regard to viral transport in the cytoplasm.

Like many other RNA viruses, the entire life cycle of AHSV occurs within the cytoplasm of infected cells. However, full particles are transported in the cytoplasm during only two stages of the viral life cycle: first, during virus adsorption and penetration, and second, during virus egress, when the virus moves through the cytoplasm to the cell surface for release into the extracellular milieu. The molecular mechanisms underlying the events leading to AHSV release is unknown, but in the case of BTV the virus encoded non-structural protein, NS3/3A, via an array of different virus-host interactions is crucial for release from infected cells (BEATON *et al.* 2002; WIRBLICH *et al.* 2006; CELMA AND ROY 2009; CELMA AND ROY 2011; BHATTACHARYA *et al.* 2015) Evidence shows that cell-mediated events leading to AHSV release may underlie the cytopathic effect observed in mammalian cells versus the lack thereof in insect cells (WIRBLICH *et al.* 2006). Elucidating the molecular mechanisms of cytoplasmic transport is therefore required for a coherent understanding of AHSV pathogenesis.

Studies on the localisation of NS3/3A (HYATT *et al.* 1991) and the intracellular localisation of virus particles (HYATT *et al.* 1991; GOULD AND HYATT 1994; CELMA AND ROY 2011; BHATTACHARYA *et al.* 2015) have implicated cellular pathways involving membrane traffic in orbivirus egress. Studies with inhibitors of cellular factors involved in membrane trafficking pathways have aided in elucidating many details of mechanisms and pathways involved in virus trafficking and release. Brefeldin A inhibition of virus replication has been shown for BTV (unpublished data by Eaton, Hyatt and Gould cited in (HYATT *et al.* 1993; GOULD AND HYATT 1994)) and poliovirus (CUCONATI *et al.* 1998). Inhibition of replication by proteasome inhibitors have been shown for BTV (BHATTACHARYA *et al.* 2015) and rotavirus (LÓPEZ *et al.* 2011). Inhibition of phosphatidylinositol 3-kinase activity has been shown to inhibit the replication of BTV (BHATTACHARYA *et al.* 2015), rotavirus (BAGCHI *et al.* 2010) and hepatitis C virus (MANNOVÁ AND BERETTA 2005).

The aim of this study was to comparatively investigate events leading to AHSV release from infected mammalian cells and insect cells. To achieve this, we first analysed the intracellular distribution of virus particles using transmission electron microscopy. We then used inhibitors to selectively inhibit cellular processes involved in membrane trafficking, and assayed AHSV progeny production and percentage release

by virus titration. Results obtained from mammalian and insect cell studies were compared with the hope of detecting underlying differences that could contribute to our understanding of AHSV pathogenesis.

2.2. Materials and Methods

2.2.1. Cell lines

BSR T7/5 cells (referred to as BSR cells from here onwards) (derived from BHK-21 cells) which stably express T7 RNA polymerase (BUCHHOLZ *et al.* 1999), kindly provided by Dr AC Potgieter (Deltamune [Pty] Ltd, South Africa) were maintained in Eagle's Minimal Essential Medium (MEM; Lonza), supplemented with 5% (v/v) foetal calf serum (FCS; Gibco® by Life Technologies™), 1% (v/v) non-essential amino acids (NEAA; Lonza), antibiotics (100 IU/ml penicillin and 100 µg/ml streptomycin; Lonza) and antifungals (2.5 µg/ml Amphotericin B; Sigma). Medium was supplemented every third cell passage with Geneticin (20 µl/ml) (Gibco® by Life Technologies™). KC cells derived from *Culicoides variipennis* (JONES 1957), obtained from Onderstepoort Veterinary Institute (OVI) (Onderstepoort, South Africa) were maintained in 50:50 TC-100 Insect Medium (Lonza) and Insect-Xpress with L-Glutamine (Lonza), supplemented with 10% (v/v) FCS, antibiotics and antifungals. Both cell lines were tested for mycoplasma contamination by the nucleic acid amplification test (NAT) method (ZHI *et al.* 2010), and were mycoplasma free. Cultures were grown in 25 cm^2 tissue culture flasks (TPP®) and split at a ratio of 1:10 twice a week by treatment with 0.125% Trypsin/ 0.1% EDTA for BSR cells and by resuspension for KC cells. BSR cells were incubated at 37°C under 5% CO_2 and 90% humidity, and KC cells at 28°C until confluent for use in assays.

2.2.2. Virus strain

Virus strain AHSV serotype 4 39/97 (AHSV-4) obtained from the OIE Reference Laboratory at OVI was used for this study. Fresh viral stocks were routinely generated for experimental use by infecting sub-confluent BSR cells grown in 75 cm^2 tissue culture flasks (TPP®) at a low multiplicity of infection (MOI). When total CPE was observed, cells were dislodged with a cell scraper and lysed using a 22-gauge (G) needle. The resultant virus suspensions were used as AHSV-4 stock inoculum and stored at 4°C.

2.2.3. Cell culture infections

Monolayers of BSR and KC cells grown in tissue culture dishes were infected with AHSV-4 at a MOI of 1 $TCID_{50}$/ml. After one hour of adsorption, the inoculum was removed and cells washed twice with medium supplemented with antibiotics. Cells were fed with fresh fully supplemented medium and incubated at appropriate conditions until indicated times post infection and/or inhibitor treatment.

2.2.4. Transmission electron microscopy

2.2.4.1. High-pressure freezing and freeze substitution reactions of cells

KC cells ($1.5x10^7$ cells/well) seeded in 6-well plates (Cellstar®) infected with AHSV-4 (section 2.2.3) were fixed by cryopreservation. At 12, 24 or 48 hpi cells were gently dislodged by scraping, and collected by low speed centrifugation at 2 000 rpm for 5 min using a Beckman JS5.3 rotor. A volume of approximately 0.5 µL loose cell pellet was transferred onto the Leica membrane specimen carrier. High-pressure freezing (HPF) of each

sample was done using the standard protocol (STUDER *et al.* 2001) with the LEICA EMPACT2 HPF apparatus. Each sample was overlain with the cryoprotectant 1-hexadecane, after which synchronized pressurization and cooling was delivered by the apparatus (MOOR AND RIEHLE 1968; STUDER *et al.* 2001). The resulting vitrified cell pellet was dehydrated over a period of 72 h using the LEICA AFS2 FS apparatus. The freeze-substitution (FS) reaction mixture consisted of ethanol and 1% water, and the reaction temperature was set to logarithmically increase from -90°C to 0°C within the 72 h period.

2.2.4.2. Chemical fixation and dehydration reaction of cells

BSR ($3.8x10^6$ cells/well) cells seeded in 6-well plates (Cellstar®) infected with AHSV-4 (section 2.2.3) were subject to chemical fixation. At 12, 24 or 48 hpi cells were gently dislodged by scraping, and collected by low speed centrifugation at 2 000 rpm for 5 min using a Beckman JS5.3 rotor. The cell pellet was then washed with 0.075 M sodium phosphate buffer, and fixed in 2.5% glutaraldehyde-formaldehyde solution for 1 h. The fixative solution was removed, and the pellet washed three times with 0.075 M sodium phosphate buffer. Each sample was then suspended in a solution of 1% osmium tetroxide for 1 h for secondary fixation. The resulting cell pellet was washed as before and dehydrated using a graded series of ethanol (30%, 50%, 70%, 90% and 100%) for 15 min.

2.2.4.3. Resin embedding and ultrathin sectioning of cell pellets

Following the HPF-FS or chemical fixation reaction, samples were washed three times with 100% ethanol and dislodged from the Leica membrane sample carriers or Eppendorf tubes and transferred to embedding capsules. Resin embedding for KC samples was done in a low viscosity resin, LR White resin (SPI Supplies) with the systematic replacement of ethanol with resin for 30 min. Resin embedding for BSR samples was done in a hard resin formulation, Quetol 651 epoxy resin (VAN DER MERWE AND COETZEE 1992) also with the systematic replacement of ethanol and resin for 30 min. Samples in complete resin was incubated overnight at 60°C to polymerize. Once embedded, ultrathin sections (100 nm) were made through the cell pellet with a Reichert-Jung Ultract E microtome using a Diatome diamond knife.

2.2.4.4. Staining and electron microscopy of cell sections

Embedded samples were stained for 15 min in 4% aqueous uranyl acetate (UA) and three min in Reynolds' lead citrate (REYNOLDS 1963). Sample visualization was done with a JEOL JEM-2100F field emission transmission electron microscope (FE-TEM). Single-section planes of twenty infected cells were analysed per time point.

2.2.5. Inhibition assays

The pharmacological agents LY294002 [2-(4-morpholinyl)-8-phenylchromone], Brefeldin A, and MG132 (Table 2) were used in inhibition assays to investigate the role of cellular transport pathways in AHSV replication. The aprotic solvent, dimethyl sulfoxide (DMSO; Merck) was used to reconstitute the listed drugs. The (R)-MG132 stereoisomer is a more effective inhibitor of proteolytic activities than the (S)-MG132

(MROCZKIEWICZ *et al.* 2010), and was used in this study. All stocks were stored at -20°C. For inhibition assays, pharmacological agents were applied to final concentrations (Table 2) in the media of AHSV-infected BSR cells ($3.8x10^5$ cells/well) and KC cells ($1.6x10^6$ cells/well) seeded in 24-well plates (Cellstar®). Cultures were infected, incubated with concentrations of pharmacological agents within these ranges and harvested for virus titration.

Table 2. Specifics of inhibitors used in this study

Specifics	Pharmacological agents		
	LY-294002 hydrochloride Sigma-Aldrich® cat. no. L9908	**Brefeldin A (BFA)** Sigma-Aldrich® cat. no. B6542	**MG-132 [(R)-MG132]** Sigma-Aldrich® cat. no. M8699
Mode of action	Phosphatidylinositol 3-kinase inhibitor	ER-Golgi transport inhibitor	Proteasome inhibitor
Form	Powder	Powder	Crystalline solid (powder)
Solubility	DMSO	DMSO	DMSO
Stock concentration	0.6 mM	5 mg/ml	1 mM and 50 µM
Final concentration in media	10 µM (LEE *et al.* 2005) 50 µM (ZHANG *et al.* 2010a) 100 µM (BHATTACHARYA *et al.* 2015)	0.5 µg/ml (WEI *et al.* 2008) 1 µg/ml (DONALDSON *et al.* 1990) 2.5 µg/ml (FUJIWARA *et al.* 1988)	0.5 µM (PROSCH *et al.* 2003) 5.0 µM (OKUMURA *et al.* 2008) 10 µM (BHATTACHARYA *et al.* 2015)

2.2.6. Cell viability assays

The cytotoxicity of the inhibitors was tested using colorimetric MTT (tetrazolium) assays (MOSMANN 1983). BSR cells ($6.0x10^4$ cells/well) and KC cells ($3.2x10^5$ cells/well) seeded in 96-well plates (Cellstar®) were incubated for approximately 24 h until confluent. Monolayers of cells were virus-infected or mock-infected (section 2.2.3) and treated with inhibitors for the indicated times and concentrations (section 2.3.3). Three biological repeats were done. MTT (3-(4,5-dimethylthiazol-2-yl)-2,5-diphenyl tetrazolium bromide; Merck) was dissolved in PBS at 5 mg/ml and filtered to sterilize and remove any insoluble residue in MTT solution. At times indicated below, medium containing virus and/or inhibitor was removed and MTT solution (10 µl stock solution per 100 µl fresh medium) was added to wells, and plates with BSR cells incubated at 37°C under 5% CO_2 and 90% humidity, and plates with KC cells incubated at 28°C for 3 h. MTT medium was then carefully removed from stained cells. Dimethyl sulfoxide (DMSO; Merck) was added (200 µl/well) to wells and mixed thoroughly to dissolve formazan crystals. After 20 min of incubation at 37°C to ensure all crystals were dissolved, the absorbance of each well at a wavelength of 570 nm was read on a SpectraMax i3X Paradigm (Molecular Devices) multi-well scanning spectrophotometer reader. This reading reflected the dehydrogenase activity of cells. Plates were normally read within 1 h of adding the DMSO. Absorbance readings of the blank (medium only) was subtracted from control and sample readings. The percentage cell viability was calculated using the following formulae:

$$\%\ viable\ cells\ = \frac{(absorbance_{sample} - absorbance_{blank})}{(absorbance_{control} - absorbance_{blank})} \times 100$$

MTT assays established inhibitor concentration ranges in which 60-90% of cells remained *via*ble.

2.2.7. Virus titration

The infectious virus titre was determined by median tissue culture infectious dose ($TCID_{50}$) assays. Serial 10-fold dilutions of samples were made in MEM supplemented with antibiotics and antifungals. For each sample, 100 µl of each virus or virus-free diluent was placed in six or four replicate wells of a 96-well plate (Cellstar®). A 100 µl cell suspension containing approximately $4.5x10^4$ BSR cells was then added to each well and incubated at 37°C under 5% CO2 and 90% humidity. Cells were observed daily and when control cells sloughed or at 3 days, monolayers were scored for CPE by light microscopy (Olympus CKX41). Signs of AHSV-induced CPE such as an area of clearing in the monolayer sheet of cells was recorded and the 50% tissue culture infectious dose per millilitre ($TCID_{50}$/ml) calculated using the Reed-Muench method (REED AND MUENCH 1938). Three biological repeats were done, and titres expressed as $log_{10}TCID_{50}$/ml were compared for statically significant differences by paired T-tests. The $TCID_{50}$/ml of virus stocks ranged from 8.0 - 8.3 $log_{10}TCID_{50}$/ml. Fresh virus stocks were generated when virus titres dropped below this range.

2.2.8. Protein resolution by polyacrylamide gel electrophoresis

Mock- or AHSV-infected BSR cells ($3.8x10^5$ cells/well) or KC cells ($1.6x10^6$ cells/well) seeded in 24-well plates (Cellstar®) untreated or treated with inhibitors were harvested directly on the plate by aspirating the medium, washing the cells with PBS, and adding 20 µl RIPA lysis buffer. Syringe rubbers were used to dislodge cells, which were incubated at 4°C for 30 min with shaking prior to being stored at -20°C or loaded onto sodium dodecyl sulphate polyacrylamide gels. Protein samples were resuspended in the appropriate amount of 6x protein solvent buffer (PSB) and boiled for 5 min at 90°C before loading. Polyacrylamide gels cast with the Invitrogen™ SureCast™ Gel Handcast System comprised of a stacking gel (5% Acrylamide-bis ready-to-use solution 30% (37.5:1) (Merck), 0.125 M Tris-HCl [pH 6.8], 0.1% SDS, 0.008% TEMED and 0.08% Ammonium persulfate) and a separating gel (12% Acrylamide-bis ready-to-use solution 30% (37.5:1) (Merck), 0.375 M Tris-HCl [pH 8.8], 0.1% SDS, 0.008% TEMED and 0.08% Ammonium persulfate). These gels were used to condense and separate proteins by electrophoresis for 1.5 h at 130 V and 400 mA in TGS buffer using the Invitrogen™ Vertical Gel System. PageRuler™ (Thermo Fisher Scientific) was used as molecular weight marker.

2.2.9. Western blot analysis and antibodies

Resolved proteins were electroblotted onto Amersham™ Protran® 0.45 µm nitrocellulose membrane (GE Healthcare Life Sciences) for 1 h at 100 V and 400 mA in transfer buffer using the Cleaver Scientific omniPAGE Blot Mini System. Gels were stained by Coomassie brilliant blue solution (0.125% Coomassie blue, 50% methanol, 10% acetic acid) for 20 min and left overnight in destain solution (5% methanol, 5% acetic acid) to

confirm protein separation and transfer. Membranes were incubated in blocking solution [5% (w/v) milk powder in PBS] for one hour at room temperature (25°C) with gentle agitation to limit non-specific antibody binding. Primary antibodies (Table 3) diluted in 1% (w/v) milk powder in PBS were incubated overnight with agitation at room temperature (25°C). Membranes were rinsed 3 times for a duration of 5 min each in wash buffer. Depending on the binding affinity (Table 3), secondary labelling was then done by horseradish peroxidase (HRP) conjugated Protein A (Calbiochem®) or anti-mouse immunoglobulin conjugated HRP (Dako) diluted in 1% (w/v) milk powder in PBS for 1 h with agitation at room temperature (25°C). To wash off unbound secondary labelling molecules, membranes were rinsed as before in wash buffer and once in PBS. Colorimetric detection of proteins was done by developing membranes in substrate solution (60 mg 4-chloro-1-naphtol in 20 ml ice cold methanol and 60 µl hydrogen peroxide in 100 ml PBS) in the dark until sufficient signal was observed. Developed membranes were then washed with dH_2O and visualised for analysis with the GelDoc™ XR+ Imaging System.

Table 3. Antibodies used in this study

Specifics	Primary antibody		
	Polyclonal anti-NS2 IgG produced in rabbit (UITENWEERDE *et al.* 1995)	**Monoclonal anti-β-actin IgG2a produced in mouse (Sigma-Aldrich® cat. no. A2228)**	**Monoclonal anti-PML IgG1 produced in mouse (Sigma-Aldrich® cat. no. P6746)**
Immunogen	Full length NS2 protein.	Modified β-cytoplasmic actin N-terminal peptide.	Recombinant full-length human PML (promyelocytic leukemia) protein.
Species reactivity	AHSV NS2	Canine, guinea pig, rabbit, bovine, chicken, rat, sheep, carp, *Drosophila*, *Hirudo medicinalis*, pig, cat, mouse, human	Mouse, hamster, human
Dilution of primary antibody used	1:500	1:200	4µg/mL
Molecular weight of detected antigen	42 kDa in BSR and KC cells	42 kDa in BSR cells	60 kDa in KC cells
Protein A binding affinity (1:10 000)	++++	++++	+
Anti-mouse immunoglobulin binding affinity (1:1000)	+++	++++	++++

2.3. Results

2.3.1 Ultrastructural investigation of AHSV particle localisation in mammalian and insect cell culture

There is limited information available regarding the series of events that lead to the release of AHSV from infected cells. To investigate the final stage of AHSV replication, the initial focus was on documenting the intracellular location of mature particles in both mammalian (BSR) and insect (KC) cells. Care was taken to record only particles measuring 55 to 70 nm diameter (OELLERMANN *et al.* 1970; ROY *et al.* 1994) so as not to mistake core particles for full virus particles. Specific time points representative of early, intermediate, and late times post infection were selected for ultrastructural investigation by transmission electron microscopy.

High-pressure freezing was the fixation method of choice, as it allows for improved structural preservation of specifically membranous components, and does not introduce significant cellular alterations (TOMOVA 2013). Cryofixed cell pellets were dehydrated by freeze-substitution and subsequently embedded in resin for sectioning and visualisation by TEM. AHSV replication was confirmed by the detection of any one of the following structures by high resolution TEM imaging: viral inclusion bodies (VIBs), virus tubules or crystals, virus core particles or full virus particles in a cell.

2.3.1.1. Ultrastructural characterisation of AHSV particle localisation in BSR cells

AHSV-infected BSR cells were examined, specifically the cytoplasm of cells, to discern the intracellular location of virus particles. At 12 hpi (Fig 4) infected cells showed typical BSR morphology, i.e. amorphous shapes, intact plasma membranes and contact between neighbouring cells (Fig 4 A). It was presumed from these observations that at 12 hpi virus-infected BSR cells were able to sustain cellular activity such as trafficking. At this time, the infected status of a cell was usually confirmed by the presence of mature virus particles, as other hallmarks of infection described above (e.g. VIBs, tubules and crystals) were not prevalent yet. Single or multiple AHSV particles were frequently observed inside membrane-bound cytoplasmic structures, often in proximity (> 0.1 µm) to the plasma membrane (Fig 4 B, C, D). Dispersed single virus particles, particles in pairs, or aggregates consisting of multiple (≥ 3) virus particles were at times observed free within the cytoplasm (Fig 4 E), or associated with the cytoplasmic face of smooth surface vesicles (Fig 4 F). Intracellular membrane-bound cytoplasmic structures larger than 100 nm are typically referred to as vacuoles, and smaller than 100 nm are referred to as vesicles (DAVIDSON 1995). Unless otherwise specified, all membrane-bound cytoplasmic structures were referred to as vesicles in this study.

At 24 hpi (Fig 5) AHSV-infected cells still showed typical BSR cell morphology (Fig 5 A). At this time point virus particles were mainly observed in the cytoplasm as single particles, pairs, and aggregates in proximity to the plasma membrane (Fig 5 B, C). Multiple virus particles were often observed on the cytoplasmic face of vesicles (Fig 5 E), and a few particles on occasion within vesicles (Fig 5 F). The hallmarks of infection such as tubules or crystals were prevalent (not shown) and confirmed the infected status of cells. Extracellular particles could also be observed at this time (Fig 5 D). Compared to 12 hpi where nearly all viruses were

present within vesicles, at 24 hpi virus particles were more often observed as cytoplasmic aggregates between vesicles (Fig 5 D) or within no proximity to vesicles (Fig 5 C).

By 48 hpi (Fig 6) cell death was markedly increased in AHSV-infected cells. These cells exhibited cell rounding, condensed granular cytoplasm, plasma membrane blebbing, and/or multiple vesicle and lysosome-like structures (Fig 6 A, B). Only cells of which the cytoplasmic boundaries were apparent and thus presumed to still sustain activities such as trafficking were used for subsequent analysis. Virus particles were most frequently observed in the cytoplasm as single particles, pairs or aggregates in proximity to the plasma membrane (Fig 6 C). Many virus particles were also observed on the cytoplasmic face of vesicles, or associated with membrane-like fragments and disrupted vesicles (Fig D). Viruses were sometimes seen within small vesicles (Fig 6 C, E-F). These vesicles mostly contained only one or two viruses, and were frequently found at or in proximity to the plasma membrane. Viral tubules and crystals were frequently observed in the cytoplasm (Fig 6 F). Compared to 24 hpi, the size of virus aggregates seemed smaller at 48 hpi, and virus particles associated with intracellular membranous-like structures were more common at this time point than at earlier times. Extracellular particles were also observed at 48 hpi.

As not many records of AHSV release exist, efforts were made to document virus release (Fig 7). Orbivirus release from mammalian cells has previously been described to result both from a locally disrupted plasma membrane, and from a budding-like mechanism (HYATT *et al.* 1989; STOLTZ *et al.* 1996; CELMA AND ROY 2011; VENTER *et al.* 2014). Correspondingly, in this study AHSV particles were observed in BSR cells in very close proximity to a locally disrupted membrane (Fig 7 A), and within a budding-like structure (Fig 7 B). However, other types of events not previously described were also observed here. At 24 hpi, a group of five particles associated with cellular-derived material appeared to have separated from the plasma membrane (Fig 7 C). At 48 hpi, two incidents where two particles were present together within the same plasma membrane protrusion were observed in close proximity to one another (Fig 7 D). A single virus particle inside a cell-derived membranous structure was observed at 48 hpi in the extracellular space in close proximity to the plasma membrane (Fig 7 E, F).

Virus particles were observed in similar intracellular locations at early, intermediate and late times post infection in BSR cells, however from the initial screening of the samples it seemed as if the frequency at which particles were observed e.g. within vesicles, associated with membranous structures or free in the cytoplasm differed at the different time points. To describe this in more detail, twenty AHSV-infected BSR cells were selected from the 12 hpi, 24 hpi and 48 hpi samples, and each of the cells scanned systematically to quantify the occurrence of the different virus particle distributions. The cytoplasm of each cell was examined at different magnifications to determine the total number of virions and intracellular location of each virion in that sample. Specific criteria were established (Figs 8-10) according to which the different types of distributions were categorised, and these were then recorded per cell for twenty cells.

Virus particles were designated as being intra-vesicular (VP-Ves) (Fig 8) when particles were separated by a lipid bilayer from the cytosol and were contained inside a vesicle/vesicle-like structure (Fig 8 A, C). If the boundaries of such structures were not visible, particles in a distinctly less dense environment were also considered intra-vesicular (Fig 8 E). The number of VP-Ves particles were counted as illustrated (Fig 8 B, D, F) and the total number of viruses inside vesicles recorded for every cell. The number of vesicles per cell containing only one virus, versus more than one virus particle, was also recorded. For example, in Fig 8 B a total of 11 VP-Ves particles were identified, and there were two vesicles recorded which both contained multiple (> 1) particles.

Membrane-associated virus particle distributions (VP-Mem) (Fig 9) were designated when particles were in contact with the cytoplasmic face of vesicles (Fig 9 A; VP-Mem^{1}), with disrupted vesicle/vesicle-like structures (Fig 9 C; VP-Mem^{2}), with membrane/membrane-like fragments (Fig 9 E; VP-Mem^{3}), or with the plasma membrane (VP-mem^{4}; Fig 9 G). If direct contact could not be established, particles in very close proximity to membrane structures were also considered VP-Mem particles (Fig 9 I; VP-Mem^{5}). The number of VP-Mem particles were counted as illustrated (Fig 9 B, D, F, H, J) and the total number of viruses showing an intracellular membrane association recorded for every cell. The number of membranous structures per cell associated with virions, and whether the association involved one or multiple (>1) particles, was also recorded. For example, in Fig 9 B a total of 4 VP-Mem particles were counted (4x VP-Mem^{1}) and this micrograph shows examples of membrane structures associated with a single particle and with multiple particles.

A cytoplasmic virus particle distribution (VP-Cyt) (Fig 10) was designated when a single virion (VP-Cyt^{1}), pairs (VP-Cyt^{2}), or aggregates (VP-Cyt^{3}) of virus particles occurred freely in the cytoplasm (Fig 10 A). Three or more particles in close contact which formed part of a distinct grouping in the cytoplasm were considered an aggregate. The number of VP-Cyt particles were counted as illustrated (Fig 10 B) and the total recorded for every cell. The number of incidents of a single / pair of viruses and the number of aggregates per cell was also noted. For example, in Fig 10 A there was a total of 40 VP-Cyt particles, and this micrograph had a single virion, one virus pair and three aggregates in the cytoplasm.

The data recorded in this fashion for AHSV-infected BRS cells at 12, 24 and 48 hpi is summarised in Tables 3-5. The percentage of viruses localising within vesicles, associated with membrane components or purely cytoplasmic was calculated for each cell. To allow comparison across time points these values were averaged across all 20 cells, or per cell (but then only considering cells in which that specific type of distribution had been recorded). The percentage of the 20 cells exhibiting a specific particle distribution, and the percentage exhibiting a specific type of distribution at least once, was also determined.

At 12 hpi (Table 4), 72% of the total number of virus particles identified were present inside vesicles (VP-Ves), while 26% distributed in the cytoplasm (VP-Cyt) and only 2% associated with membranous structures (VP-Mem). VP-Ves particles occurred in all twenty cells, while both VP-Mem and VP-Cyt particle distributions occurred in only 25% of cells, even though more particles in total were recorded as being cytoplasmic compared to membrane-associated. This was attributed to the large number of viruses present per aggregate in three of the cells at this time post infection (Table 4; sample 2, 6 and 9), while membrane fragments were usually associated with only a single virus. On average, 85% of particles were inside vesicles, 12% were free in the cytoplasm, and only 3% were in membrane association across all 20 cells. The majority of virus particles detected at 12 hpi were therefore present inside vesicle-type structures, and most vesicles contained multiple particles.

At 24 hpi (Table 5), 91% of the total number of virus particles were distributed freely in the cytoplasm, 8% into vesicles and only 1% associated with membranous structures. VP-Cyt distributions were recorded in 95% of cells, while 60% and 30% of cells showed incidents of VP-Ves and VP-Mem distributions respectively. VP-Cyt distributions were characterised by virus particles aggregates, rather than by the presence of single virions or pairs of particles. Across all 20 cells, an average of 83% of particles were in the cytoplasm, while 15% and 2% of particles were on average inside vesicles or membrane-associated. Compared to 12 hpi, more cells showed multiple types of particle distribution profiles at this time post infection. However, at 24 hpi particles were predominantly present as virus aggregates in the cytoplasm.

At 48 hpi (Table 6), 70% of the total number of virus particles were distributed in the cytoplasm, while 27% were associated with membranous structures, and only 3% were inside vesicles. An average of 69% of particles recorded across 20 cells were in the cytoplasm, while averages of 27% and 3% of particles were either membrane-associated or inside vesicles. All cells also showed VP-Cyt distributions, and 80% and 55% showed VP-Mem and VP-Ves distributions respectively. Even though incidents of VP-Ves distributions were recorded for half of the total number cells, the percentage of intra-vesicular distributed virus particles of was very low. This was explained by the frequent detection of vesicles containing a single virion rather than multiple particles at this time post infection.

Compared to earlier time points, VP-Mem incidents were the highest at this time point with many of the cells showing membranous components associated with either single or multiple particles. A decrease was found from 24 hpi to 48 hpi in the number of total virus particles in aggregates (from 73% to 45%), in the average incidence of aggregates in cells (from 95% to 75%), and in the average size of aggregates i.e. the average number of virus particles in an aggregate (from 22 to 18). The average number of aggregates across 20 cells remained 3 between 24 hpi and 48 hpi. The average size of aggregates therefore appears to be smaller at 48 hpi. Viruses were therefore predominantly present in the cytoplasm at 48 hpi as single virions, pairs of viruses, or smaller aggregates.

To summarise, the intracellular distribution profile of virus particles appeared to change over time in infected BSR cells (Fig 11). At 12 hpi most of the particles were inside vesicles, at 24 hpi the bulk of the particles were free in the cytoplasm, and by 48 hpi most of the particles were still cytoplasmic but with a larger component showing a membrane component association (Fig 11). This was subsequently followed up by an investigation into the localisation of virus particles in insect cells.

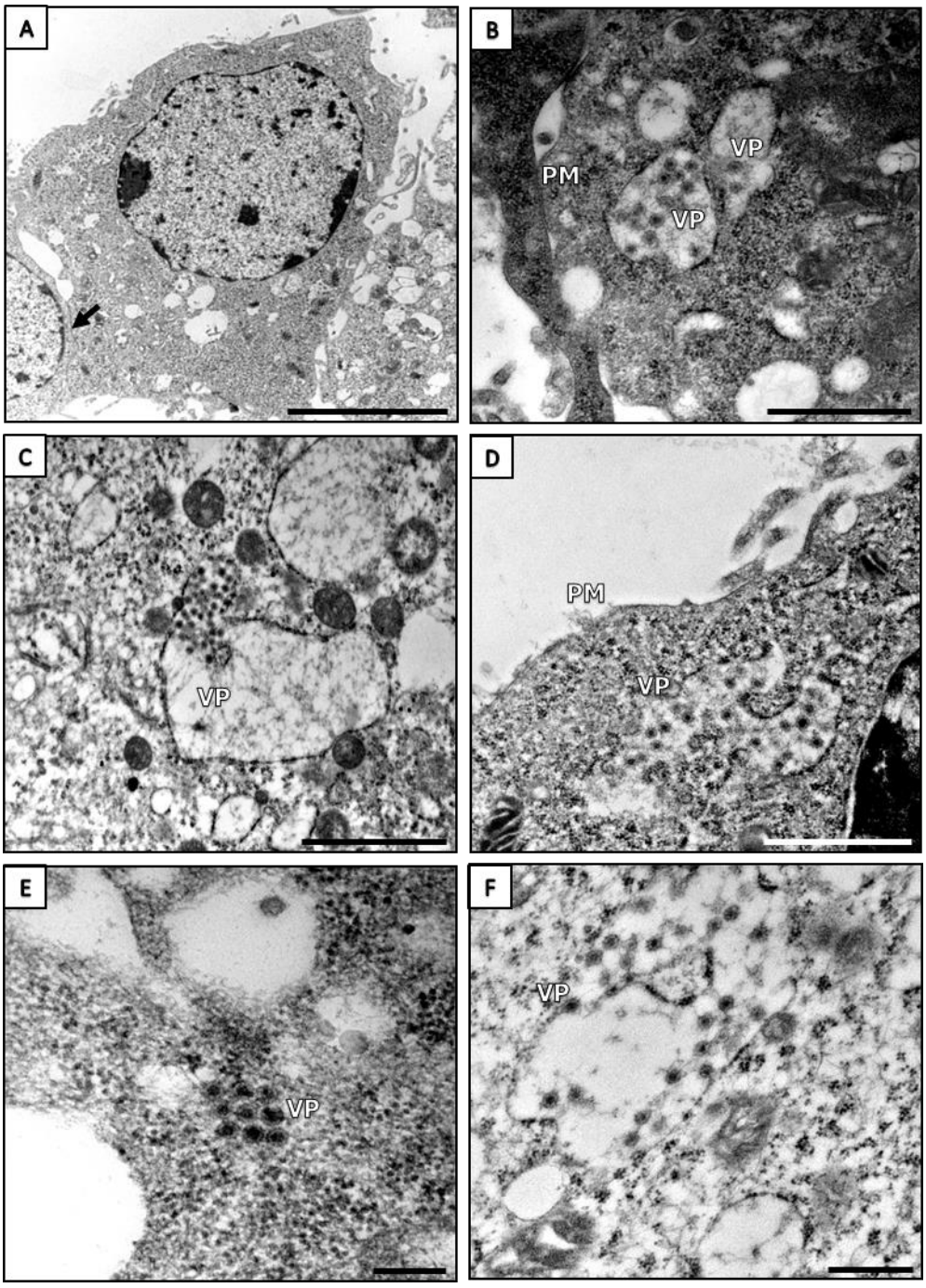

Figure 4. TEM micrographs of AHSV-infected BSR cells at 12 hpi. (A) AHSV-infected cell exhibiting typical BSR morphology with contact between neighbouring cells indicated by arrow. (B-D) Mature ~ 70 nm spherical virus particles (VP) were present inside vesicle-like structures, often in proximity to the plasma membrane (PM). (E) Free virus particles were present within the cytoplasm. (F) Virus particles observed in association with the cytoplasmic face of intracellular membranes. Scale bars, 5 µm (A); 2 µm (C); 1 µm (D); 0,5 µm (B, F); 0,2 µm (E).

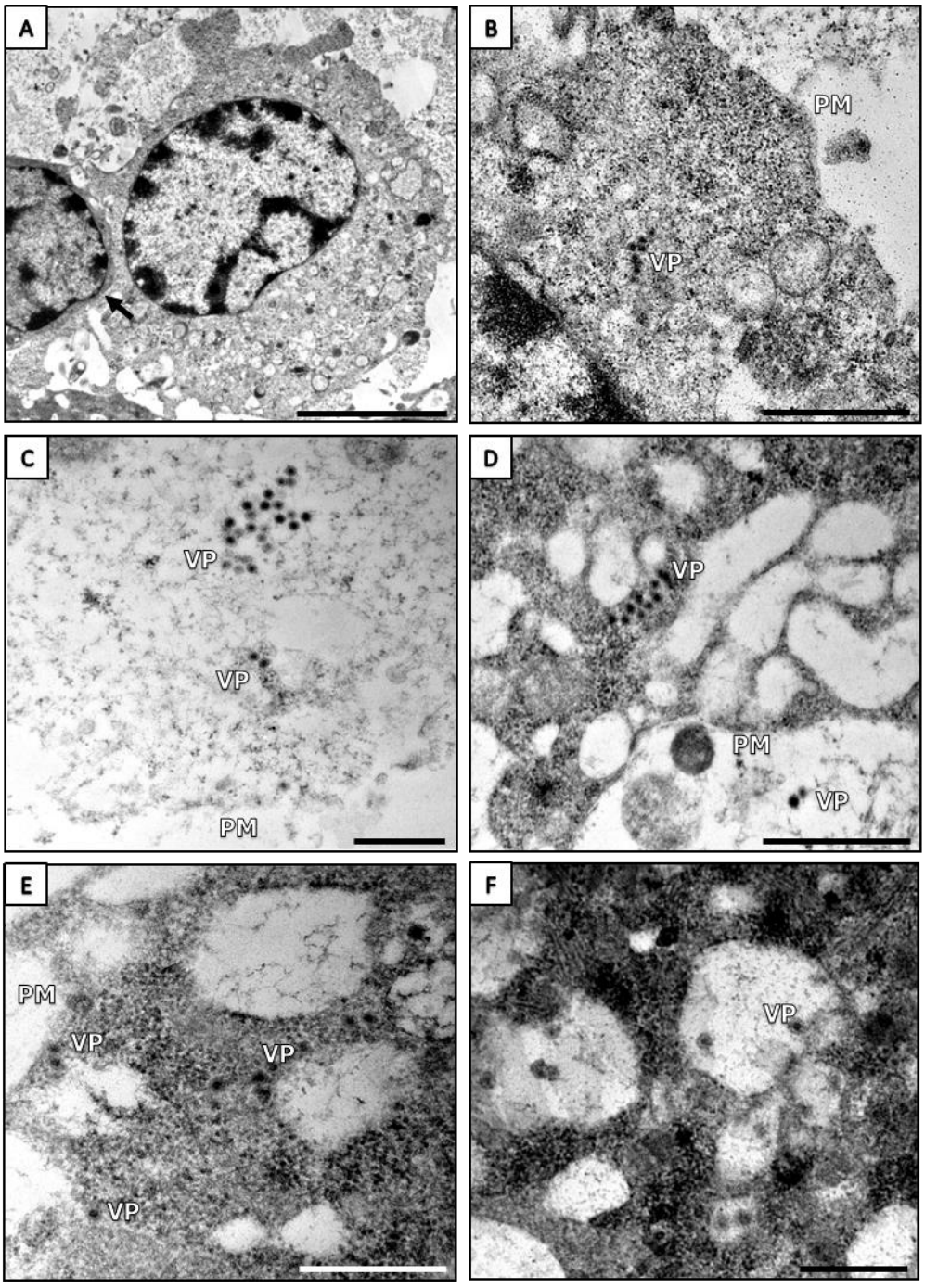

Figure 5. TEM micrographs of AHSV-infected BSR cells at 24 hpi. (A) AHSV-infected cell exhibiting typical BSR morphology, with contact between neighbouring cells indicated by arrow. (B-F) Observation of intracellular mature ~ 70 nm spherical virus particles (VP). (B-D) Viruses were freely distributed in the cytoplasm, (E) in association with the cytoplasmic face of vesicles in proximity to the plasma membrane (PM) or (F) inside vesicles. (D) Virus particles were occasionally detected outside the plasma membrane. Scale bars, 5 µm (A); 1 µm (B); 0,5 µm (C-F).

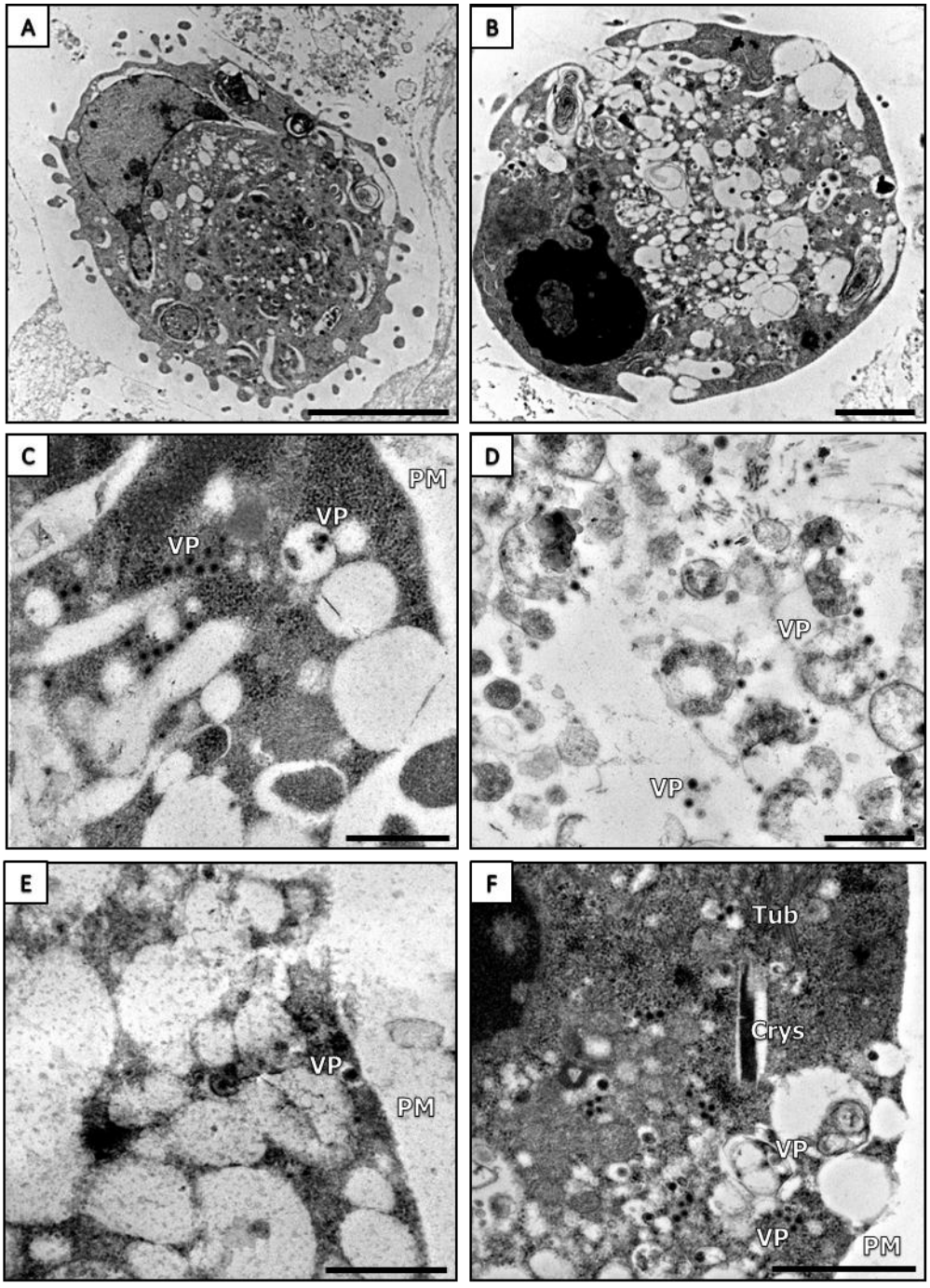

Figure 6. TEM micrographs of AHSV-infected BSR cells at 48 hpi. (A-B) AHSV-infected BSR cells displaying condensed granular cytoplasm, irregular cell membrane protrusions, and multiple cytoplasmic vesicle- and lysosome-like structures. (C-F) Mature ~ 70 nm spherical virus particles (VP) were frequently observed in infected cells. (F) Observation of virus-specific NS1 tubules (Tub) and VP7 crystals (Crys). Plasma membrane was abbreviated PM. Scale bars, 5 µm (A); 2 µm (B); 1 µm (F); 0,5 µm (C, D, E).

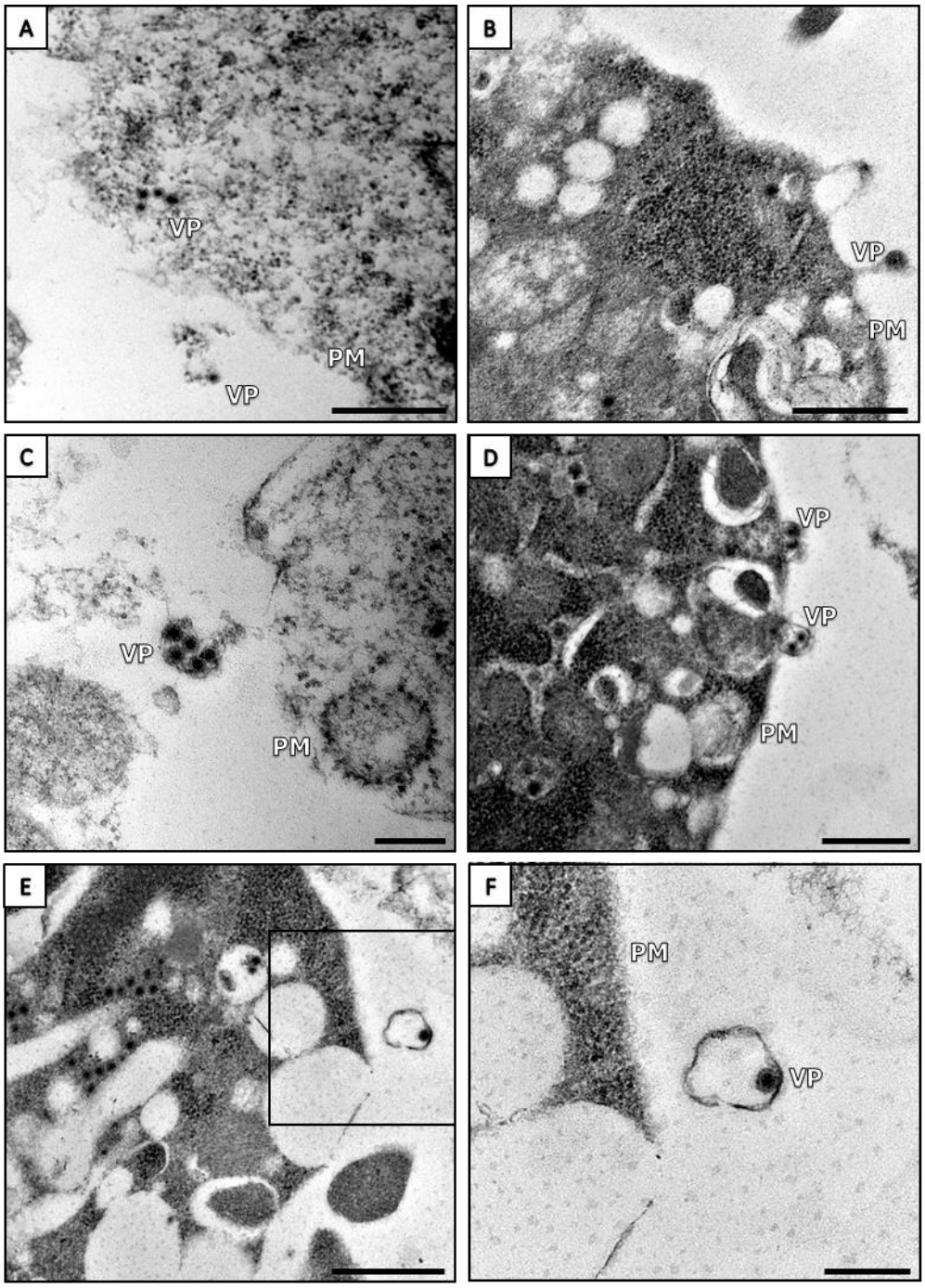

Figure 7. TEM micrographs depicting AHSV particles at the plasma membrane of virus-infected BSR cells. (A) A cell at 24 hpi with four intracellular virus particles and one released particle in close proximity to locally disrupted plasma membrane (PM). (B) A single virus particle inside a budding-type structure at 48 hpi. (C) Multiple virus particles released at 24 hpi and associated with membranous structure from plasma membrane. (D) Two pairs of particles at 48 hpi inside plasma membrane protrusion structures. (E) Released virus particle inside intact vesicle. (F) Enlargement of demarcated area from (E). Scale bars, 0,5 µm (A, B, D, E); 0,2 µm (C, F).

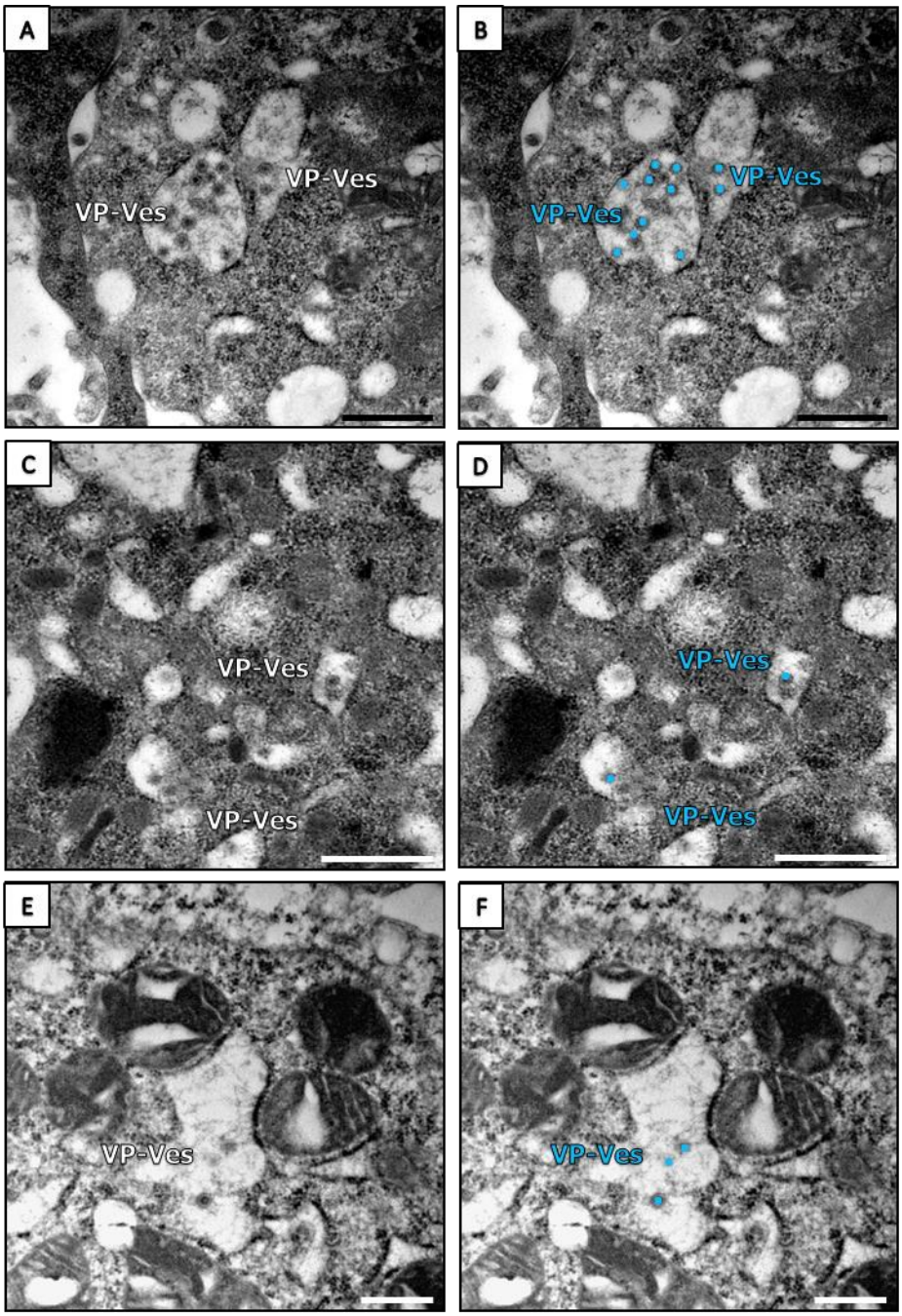

Figure 8. Quantification of intra-vesicular viruses. (A, C, E) TEM micrograph of AHSV-infected BSR cells. (B, D, F) Duplicate images of micrographs in left panel. Blue bullets illustrate how virus particles inside vesicles (VP-Ves) were counted. (A) Multiple (> 1) virus particles inside vesicles in BSR cell at 12 hpi. (C) Single virus particles inside vesicles at 24 hpi. (E) Virus particles designated as VP-Ves due to its presence in a less dense cytoplasmic environment. Scale bar, 1 µm (C-D); 0,5 µm (A-B, E-F).

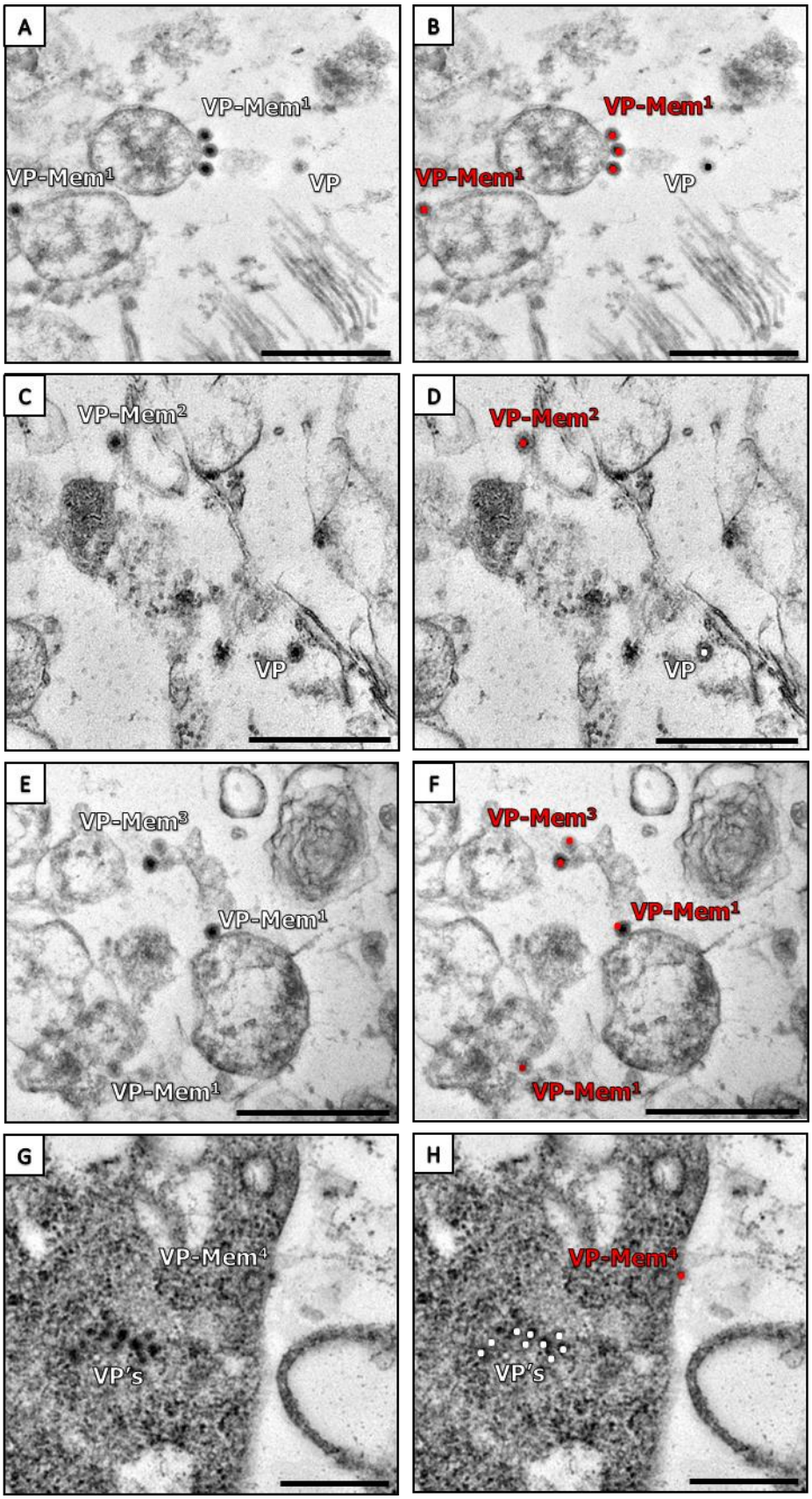
A
VP-Mem1
VP-Mem1
VP
B
VP-Mem1
VP-Mem1
VP
C
VP-Mem2
VP
D
VP-Mem2
VP
E
VP-Mem3
VP-Mem1
VP-Mem1
F
VP-Mem3
VP-Mem1
VP-Mem1
G
VP-Mem4
VP's
H
VP-Mem4
VP's

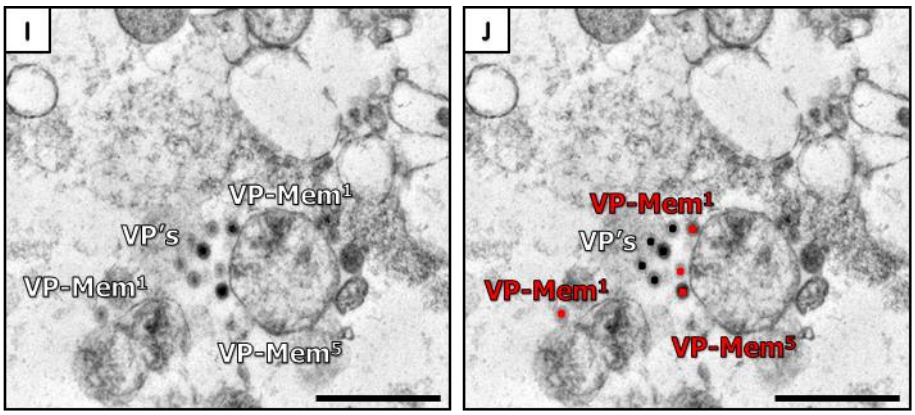

Figure 9. Quantification of membrane-associated viruses. (A, C, E, G, I) TEM micrographs of AHSV-infected BSR cells at 24 hpi (G) and 48 hpi (A, C, E, I). (B, D, F, H, J) Duplicate images of micrographs in left panel. Red bullets illustrate how particles associated with membrane structures (VP-Mem) were counted. (A) Virus particles (VP) on the cytoplasmic face of vesicles (VP-Mem^1), (C) disrupted vesicles (VP-Mem^2), (E) membrane fragments (VP-Mem^3), and (G) embedded in the plasma membrane (VP-Mem^4). (I) Particles in close proximity to vesicle (VP-Mem^5). Scale bars, 0,5 µm (A-J).

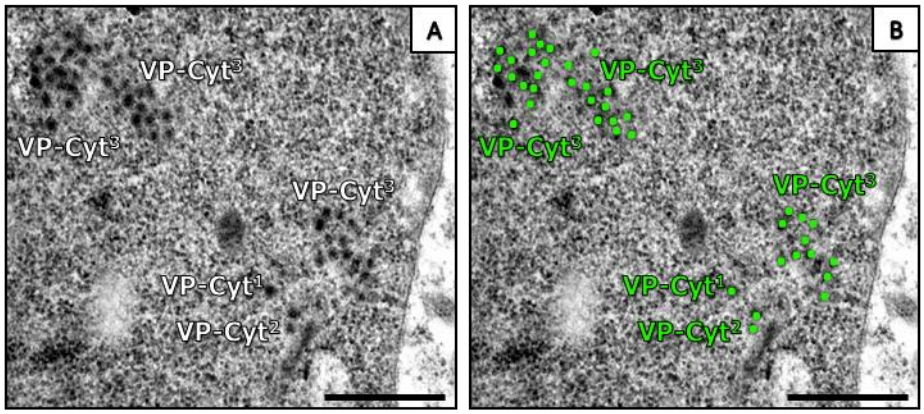

Figure 10. Quantification of cytoplasmic viruses. (A) TEM micrographs of a AHSV-infected BSR cell at 24 hpi. (B) Duplicate of the image on the left, with green bullets indicating how cytoplasmic viruses (VP-Cyt) were counted. (A) Virus particles occurred freely in the cytoplasm as single virions (VP-Cyt^1), pairs (VP-Cyt^2), and aggregates (VP-Cyt^3). Scale bars, 0,5 µm (A-B).

Table 4. AHSV distribution profile at 12 hpi in BSR cells

Cell sample	Total number of virus particles	Intra-vesicular (VP-Ves)				Membrane-associated (VP-Mem)				Cytoplasmic (VP-Cyt)				
		Number of virus particles in cell inside vesicles	Percentage of total particles in cell inside vesicles	Number of vesicles in cell containing one particle	Number of vesicles in cell containing 2 or more particles	Number of membrane-associated virus particles in cell	Percentage of total virus particles in cell showing membrane association	Number of membranous structures in cell associated with a single particle	Number of membranous structures in cell associated with 2 or more particles	Number of virus particles free in cytoplasm in cell	Percentage of total particles in cell free in cytoplasm	Number of cytoplasmic particles in cell distributed individually or in pairs	Number of cytoplasmic particles in cell forming part of aggregates	Number of aggregates in cytoplasm of cell
1	**35**	35	100%		5		0%				0%			
2	**77**	1	1%	1			0%			76	99%		76	1
3	**7**	7	100%	1	2		0%				0%			
4	**9**	9	100%	1	2		0%				0%			
5	**7**	7	100%	3	2		0%				0%			
6	**31**	1	3%	1		2	6%		1	28	90%	2	26	4
7	**20**	20	100%	1	2		0%				0%			
8	**15**	15	100%	1	1		0%				0%			
9	**46**	21	46%	5	2	4	9%	1	1	21	46%	7	14	2
10	**40**	40	100%		5		0%				0%			
11	**37**	37	100%	2	4		0%				0%			
12	**22**	22	100%	7	5		0%				0%			
13	**22**	22	100%		2		0%				0%			
14	**47**	47	100%	3	5		0%				0%			
15	**23**	20	87%	7	4	2	9%	2		1	4%	1		
16	**22**	19	86%		1	1	5%	1		2	9%	2		
17	**23**	23	100%		1		0%				0%			
18	**4**	4	100%	1	1		0%				0%			
19	**3**	2	67%		1	1	33%	1			0%			
20	**8**	8	100%	5	1		0%				0%			
TOTAL	**498**	360	-	39	46	10	-	5	2	128	-	12	116	7
Percentage of total viruses	**-**	72,29%	-	7,83%	9,24%	2,01%	-	1,00%	0,40%	25,70%	-	2,41%	23,29%	-
Percentage of cells displaying event	**-**	100%	-	-	-	25%	-	-	-	25%	-	-	-	-
Percentage of cells with ≥ 1 incidence	**-**	-	-	70%	90%	-	-	20%	10%	-	-	20%	15%	15%
AVG (across all 20 cells)	**24,90**	18,00	84,51%	1,95	2,30	0,50	3,09%	0,25	0,10	6,40	12,41%	0,60	5,80	0,35
SD (across all 20 cells)	**18,37**	13,60	31,40%	2,31	1,72	1,05	7,73%	0,55	0,31	18,04	29,92%	1,64	17,73	0,99
AVG (only cells displaying event)	**24,90**	18,00	84,51%	2,79	2,56	2,00	12,34%	1,25	1,00	25,60	49,62%	3,00	38,67	2,33
SD (only cells displaying event)	**18,37**	13,60	31,40%	2,29	1,62	1,22	11,86%	0,50	0,00	30,53	44,08%	2,71	32,88	1,53

Table 5. AHSV distribution profile at 24 hpi in BSR cells

Cell sample	Total number of virus particles	Intra-vesicular (VP-Ves)				Membrane-associated (VP-Mem)				Cytoplasmic (VP-Cyt)				
		Number of virus particles in cell inside vesicles	Percentage of total particles in cell inside vesicles	Number of vesicles in cell containing one particle	Number of vesicles in cell containing 2 or more particles	Number of membrane-associated virus particles in cell	Percentage of total virus particles in cell showing membrane association	Number of membranous structures in cell associated with a single particle	Number of membranous structures in cell associated with 2 or more particles	Number of virus particles free in cytoplasm in cell	Percentage of total particles in cell free in cytoplasm	Number of cytoplasmic particles in cell distributed individually or in pairs	Number of cytoplasmic particles in cell forming part of aggregates	Number of aggregates in cytoplasm of cell
1	**24**	2	8%	2		1	4%	1		21	88%		21	4
2	**39**		0%			1	3%	1		38	97%	1	37	5
3	**81**	9	11%	1	3	1	1%	1		71	88%	1	70	7
4	**18**	12	67%	2	3		0%			6	33%	2	4	1
5	**36**	2	6%	2		1	3%			33	92%		33	1
6	**14**	1	7%	1	1		0%			13	93%	5	8	1
7	**9**	2	22%		1		0%			7	78%	3	4	1
8	**9**	2	22%		1	1	11%	1		6	67%	2	4	1
9	**52**	1	2%	1			0%			51	98%	21	30	7
10	**23**	4	17%		1		0%			19	83%		19	4
11	**15**	5	33%	3	1		0%			10	67%	4	6	1
12	**22**		0%			2	9%		1	20	91%	1	19	4
13	**137**		0%				0%			137	100%	60	77	8
14	**21**		0%				0%			21	100%	2	19	4
15	**59**		0%				0%			59	100%	7	52	8
16	**19**		0%				0%			19	100%		19	5
17	**4**	4	100%		1		0%				0%			
18	**7**		0%				0%			7	100%		7	2
19	**3**		0%				0%			3	100%		3	1
20	**11**	1	9%	1			0%			10	91%		10	1
TOTAL	**603**	45	-	13	12	7	-	4	1	551	-	109	442	66
Percentage of total viruses	**-**	7,46%	-	2,16%	1,99%	1,16%	-	0,66%	0,17%	91,38%	-	18,08%	73,30%	-
Percentage of cells displaying event	**-**	60%	-	-	-	30%	-	-	-	95%	-	-	-	-
Percentage of cells with ≥ 1 incidence	**-**		-	40%	40%	-	-	20%	5%	-	-	60%	95%	95%
AVG (across all 20 cells)	**30,15**	2,25	15,25%	0,65	0,60	0,35	1,55%	0,21	0,05	27,55	83,20%	5,45	22,10	3,30
SD (across all 20 cells)	**32,15**	3,24	25,71%	0,93	0,94	0,59	3,17%	0,42	0,22	32,28	25,57%	13,69	22,14	2,66
AVG (only cells displaying event)	**30,15**	3,75	25,42%	1,63	1,50	1,17	5,16%	1,00	1,00	29,00	87,58%	9,08	23,26	3,47
SD (only cells displaying event)	**32,15**	3,47	29,32%	0,74	0,93	0,408	3,99%	0,00	n/A	32,49	16,89%	16,96	22,11	2,61

Table 6. AHSV distribution profile at 48 hpi in BSR cells

Cell sample	Total number of virus particles	Intra-vesicular (VP-Ves)				Membrane-associated (VP-Mem)				Cytoplasmic (VP-Cyt)				
		Number of virus particles in cell inside vesicles	Percentage of total particles in cell inside vesicles	Number of vesicles in cell containing one particle	Number of vesicles in cell containing 2 or more particles	Number of membrane-associated virus particles in cell	Percentage of total virus particles in cell showing membrane association	Number of membranous structures in cell associated with a single particle	Number of membranous structures in cell associated with 2 or more particles	Number of virus particles free in cytoplasm in cell	Percentage of total particles in cell free in cytoplasm	Number of cytoplasmic particles in cell distributed individually or in pairs	Number of cytoplasmic particles in cell forming part of aggregates	Number of aggregates in cytoplasm of cell
1	**40**	1	3%	1		24	60%	17	1	15	38%	9	6	1
2	**129**	5	4%	1	1	85	66%	28	21	39	30%	24	15	4
3	**19**		0%			14	74%	4	2	5	26%	5		
4	**100**	3	3%	3			0%			97	97%	13	84	14
5	**40**	2	5%	2			0%			38	95%	6	32	6
6	**7**		0%			3	43%	1	1	4	57%	4		
7	**34**	2	6%	2		21	62%	9	4	11	32%	8	3	1
8	**36**		0%			12	33%	9	2	24	67%	10	14	3
9	**10**		0%			1	10%	1		9	90%	6	3	1
10	**60**		0%			7	12%	4	1	53	88%	13	40	7
11	**52**	5	10%	3	1	4	8%		1	43	83%	9	34	6
12	**33**		0%			2	6%		1	31	94%	3	28	3
13	**30**	1	3%	1		3	10%	1	1	26	87%	26		
14	**10**		0%			8	80%	6	1	2	20%	2		
15	**14**	2	14%	2			0%			12	86%	2	10	2
16	**16**		0%	3	1		0%			16	100%	16		
17	**9**	1	11%	1		3	33%	3		5	56%	2	3	1
18	**109**	1	1%	1		21	19%	13	3	87	80%	30	57	12
19	**46**		0%			8	17%	6	1	38	83%	8	30	6
20	**8**	1	13%			1	13%	1		6	75%	3	3	1
TOTAL	**802**	24	-	20	3	217	-	103	40	561	-	199	362	68
Percentage of total viruses	**-**	2,99%	-	2,49%	0,37%	27,06%	-	12,84%	4,99%	69,95%	-	24,81%	45,14%	-
Percentage of cells displaying event	**-**	55%	-	-	-	80%	-	-	-	100%	-	-	-	-
Percentage of cells with ≥ 1 incidence	**-**	-	-	55%	15%	-	-	70%	65%	-	-	100%	75%	75%
AVG (across all 20 cells)	**40,10**	1,20	3,60%	1,00	0,15	10,85	27,27%	5,15	2,00	28,05	69,13%	9,95	18,10	3,40
SD (across all 20 cells)	**35,27**	1,58	4,69%	1,12	0,37	19,05	27,18%	7,22	4,60	26,61	26,52%	8,27	22,72	4,03
AVG (only cells displaying event)	**40,10**	2,18	6,55%	1,82	1,00	13,56	34,09%	7,36	3,08	28,05	69,13%	9,95	24,13	4,53
SD (only cells displaying event)	**35,27**	1,54	4,54%	0,87	0,00	20,50	26,22%	7,66	5,47	26,61	26,52%	8,27	23,34	4,07

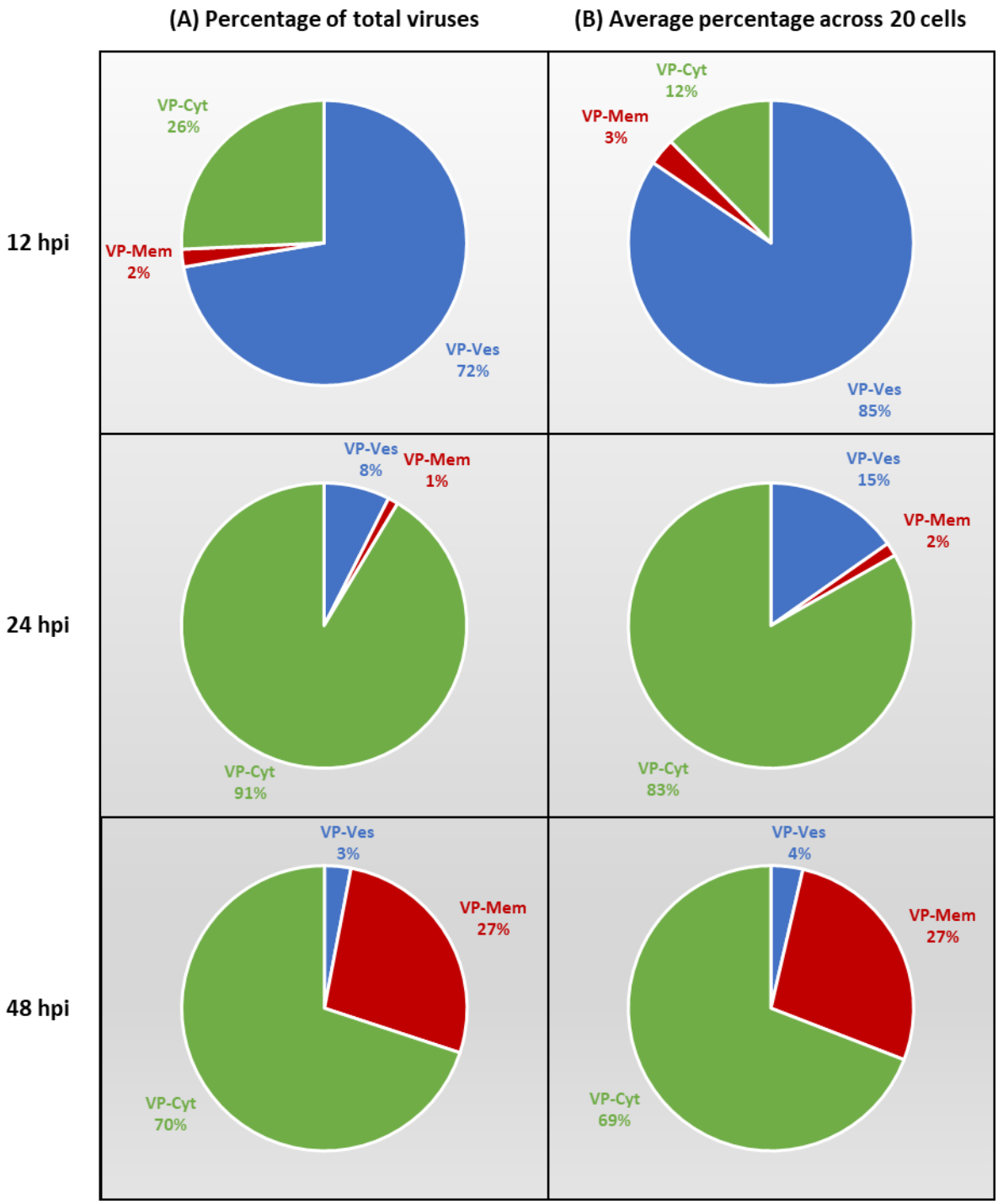

Figure 11. Summary of the AHSV distribution profile in BSR cells over time. All viruses identified in the cytoplasm of AHSV-infected BSR cells were categorised as VP-Ves, VP-Mem or VP-Cyt particles. (A) Percentage of total virus particles in a particular intracellular virus distribution at a specific time post infection. The total number of virus particles in a specific intracellular distribution was divided by the total number of particles identified in the cytoplasm of 20 cells. (B) Average percentage of a particular intracellular virus distribution across 20 cells at a specific time post infection. The number of total viruses per cell identified in a particular intracellular distribution was determined and the percentage of each distribution category averaged across 20 cells.

2.3.1.2 Ultrastructural characterisation of AHSV particle localisation in KC cells

To determine the intracellular location of virus particles in insect cells, AHSV-infected KC cells were examined by high resolution TEM imaging. At 12 hpi (Fig 12) infected cells showed typical KC cell morphology, i.e. rounded shapes, intact plasma membranes and contact between neighbouring cells (Fig 12 A). From these observations, AHSV-infected KC cells were presumed to sustain cellular activities such as trafficking. The infection status of cells was confirmed by the presence of mature virus particles, and often by the presence of other viral structures such as tubules and VIBs (Fig 12 E). Virus particles were frequently observed in the cytoplasm as aggregates or freely dispersed virions in proximity to the plasma membrane (Fig 12 B, C). Many particles were also seen within small vesicles containing one virus particle in close proximity to the plasma membrane (Fig 12 D). Large vesicle-like structures containing cellular-derived material, and at times virus particles and viral structures such as tubules, were also observed in cells (Fig 12 E, F). At this time post infection, observations of membrane-associated virus particles were rare (Fig 12 F).

At 24 hpi (Fig 13) infected cells still showed typical KC cell morphology (Fig 13 A). Virus particles were mainly observed as cytoplasmic aggregates (≥ 3), pairs, or single virions in proximity to the plasma membrane (Fig 13 B, C). Dispersed single virions were frequently seen within plasma membrane protrusions (Fig 13 C, D). Virus particles were on occasion observed inside vesicles in close proximity to the plasma membrane (Fig 13 E), and at times associated with the cytoplasmic face of vesicles (Fig 13 F). Virus infection was confirmed by the presence of mature virus particles and the other hallmarks of infection (e.g. VIBs, tubules and crystals) (not shown). Compared to 12 hpi where viruses were mostly in the cytoplasm and some inside vesicles, at 24 hpi most viruses were in the cytoplasm as single virus particles, pairs or aggregates.

At this time post infection virus particles were frequently observed at the plasma membrane (Fig 14). Orbivirus release from insect cells has not been described in detail, but is expected to be non-lytic due to the ability of KC cells to sustain continued AHSV infection (VENTER *et al.* 2014). In this study virus particles were observed at irregular plasma membranes (Fig 14 A-B), within budding-like structures (Fig 14 C-D) and on the extracellular side of the plasma membrane (Fig 14 E-F).

Vesicles containing cellular-derived material were also observed at 24 hpi in AHSV-infected cells (Fig 15). Some cells showed more than one of these vesicle structures (Fig 15 A), and virus particles were frequently located in close proximity to (Fig 15 B) or inside these structures (Fig 15 C, D). Vesicles containing cellular material and sometimes viral material were also detected at the plasma membrane of cells (Fig 15 C, D). These observations support the non-lytic virus release mechanism from KC cells previously proposed (VENTER *et al.* 2014), as the fusion of these vesicles with the plasma membrane would release viruses into the extracellular space and preserve the integrity of the plasma membrane (Fig 15 E, F).

At 48 hpi (Fig 16) cells continued to show typical KC cell morphology (Fig 16 A). Virus particles were present in several distinct intracellular locations in single cells (Fig 16 A-F). Viruses were most frequently observed in cytoplasmic aggregates, pairs and single virions in proximity to the plasma membrane (Fig 16 B, C, G). Single virions in the cytoplasm were also observed within plasma membrane protrusions (Fig 16 E). Viruses were sometimes seen associated with the plasma membrane (Fig 16 D) and with the cytoplasmic face of vesicles (Fig 16 F, G). Multiple and single particles were on occasion observed inside vesicles (Fig 16 C, H). Some of the intra-vesicular virus particles were observed in dense intra-vesicular environments (Fig 16 H; vesicle containing > 2 virus particles). The infection status of cells was confirmed by the presence of virus particles and virus structures such as VIBs, which at times were present more than once in a single cell (Fig 16 B, F). At 48 h virus particles were also, as at 24 hpi, mainly observed in the cytoplasm as single virus particles, pairs and aggregates.

Similar to 24 hpi, at 48 hpi virus particles were also observed at irregular or potentially disrupted plasma membranes (Fig 17 A-C). Particles were also detected inside extracellular vesicles (Fig 17 D), associated with membrane structures connected to the plasma membrane (Fig 17 E) and in the extracellular space (Fig 17 F). Compared to earlier time points, at 48 hpi viruses were not as often observed inside or in close proximity to vesicles containing cellular-derived material.

At 7 dpi (Fig 18) cells still showed typical KC cell morphology (Fig 18 A). Virus structures such as tubules were prevalent and confirmed virus infection (Fig 18 A). Aggregates of virus particles were frequently observed at several distinct locations in the cytoplasm (Fig 18 B). Virus particles were on occasion observed on the cytoplasmic face of vesicles (Fig 18 C) or inside vesicles (Fig 18 D). At this time point virus particles were also observed in proximity to vesicles containing cellular-derived material (Fig 18 E) and at the plasma membrane (Fig 18 F). Similar to 48 hpi, virus particles were most frequently present in the cytoplasm as aggregates, pairs, and single particles

Virus particles were observed in similar intracellular locations at early, intermediate and late times post infection in KC cells. However, as in BSR cells, the frequency at which particles were observed at different intracellular locations seemed to differ in KC cells at different time points. The same procedure used to document this in more detail for BSR samples was subsequently also applied to the KC samples. Twenty AHSV-infected KC cells were selected from 12 hpi, 24 hpi, 48 hpi, and 7 dpi samples, and each of the cells examined systematically to quantify the occurrence of the different virus particle distributions. The criteria according to which the different types of distributions were categorised is as described in section 2.3.1.1. The data recorded in this fashion for AHSV-infected KC cells at 12 hpi, 24 hpi, 48 hpi, and 7 dpi is summarised in Tables 6-9. Data analysis was subsequently done for KC samples as described in section 2.3.1.1.1 for BSR samples.

At 12 hpi (Table 7), 78% of the total number of virus particles detected were distributed in the cytoplasm, 18% into vesicles, and only 4% associated with membranous structures. Eighty percent of cells showed VP-Cyt distributions and 75% showed VP-Ves distributions. Vesicles typically contained single particles and cytoplasmic virus distributions were single and pairs of virus particles. Despite the low total number of membrane-associated viruses, 35% of cells showed VP-Mem distributions. On average, 52% of particles were dispersed in the cytoplasm, 40% were inside vesicles, and only 8% were membrane-associated across all 20 cells. The majority of virus particles detected at 12 hpi were therefore freely dispersed in the cytoplasm as single virions or virus pairs.

At 24 hpi (Table 8), 89% of the total number of virus particles present were in the cytoplasm, while 6% were inside vesicles, and only 5% were associated with membranous structures. VP-Cyt distributions were recorded in 85% of cells, while 25% and 15% of cells showed VP-Mem and VP-Ves distributions respectively. VP-Mem distributions were characterised by single particle membrane associations which explained the high incidence but low total number of VP-Mem particles. The predominant distribution, VP-Cyt, was characterised by freely dispersed single virions and pairs of virus, rather than aggregates. Across all twenty cells, an average of 81% of particles were in the cytoplasm, whereas 10% and 9% of particles were inside vesicles and membrane-associated respectively. Compared to the averages at 12 hpi, VP-Cyt distributions increased while VP-Ves distributions decreased at 24 hpi. The total number of identified virus particles was lower at 24 hpi than at 12 hpi. Similar to 12 hpi, at 24 hpi particles were predominantly present as single virus particles and pairs in the cytoplasm.

At 48 hpi (Table 9), 87% of the total number of virus particles present distributed in the cytoplasm, 9% into vesicles, and only 4% associated with membranous structures. All cells showed VP-Cyt distributions characterised by aggregates, pairs of viruses and single virions alike. Fifty percent and 55% of cells showed VP-Ves and VP-Mem distributions respectively. This high incidence but low total number of VP-Ves and VP-Mem virus particles was explained by the more frequent detection of single virus particles in these distributions. An average of 90% of particles recorded across 20 cells were in the cytoplasm, while 7% were inside vesicles and only 3% were membrane-associated. Like 24 hpi, the majority of viruses were cytoplasmic at 48 hpi, however, particles were as this time point mainly present as cytoplasmic aggregates.

At 7 dpi (Table 10), 94% of the total number of virus particles were in the cytoplasm, while only 4% were inside vesicles and 2% were membrane-associated. Ninety-five percent of cells showed VP-Cyt distributions, while 25% of cells showed incidents of VP-Ves and VP-Mem. The total number of identified particles in 7 dpi samples was lower than the total of 48 hpi samples. Across all 20 cells, an average of 90% of particles were in the cytoplasm, 6% were inside vesicles, and only 4% showed membrane-associated particles. Similar to 48 hpi, at 7 dpi particles mainly dispersed as cytoplasmic aggregates.

To summarise, the intracellular distribution profile appeared to also change over time in infected KC cells (Fig 19). At 12 hpi, a large component of particles were cytoplasmic, but many particles were also inside vesicles. At 24 hpi, the majority of particles were dispersed in the cytoplasm, and few particles were inside vesicles. Similar observations were made at 48 hpi and 7 dpi. Compared to the AHSV distribution profile in BSR cells, wherein particles disperse predominantly into vesicles at early times post infection and freely in the cytoplasm at later times, the profile in KC cells was different. Viruses were predominantly distributed in the cytoplasm over all time points.

Transmission electron microscopy imaging of infected BSR and KC cells revealed that viruses either distribute freely in the cytoplasm, into vesicles or associate with membranous structures. Given the time points, observed virus particle were newly synthesised particles and due to the size of AHSV particles, the distribution profiles may be the result of cellular transport pathways. The possible viral usurpation of cellular transport pathways was therefore subsequently investigated.

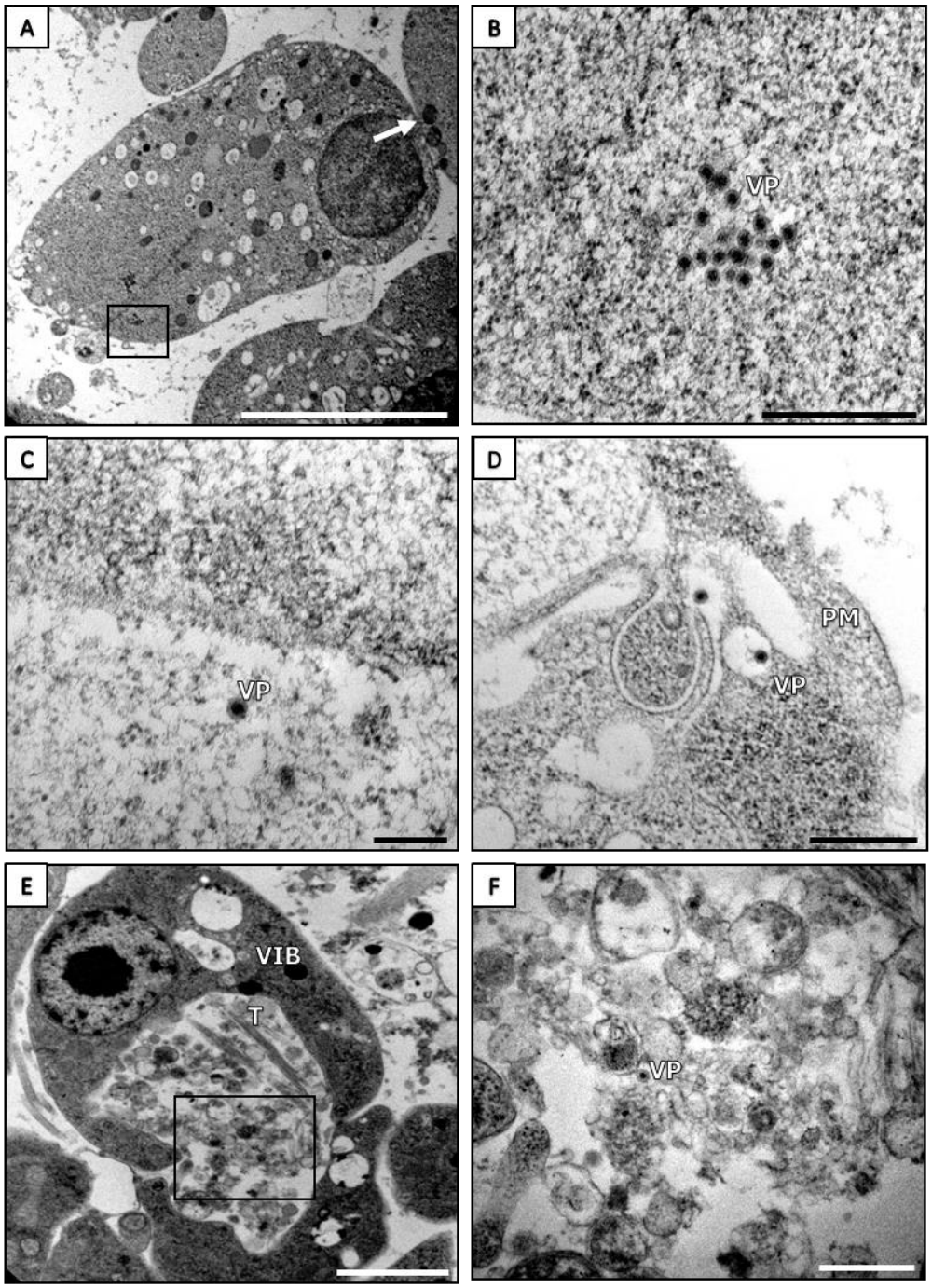

Figure 12. TEM micrographs of AHSV-infected KC cells at 12 hpi. (A) AHSV-infected cell exhibiting typical KC morphology, with contact between neighbouring cells indicated by arrow. (B) Enlargement of demarcated area in A showing an aggregate of virus particles (VP) in cytoplasm. (C) Single virion dispersed in cytoplasm. (D) Vesicles in close proximity to the plasma membrane (PM) containing only one virion. (E) Observation of tubules (T) and cellular-derived material inside vesicle-like structure in cytoplasm. A viral inclusion body (VIB) was also detected. (F) Enlargement of demarcated area in E showing membrane-associated virus particle. Scale bars, 5 µm (A); 2 µm (E); 0,5 µm (B, D, F); 0,2 µm (C).

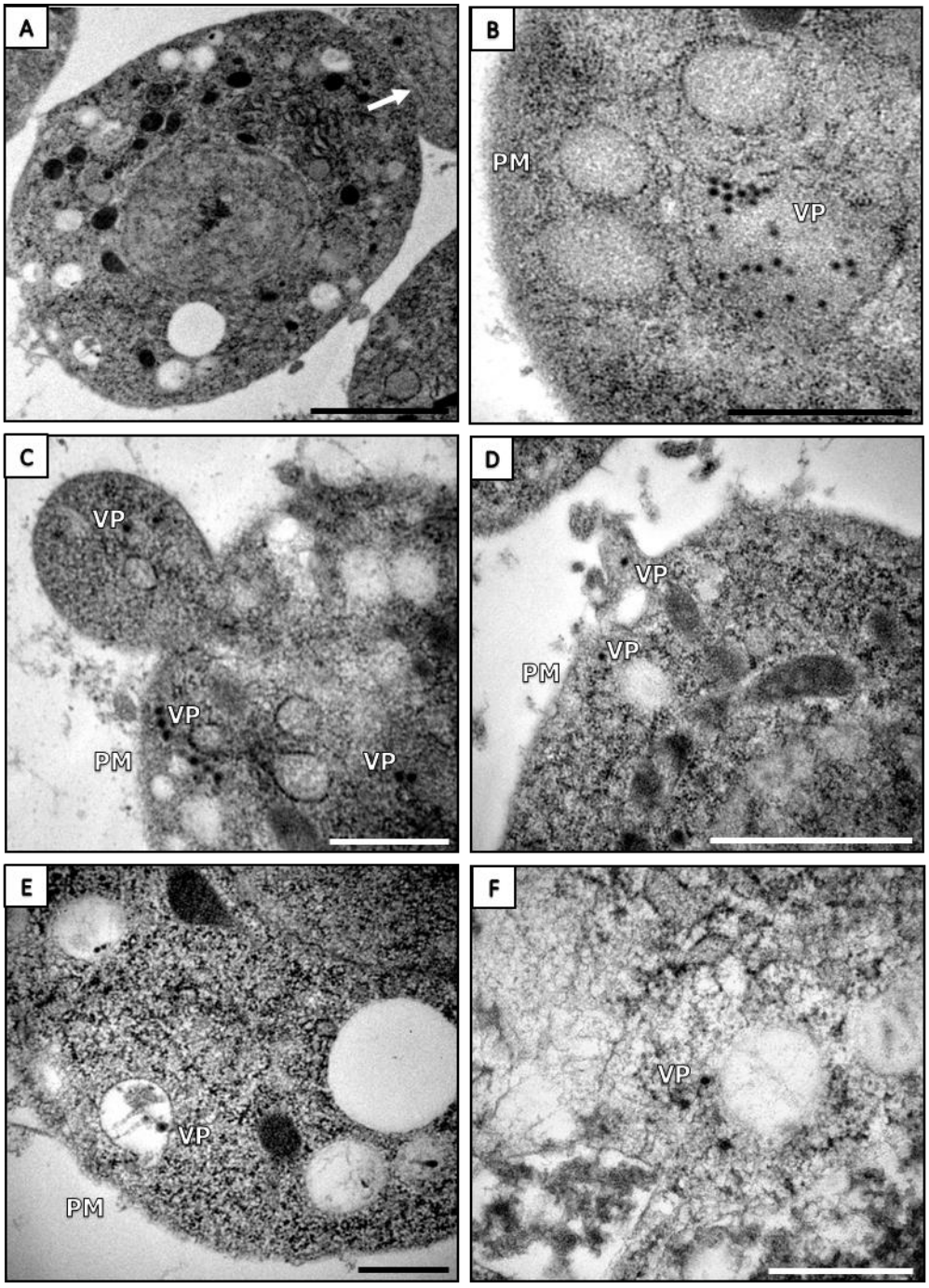

Figure 13. TEM micrographs of AHSV-infected KC cells at 24 hpi. (A) AHSV-infected cell showing typical KC morphology, with contact between neighbouring cells indicated by arrow. (B) Observation of mature ~ 70 nm spherical virus particles (VP) in the cytoplasm. (C-D) Single and aggregates of virus particles in close proximity to the plasma membrane (PM). (E-F) Viruses inside and on the cytoplasmic face of vesicles. Scale bar, 2 µm (A); 0,5 µm (B-F).

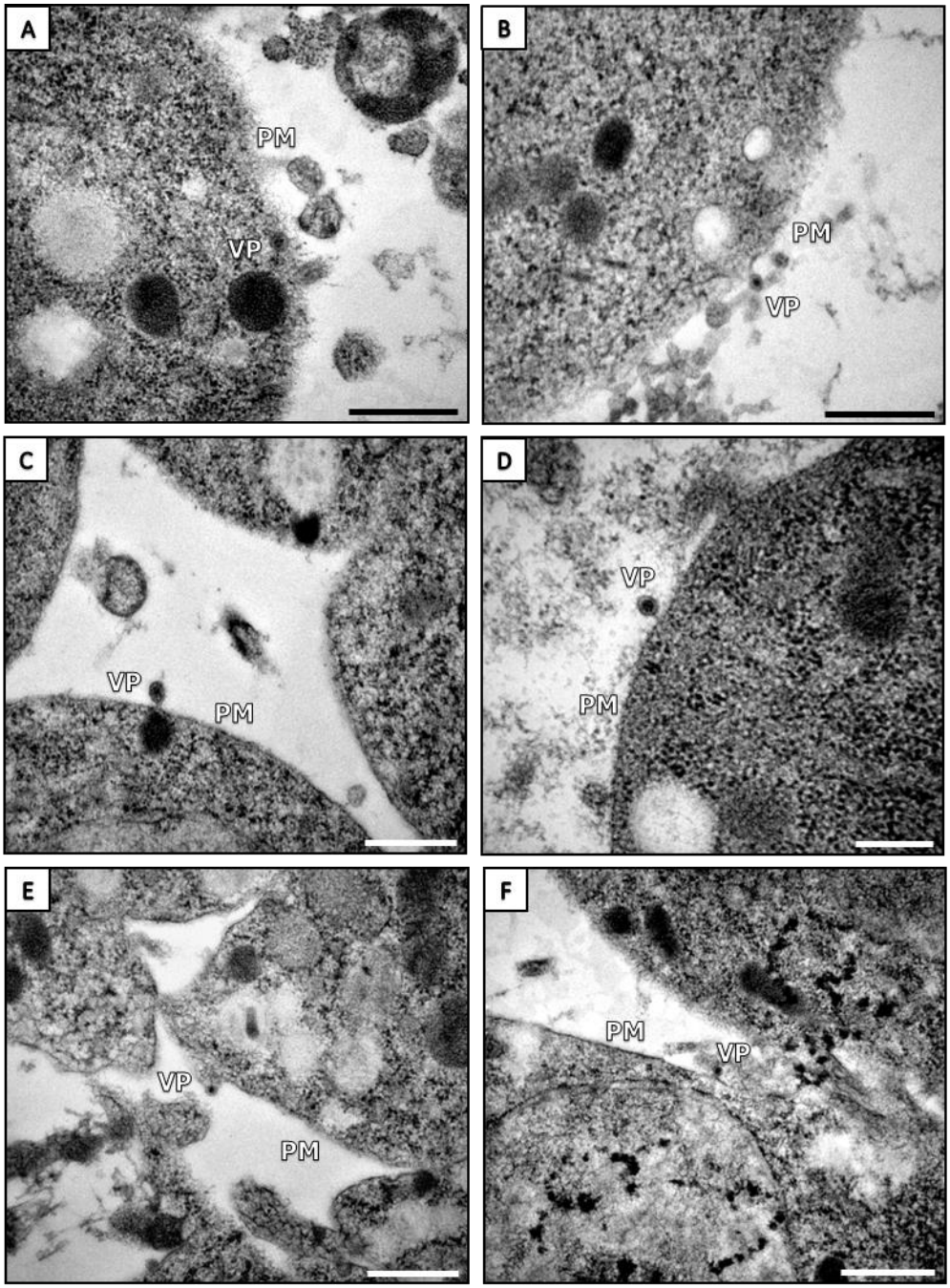

Figure 14. TEM micrographs of virus localisations in KC cells at 24 hpi. (A-B) Virus particle (VP) at plasma membrane (PM). (C-D) Single particles in budding-like structure. (E-F) Virus particles associated with the extracellular side of the plasma membrane. Scale bar, 0,5 µm (A-C, E-F); 0,2 µm (D).

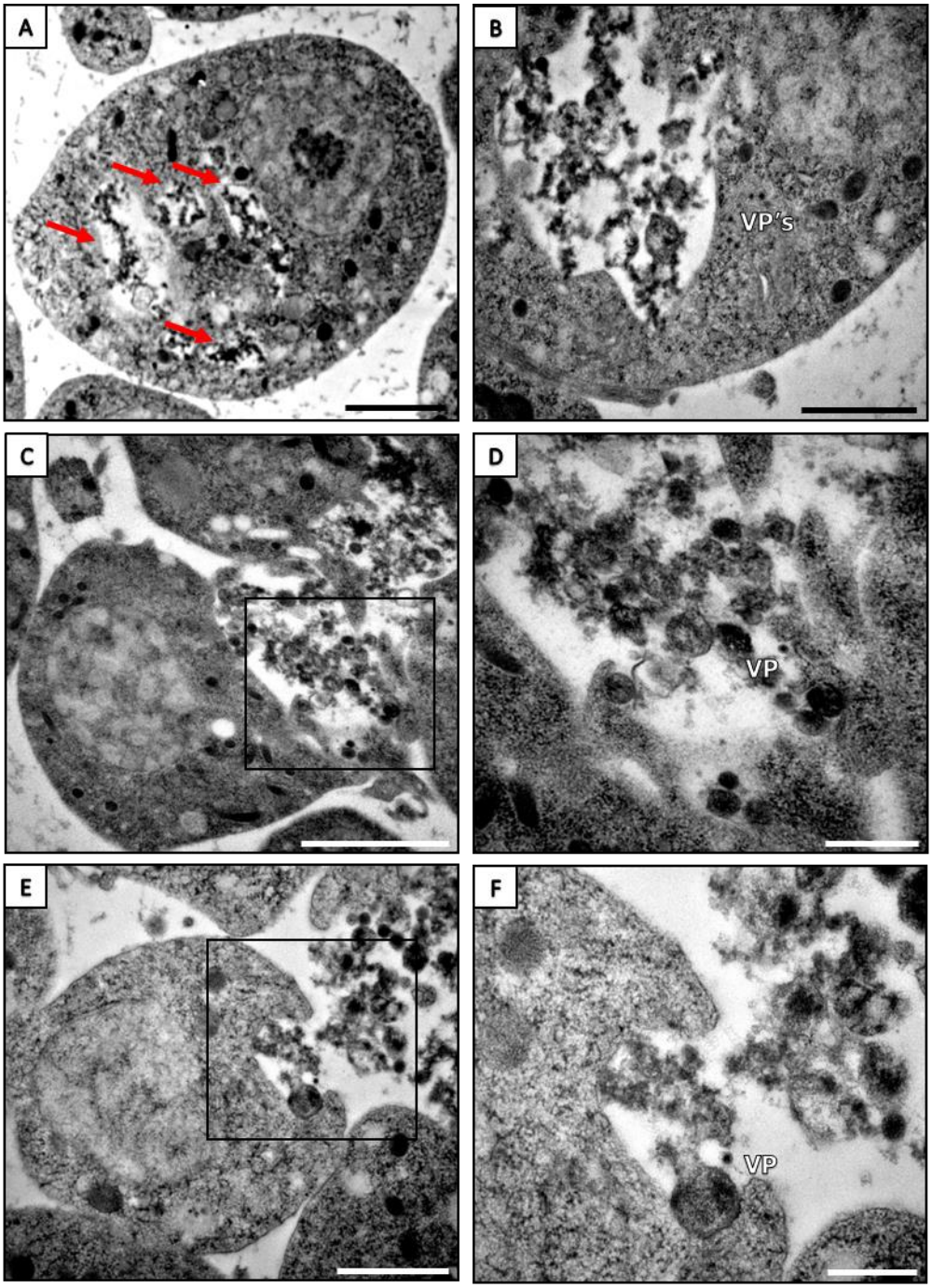

Figure 15. TEM micrographs of vesicles containing cellular-derived material in KC cells at 24 hpi. (A) Multiple vesicles containing cellular-derived material indicated by arrows in the cytoplasm. (B) Virus particles (VP) in close proximity to vesicle. (C) Vesicle containing cellular-derived material and virus particle at plasma membrane of cell. (D) Enlargement of demarcated area in C. (E) Cellular-derived material and virus particle in the extracellular space. (F) Enlargement of demarcated area in E. Scale bar, 2 µm (A, C); 1 µm (B, E); 0,5 µm (D, F).

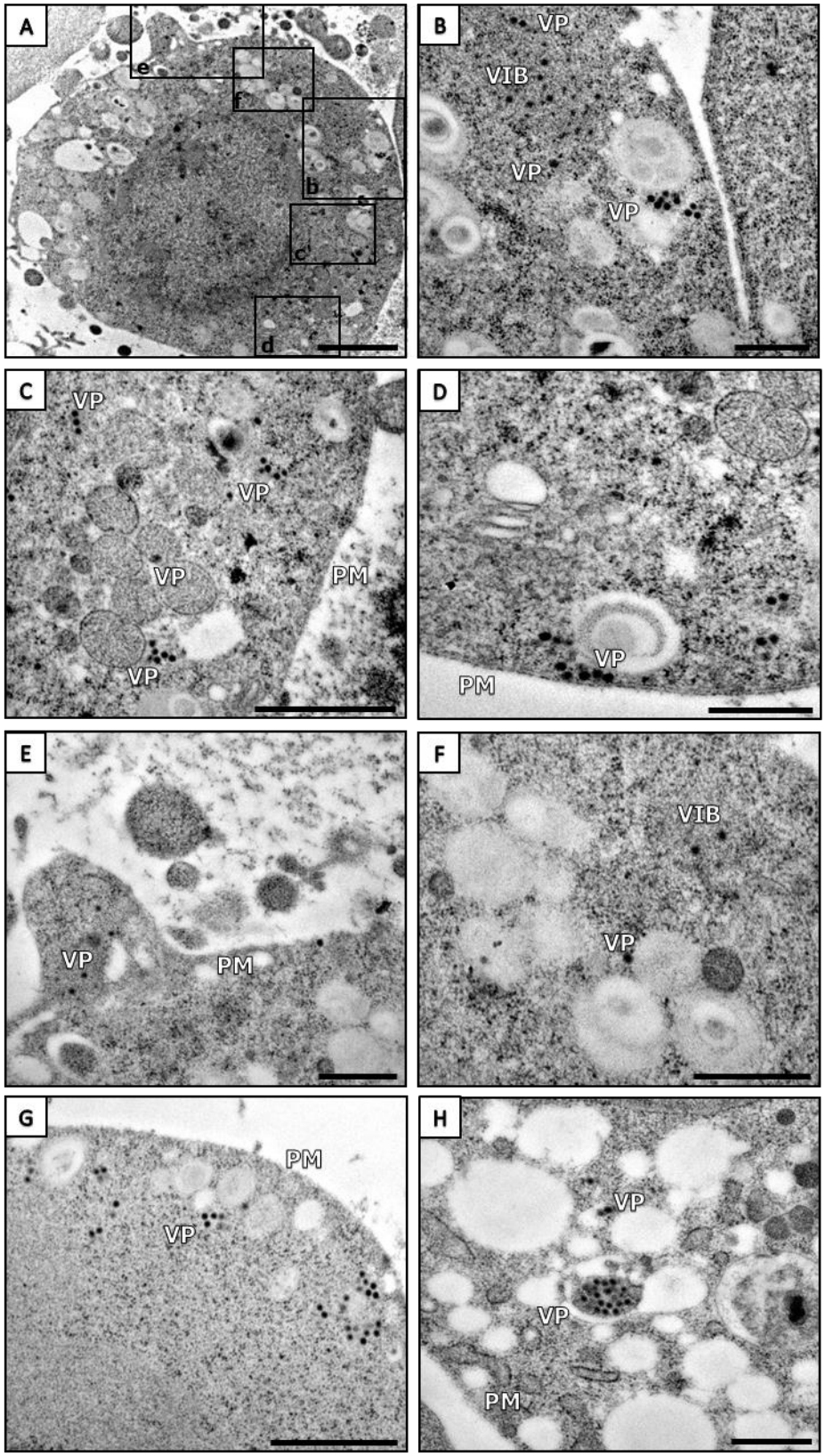

Figure 16. TEM micrographs of vesicles containing cellular-derived material in KC cells at 24 hpi. (A) Multiple vesicles containing cellular-derived material in the cytoplasm. (B) Virus particles (VP) in close proximity to vesicle. (C) Vesicle containing cellular-derived material and virus particle at plasma membrane of cell. (D) Enlargement of demarcated area in C. (E) Cellular-derived material and virus particle in the extracellular space. (F) Enlargement of demarcated area in E. Scale bar, 2 µm (A, C); 1 µm (B, E); 0,5 µm (C, D, F).

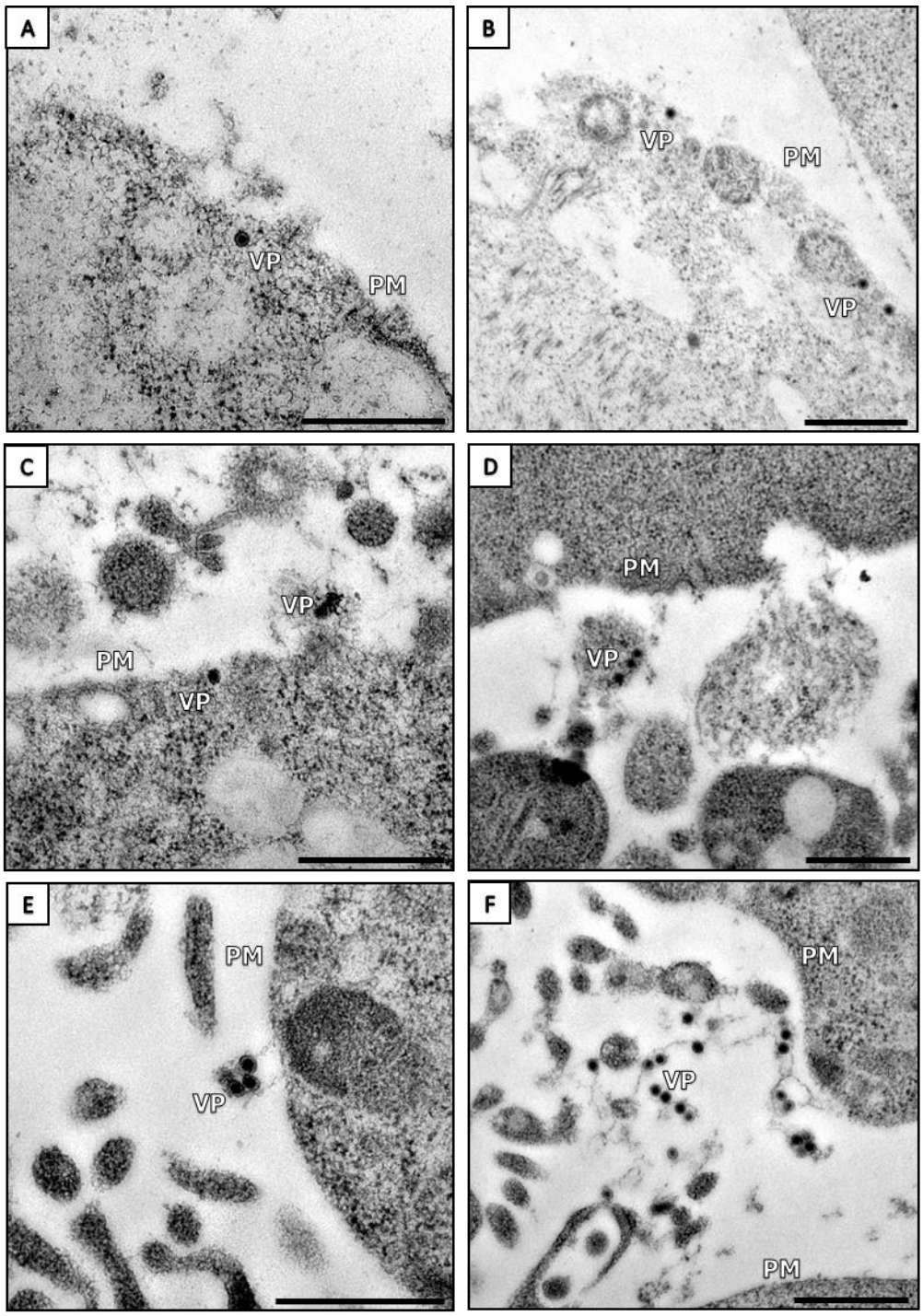

Figure 17. TEM micrographs illustrating virus localisations in KC cells at 48 hpi. (A-C) Virus particle (VP) at plasma membrane (PM). (D) Particles in extracellular vesicle. (E-F) Virus particles in the extracellular space. Scale bar, 0,5 µm (A-F).

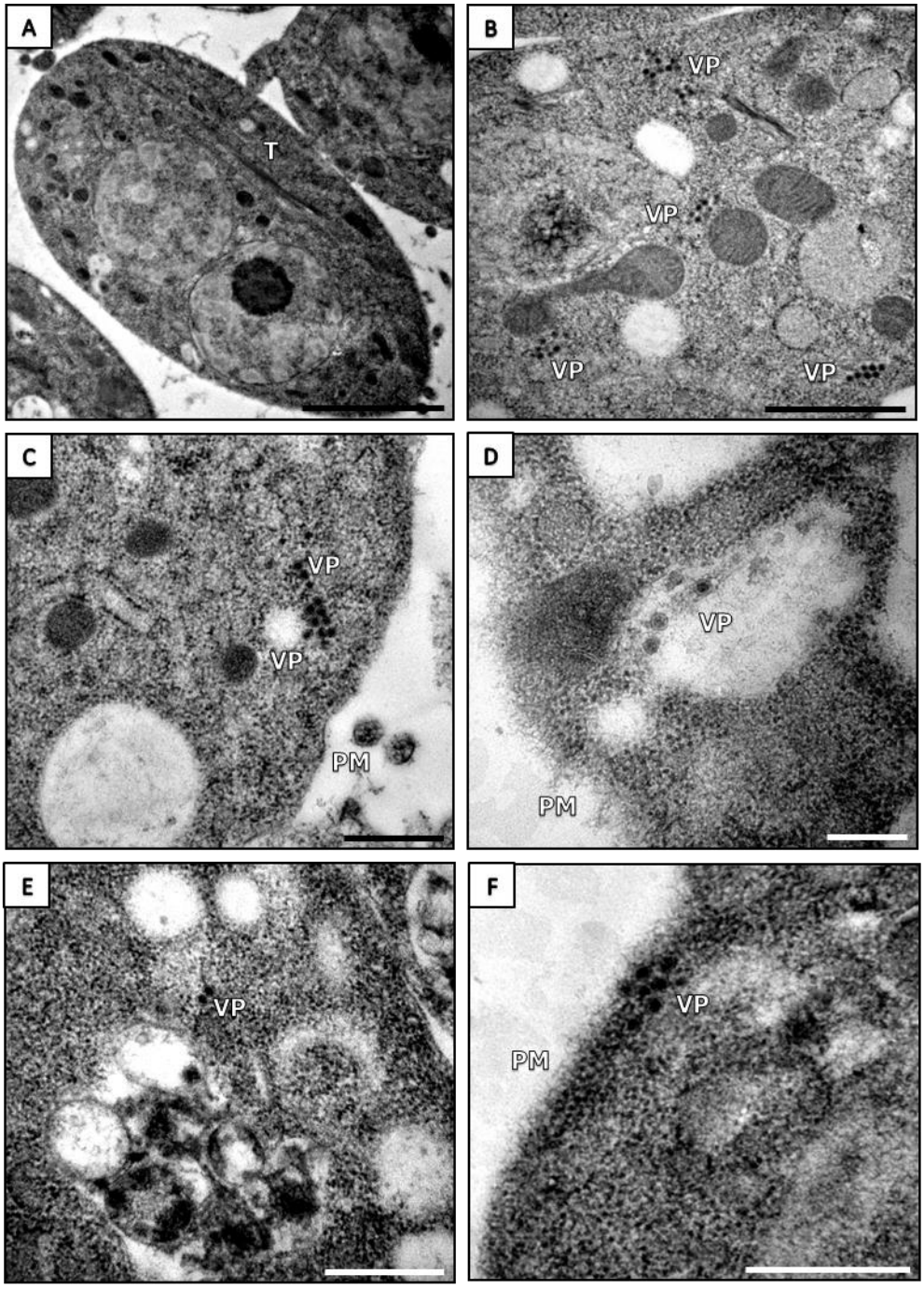

Figure 18. TEM micrographs of AHSV-infected KC cells at 7 dpi. (A) AHSV-infected cell exhibiting healthy cell morphology and tubules (T). (B) Aggregates of virus particles in the cytoplasm. (C) Single virus particle associated with the cytoplasmic face of vesicle and aggregate virus particles in proximity to the plasma membrane (PM). (D) Multiple virus particles inside vesicle. (E) Pair of virus particles in close proximity to vesicle containing cellular-derived material. (F) Virus particles at the plasma membrane. Scale bar, 2 µm (A); 1 µm (B); 0,5 µm (C, E, F); 0,2 µm (D).

Table 7. AHSV distribution profile at 12 hpi in KC cells

Cell sample	Total number of virus particles	Intra-vesicular (VP-Ves)				Membrane-associated (VP-Mem)				Cytoplasmic (VP-Cyt)				
		Number of virus particles in cell inside vesicles	Percentage of total particles in cell inside vesicles	Number of vesicles in cell containing one particle	Number of vesicles in cell containing 2 or more particles	Number of membrane-associated virus particles in cell	Percentage of total virus particles in cell showing membrane association	Number of membranous structures in cell associated with a single particle	Number of membranous structures in cell associated with 2 or more particles	Number of virus particles free in cytoplasm in cell	Percentage of total particles in cell free in cytoplasm	Number of cytoplasmic particles in cell distributed individually or in pairs	Number of cytoplasmic particles in cell forming part of aggregates	Number of aggregates in cytoplasm of cell
1	**4**	2	50%		1	1	25%	1		1	25%	1		
2	**55**		0%				0%			55	100%		55	3
3	**11**		0%				0%			11	100%	1	10	1
4	**45**	5	11%	5		3	7%		1	37	82%	19	18	4
5	**55**		0%				0%			55	100%	8	47	12
6	**6**	4	67%	4			0%			2	33%	2		
7	**5**	4	80%	1	1		0%			1	20%	1		
8	**3**	2	67%	2		1	33%	1			0%			
9	**4**	3	75%	3		1	25%	1			0%			
10	**10**	10	100%	4	3		0%				0%			
11	**9**	2	22%	2			0%			7	78%		7	1
12	**8**	1	13%	1		4	50%	1	1	3	38%	3		
13	**21**	1	5%	1		1	5%	1		19	90%	15	4	1
14	**7**	6	86%	2	2		0%			1	14%	1		
15	**7**	5	71%	3	1	1	14%	1		1	14%	1		
16	**29**		0%				0%			29	100%	11	18	2
17	**9**	2	22%	2			0%			7	78%	2	5	1
18	**3**	3	100%	3			0%				0%			
19	**5**		0%				0%			5	100%	5		
20	**18**	6	33%	2	1		0%			12	67%	3	9	2
TOTAL	**314**	56	-	35	9	12	-	6	2	246	-	73	173	27
Percentage of total viruses	**-**	17,83%	-	11,15%	2,87%	3,82%	-	1,91%	0,64%	78,34%	-	23,25%	55,10%	-
Percentage of cells displaying event	**-**	75%	-	-	-	35%	-	-	-	80%	-	-	-	-
Percentage of cells with ≥ 1 incidence	**-**	-	-	70%	30%	-	-	30%	10%	-	-	70%	45%	45%
AVG (across all 20 cells)	**15,70**	2,80	40,08%	1,75	0,45	0,60	7,95%	0,30	0,10	12,30	51,97%	3,65	8,65	1,35
SD (across all 20 cells)	**16,91**	2,65	37,09%	1,55	0,83	1,10	14,27%	0,47	0,31	17,77	40,67%	5,43	15,66	2,76
AVG (only cells displaying event)	**15,70**	3,73	53,44%	2,50	1,50	1,71	22,72%	1,00	1,00	15,38	64,96%	5,21	19,22	3,00
SD (only cells displaying event)	**16,91**	2,40	33,19%	1,22	0,84	1,25	15,91%	0,00	0,00	18,70	34,57%	5,86	18,80	3,54

Table 8. AHSV distribution profile at 24 hpi in KC cells

Cell sample	Total number of virus particles	Intra-vesicular (VP-Ves)				Membrane-associated (VP-Mem)				Cytoplasmic (VP-Cyt)				
		Number of virus particles in cell inside vesicles	Percentage of total particles in cell inside vesicles	Number of vesicles in cell containing one particle	Number of vesicles in cell containing 2 or more particles	Number of membrane-associated virus particles in cell	Percentage of total virus particles in cell showing membrane association	Number of membranous structures in cell associated with a single particle	Number of membranous structures in cell associated with 2 or more particles	Number of virus particles free in cytoplasm in cell	Percentage of total particles in cell free in cytoplasm	Number of cytoplasmic particles in cell distributed individually or in pairs	Number of cytoplasmic particles in cell forming part of aggregates	Number of aggregates in cytoplasm of cell
1	**6**	5	83%		1	1	17%	1			0%			
2	**15**		0%				0%			15	100%		15	1
3	**2**		0%				0%			2	100%	2		
4	**1**		0%			1	100%	1			0%			
5	**5**		0%				0%			5	100%		5	1
6	**3**		0%			1	33%	1		2	67%	2		
7	**3**		0%				0%			3	100%		3	1
8	**2**		0%				0%			2	100%	2		
9	**5**		0%				0%			5	100%	5		
10	**1**	1	100%	1			0%				0%			
11	**6**		0%			1	17%	1		5	83%	5		
12	**1**		0%				0%			1	100%	1		
13	**3**		0%				0%			3	100%		3	1
14	**5**		0%				0%			5	100%		5	1
15	**28**		0%				0%			28	100%	5	23	4
16	**14**	1	7%	1		2	14%	2		11	79%	8	3	1
17	**5**		0%				0%			5	100%	2	3	1
18	**2**		0%				0%			2	100%	2		
19	**2**		0%				0%			2	100%	2		
20	**7**		0%				0%			7	100%	7		
TOTAL	**116**	7	-	2	1	6	-	6	0	103	-	43	60	11
Percentage of total viruses	**-**	6,03%	-	1,72%	0,86%	5,17%	-	5,17%	0,00%	88,79%	-	37,07%	51,72%	-
Percentage of cells displaying event	**-**	15%	-	-	-	25%	-	-	-	85%	-	-	-	-
Percentage of cells with ≥ 1 incidence	**-**	-	-	10%	5%	-	-	25%	0%	-	-	60%	40%	40%
AVG (across all 20 cells)	**5,80**	0,35	9,52%	0,10	0,05	0,30	9,05%	0,30	0,00	5,15	81,43%	2,15	3,00	0,55
SD (across all 20 cells)	**6,49**	1,14	28,27%	0,31	0,22	0,57	23,21%	0,57	0,00	6,54	36,24%	2,52	5,89	0,94
AVG (only cells displaying event)	**5,80**	2,33	63,49%	1,00	1,00	1,20	36,19%	1,20	n/A	6,06	95,80%	3,58	7,50	1,38
SD (only cells displaying event)	**6,49**	2,31	49,51%	0,00	n/A	0,45	36,48%	0,45	n/A	6,70	9,84%	2,31	7,46	1,06

Table 9. AHSV distribution profile at 48 hpi in KC cells

Cell sample	Total number of virus particles	Intra-vesicular (VP-Ves)				Membrane-associated (VP-Mem)				Cytoplasmic (VP-Cyt)				
		Number of virus particles in cell inside vesicles	Percentage of total particles in cell inside vesicles	Number of vesicles in cell containing one particle	Number of vesicles in cell containing 2 or more particles	Number of membrane-associated virus particles in cell	Percentage of total virus particles in cell showing membrane association	Number of membranous structures in cell associated with a single particle	Number of membranous structures in cell associated with 2 or more particles	Number of virus particles free in cytoplasm in cell	Percentage of total particles in cell free in cytoplasm	Number of cytoplasmic particles in cell distributed individually or in pairs	Number of cytoplasmic particles in cell forming part of aggregates	Number of aggregates in cytoplasm of cell
1	**49**	1	2%	1		4	8%	4		44	90%	7	37	4
2	**46**	4	9%		1	2	4%	2		40	87%	10	30	7
3	**27**	1	4%	1		3	11%	3		23	85%	10	13	3
4	**99**	2	2%	2		4	4%	2	1	93	94%	5	88	9
5	**44**		0%				0%			44	100%	4	40	5
6	**26**		0%				0%			26	100%	0	26	1
7	**24**		0%				0%			24	100%	4	20	3
8	**38**		0%			1	3%	1		37	97%	12	25	4
9	**30**		0%				0%			30	100%	3	27	4
10	**43**	2	5%		1	1	2%	1		40	93%	11	29	1
11	**84**	47	56%		7	1	1%	1		36	43%	12	24	5
12	**23**		0%			5	22%	5		18	78%	7	11	3
13	**51**	1	2%	1		6	12%	4	1	44	86%	15	29	6
14	**42**		0%				0%			42	100%	3	39	6
15	**38**	17	45%		2	1	3%	1		20	53%	8	12	3
16	**27**	2	7%	2			0%			25	93%	9	16	5
17	**32**		0%				0%			32	100%	9	23	7
18	**25**		0%				0%			25	100%	9	16	1
19	**52**		0%			1	2%	1		51	98%	9	42	8
20	**32**	1	3%	1			0%			31	97%	1	30	3
TOTAL	**832**	78	-	8	11	29	-	25	2	725	-	148	577	88
Percentage of total viruses	**-**	9,38%	-	0,96%	1,32%	3,49%	-	3,00%	0,24%	87,14%	-	17,79%	69,35%	-
Percentage of cells displaying event	**-**	50%	-	-	-	55%	-	-	-	100%	-	-	-	-
Percentage of cells with ≥ 1 incidence	**-**	-	-	30%	20%	-	-	55%	10%	-	-	100%	100%	100%
AVG (across all 20 cells)	**41,60**	3,90	6,71%	0,40	0,55	1,45	3,59%	1,25	0,10	36,25	89,69%	7,40	28,85	4,40
SD (across all 20 cells)	**19,62**	10,82	15,25%	0,68	1,61	1,90	5,63%	1,59	0,31	16,30	15,73%	3,98	16,72	2,28
AVG (only cells displaying event)	**41,60**	7,80	13,43%	1,33	2,75	2,64	6,53%	2,27	1,00	36,25	89,69%	7,40	28,85	4,40
SD (only cells displaying event)	**19,62**	14,61	19,77%	0,52	2,87	1,86	6,25%	1,49	0,00	16,30	15,73%	3,98	16,72	2,28

Table 10. AHSV distribution profile at 7 dpi in KC cells

Cell sample	Total number of virus particles	Intra-vesicular (VP-Ves)				Membrane-associated (VP-Mem)				Cytoplasmic (VP-Cyt)				
		Number of virus particles in cell inside vesicles	Percentage of total particles in cell inside vesicles	Number of vesicles in cell containing one particle	Number of vesicles in cell containing 2 or more particles	Number of membrane-associated virus particles in cell	Percentage of total virus particles in cell showing membrane association	Number of membranous structures in cell associated with a single particle	Number of membranous structures in cell associated with 2 or more particles	Number of virus particles free in cytoplasm in cell	Percentage of total particles in cell free in cytoplasm	Number of cytoplasmic particles in cell distributed individually or in pairs	Number of cytoplasmic particles in cell forming part of aggregates	Number of aggregates in cytoplasm of cell
1	**14**		0%			1	7%	1		13	93%	2	11	1
2	**29**	3	10%		1		0%			26	90%		26	4
3	**15**		0%			1	7%	1		14	93%	4	10	1
4	**13**		0%				0%			13	100%	4	9	1
5	**17**		0%				0%			17	100%	2	15	2
6	**16**		0%				0%			16	100%		16	3
7	**7**		0%				0%			7	100%		7	1
8	**19**		0%				0%			19	100%	3	16	4
9	**12**		0%				0%			12	100%	3	9	3
10	**31**		0%				0%			31	100%		31	5
11	**35**		0%				0%			35	100%		35	1
12	**20**		0%				0%			20	100%		20	1
13	**28**		0%				0%			28	100%		28	5
14	**11**	3	27%	3			0%			8	73%	2	6	2
15	**16**	1	6%	1		1	6%	1		14	88%	2	12	3
16	**21**		0%				0%			21	100%		21	1
17	**8**	5	63%		1	3	38%	1	1		0%			
18	**7**	1	14%	1			0%			6	86%	1	5	2
19	**12**		0%				0%			12	100%	3	9	1
20	**6**		0%			1	17%	1		5	83%	5		1
TOTAL	**337**	13	-	5	2	7	-	5	1	317	-	31	286	42
Percentage of total viruses	**-**	3,86%	-	1,48%	0,59%	2,08%	-	1,48%	0,30%	94,07%	-	9,20%	84,87%	-
Percentage of cells displaying event	**-**	25%	-	-	-	25%	-	-	-	95%	-	-	-	-
Percentage of cells with ≥ 1 incidence	**-**	-	-	15%	10%	-	-	25%	5%	-	-	55%	90%	95%
AVG (across all 20 cells)	**16,85**	0,65	6,03%	0,25	0,10	0,35	3,71%	0,25	0,05	15,85	90,26%	1,55	14,30	2,10
SD (across all 20 cells)	**8,37**	1,39	15,00%	0,72	0,31	0,75	9,01%	0,44	0,22	9,06	22,58%	1,67	9,87	1,48
AVG (only cells displaying event)	**16,85**	2,60	24,13%	1,67	1,00	1,40	14,85%	1,00	1,00	16,68	95,01%	2,82	15,89	2,21
SD (only cells displaying event)	**8,37**	1,67	22,85%	1,15	0,00	0,89	13,39%	0,00	n/A	8,49	7,85%	1,17	9,07	1,44

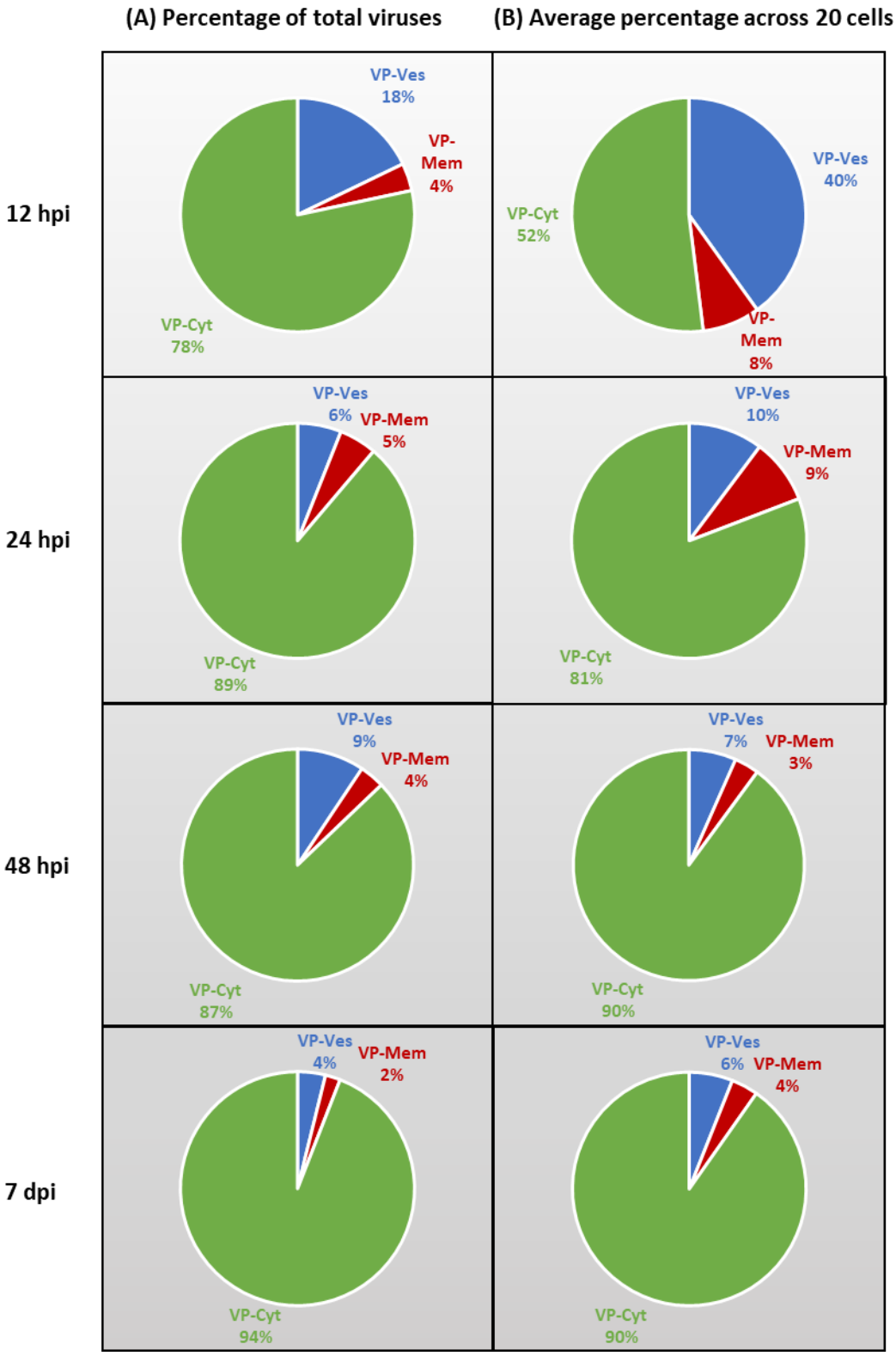

Figure 19. Summary of the AHSV distribution profile in KC cells over time. All viruses identified in the cytoplasm of AHSV-infected KC cells were categorised as VP-Ves, VP-Mem or VP-Cyt particles. (A) Percentage of total virus particles in a particular intracellular virus distribution at a specific time post infection. The total number of virus particles in a specific intracellular distribution was divided by the total number of particles identified in the cytoplasm of 20 cells. (B) Average percentage of a particular intracellular virus distribution across 20 cells at a specific time post infection. The number of total viruses per cell identified in a particular intracellular distribution was determined and the percentage of each distribution category averaged across 20 cells.

2.3.2. Investigating the role of cellular transport pathways in AHSV trafficking

Transmission electron microscopy imaging indicated that AHSV particle distribution profiles in mammalian (BSR) and insect (KC) cells changed over time. These distribution profiles are probably the combined result of AHSV replication processes such as progeny virus production, trafficking and release; and the host cell's response to virus infection.

2.3.2.1. AHSV replication in mammalian and insect cell systems

Virus growth was studied by quantifying virus yield in mammalian and insect cell systems at 12 hpi, 18 hpi, 24 hpi and 48 hpi in BSR cells, and additionally at 70 hpi and 7 dpi in KC cells. Monolayers of BSR and KC cells seeded in 24-well plates were infected with AHSV-4 (section 2.2.3), and harvested at the indicated times after infection. Supernatants were separated from the cells by low speed centrifugation and both fractions were subjected to median tissue culture infective dose ($TCID_{50}$) assays (section 2.2.7). The virus titre from the supernatant was considered to be the released virus yield, while the titre from the cellular fraction represented the cell-associated virus yield. Total virus titres were obtained by combining the released and cell-associated titres. Three biological repeats were done for each time point.

Viral titres (Fig 20) reached a maximum of 7.6±0.4 $log_{10}TCID_{50}$/ml at 18 hpi in BSR cells, and 7.8±0.2 $log_{10}TCID_{50}$/ml at 48 hpi in KC cells. After these time points virus titres remained relatively unchanged in the respective cell lines. Initial virus titres at 12 hours post infection were comparable in BSR and KC cells. However, AHSV replication seemed to be slightly delayed in KC cells compared to BSR (Fig 20). In BSR cells, a noticeable increase in virus titre was observed between 12 hpi and 18 hpi, while in KC cells this was only observed between 24 hpi and 48 hpi. Cell-associated titres were highest at 18 hpi in BSR cells and at 48 hpi in KC cells, and formed the bulk of total titres in both cell lines at all of the time points. Released virus titres were highest at 48 hpi in BSR and KC cells. The growth of AHSV on BSR and KC cells was different, and reflects the prominent role of host cell processes in AHSV replication.

TEM analyses showed a proportion of the viruses associated with membranous cellular structures, specifically inside or associated with the cytoplasmic face of vesicles in close proximity to the plasma membrane. This alludes to the importance of vesicles in the late stages of AHSV replication. Membrane-trafficking pathways were subsequently targeted for biochemical inhibition.

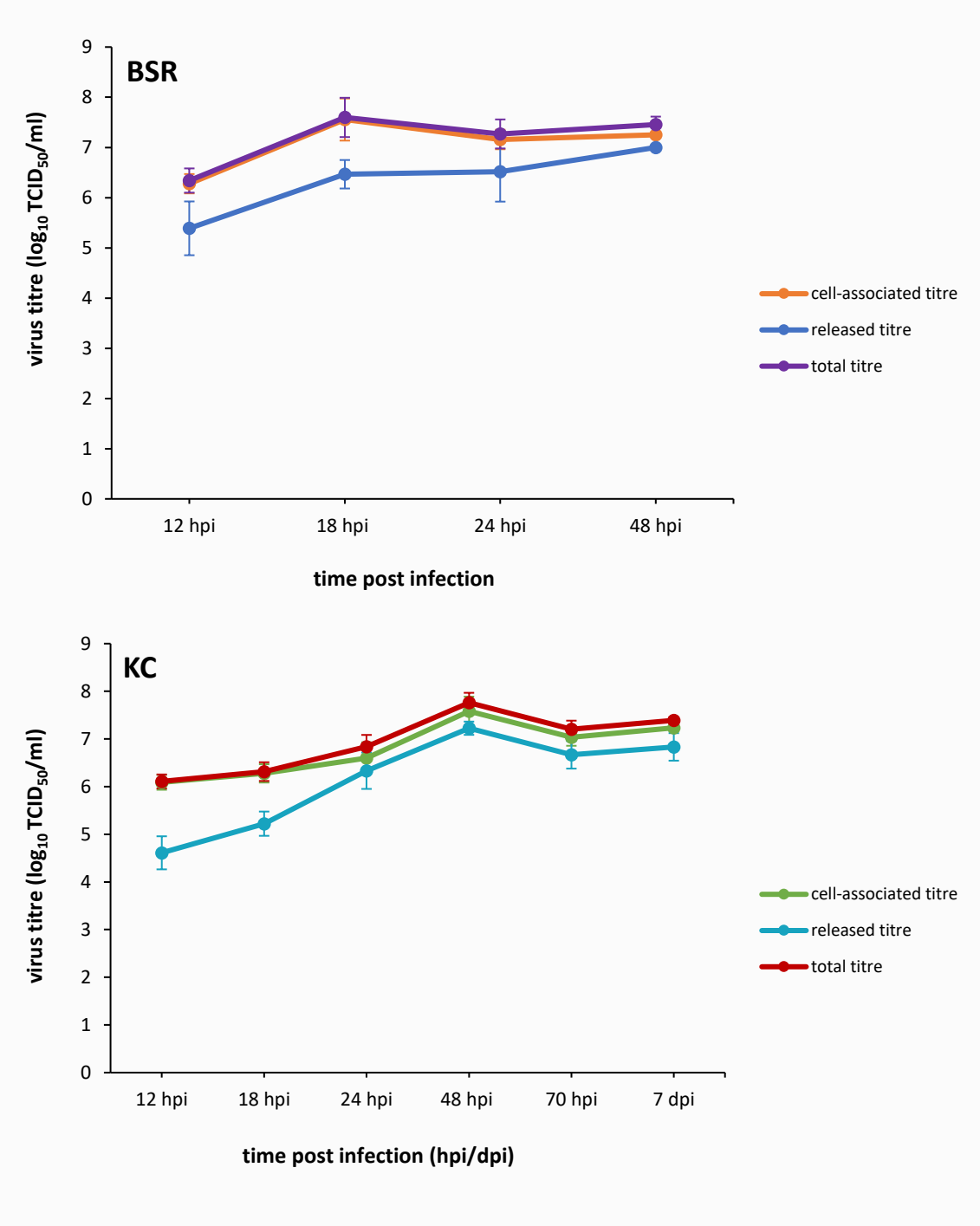

Figure 20. Virus growth after AHSV infection of mammalian and insect cells. Monolayers of BSR or KC cells were synchronously infected (MOI 1) and cell-associated, released and total (cell-associated + released) titres were determined at the indicated time points. Values represent the average of three independent titration experiments and bars represent the standard deviation.

2.3.2.2. Effect of inhibited cellular pathways on AHSV replication

In order to identify potential cellular pathways specifically involved in AHSV maturation and/or trafficking, components of the membrane-trafficking system were inhibited and virus replication assayed by virus titration. The effect of inhibition on total virus yield and virus release was determined by comparing treated and control samples.

Secretory pathway

Brefeldin A (BFA), a heterocyclic lactone produced by several fungi (HÄRRI *et al.* 1963), was used to investigate the role of the secretory pathway in AHSV replication. This system is made up of distinct organelles including the endoplasmic reticulum (ER), the Golgi apparatus, secretory vesicles, endosomes and the plasma membrane (KLAUSNER *et al.* 1992). It allows cells to regulate delivery of newly synthesised proteins, carbohydrates and lipids to the cell surface (LIPPINCOTT-SCHWARTZ *et al.* 2000). Applied to cells, BFA effectively halts ER- Golgi membrane-trafficking, inhibits a wide variety of membrane transformations of the trans-Golgi network, endosomal system and lysosomes and ultimately blocks protein secretion (FUJIWARA *et al.* 1988; HUNZIKER *et al.* 1991; LIPPINCOTT-SCHWARTZ *et al.* 1991; WOOD *et al.* 1991; KLAUSNER *et al.* 1992).

To evaluate the effect of BFA on AHSV replication, MTT cell viability assays were first done to determine the cytotoxicity of BFA on cells. Viability assays were done on uninfected and AHSV-infected cells, as BTV infection has been shown to affect the viability of cell lines differently (WECHSLER AND MCHOLLAND 1988). The pharmacological effect of BFA occurs within minutes of application, evident from the morphological changes in the Golgi apparatus (DONALDSON *et al.* 1990). Concentration and application time experiments were done for 4 h and 22 h exposure periods for BFA concentrations of 0.5 µg/ml, 1 µg/ml, 2.5 µg/ml, 5 µg/ml, and 10 µg/ml (MISUMI *et al.* 1986a; FUJIWARA *et al.* 1988; DONALDSON *et al.* 1990; REAVES AND BANTING 1992; WEI *et al.* 2008) to determine BFA tolerance in BSR and KC cells.

DMSO was used to reconstitute BFA. The effect of the BFA in DMSO, or DMSO only, on cell viability was therefore evaluated by comparing the viability of treated cells to untreated control cells. In addition, the tolerance of AHSV-infected culture was determined by incubating cells already infected with virus in the presence of BFA in DMSO, or only DMSO, for a 22 h period from 2 hpi to 24 hpi or for a 4 h period from 20 hpi to 24 hpi. After the incubation period, the media containing BFA was removed, cells stained with MTT, and the absorbance read by spectrophotometry (section 2.2.6). The percentage viable cells was calculated by dividing the average absorbance values of treated samples by control samples. Absorbance values greater than control indicated cell proliferation and lower values suggested cell death or inhibition of proliferation. The data from 22 h BFA exposure is summarised in Fig 21, controls were confluent monolayers of untreated mock-infected or AHSV-infected (MOI 1) cells incubated for 24 h.

A reduction in the viability of both mock and AHSV-infected BSR and KC cells (Fig 21 A, B) was observed in a dose-dependent manner with treatment of BFA or DMSO. KC cells seemed more sensitive to DMSO than BSR cells. The viability of KC cells decreased steadily with increasing concentrations of DMSO, while the viability of BSR cells remained comparable to the control at low DMSO concentrations (Fig 21; 0.4% (v/v) and 0.7% (v/v) DMSO). When BSR cells were treated with DMSO concentrations at or less than 1.8% (v/v), at least 60% of cells remained viable, which was only observed across all of the KC samples with DMSO concentrations at or less than 0.7% (v/v). The cell viability was comparable with regard to BFA and DMSO treatment at different concentrations, with the only exception being the viabilities of mock-infected KC cells treated with 2.5 µg/ml BFA and mock-infected KC cells treated with 1.8% (v/v) DMSO. Nevertheless, the comparability of BFA and DMSO sample viability suggested that the final DMSO concentration, and not the final BFA concentration, affected tolerance.

For the 4 h treatment period, similar results were obtained with DMSO concentrations at or less than 1.8% (v/v) in BSR cells and at or less than 0.7% (v/v) in KC cells (results not shown). At high concentrations of DMSO the viability of BSR cells treated for 4 h periods were higher than BSR cells treated for 22 h periods. In KC cells, DMSO treatment for 4 h periods opposed to 22 h periods resulted in higher viabilities at all concentrations. Constant DMSO levels with varying concentrations of BFA would have been optimal in this study, but was not done due to experimental constraints linked to stock reconstitution and dilution. It was decided to treat BSR cells with 0.5 - 2.5 µg/ml BFA, and KC cells with 0.5 - 1.0 µg/ml BFA for 22 h and then assay total virus yield and the percentage virus release.

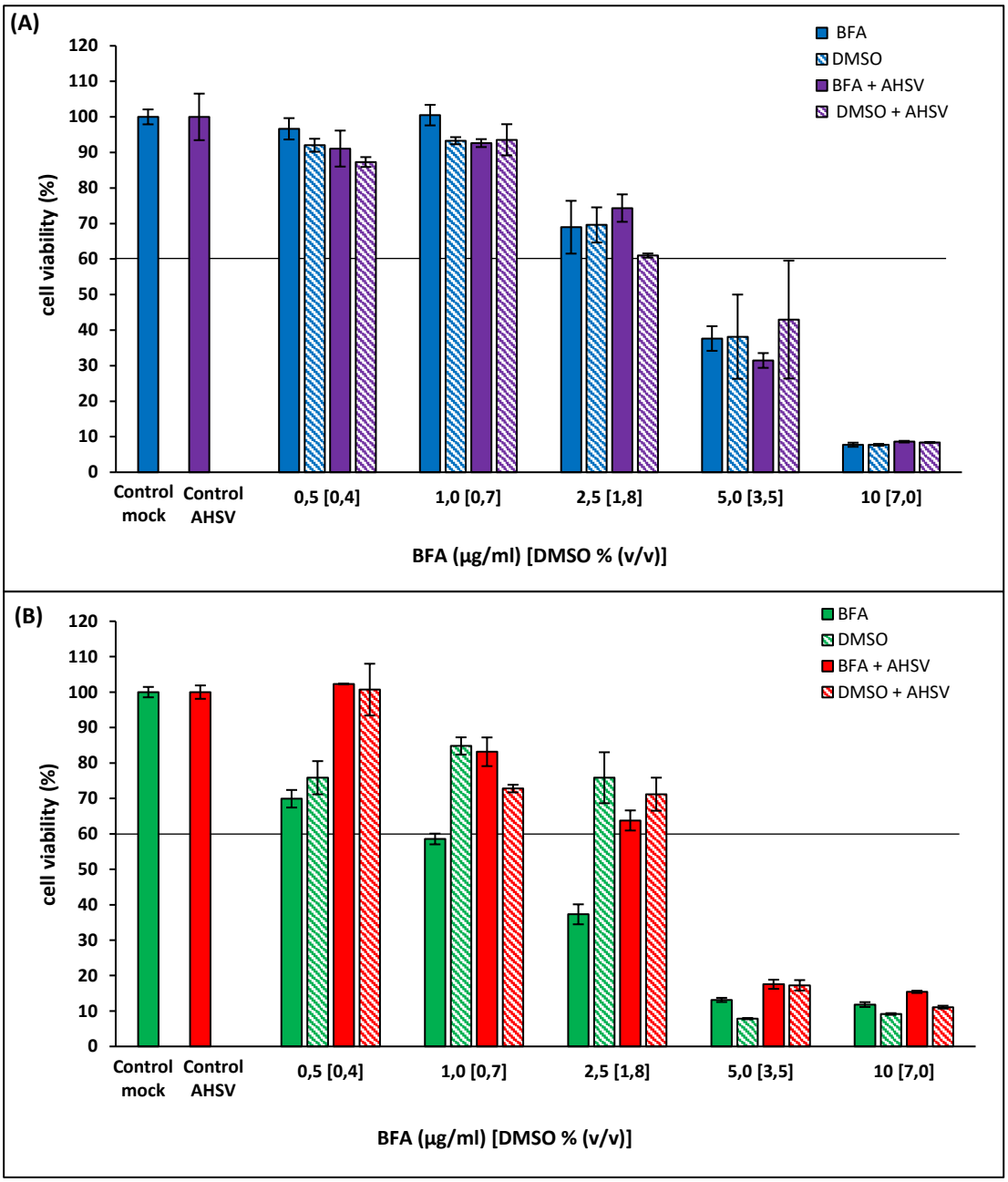

Figure 21. Evaluation of BFA and DMSO tolerance. (A) BSR cells and (B) KC cells were incubated in media containing different concentrations of BFA in DMSO (BFA) or DMSO only (DMSO). Controls were confluent monolayers of untreated mock- or AHSV-infected cells incubated only in media for 24 hours. Each value represents the average of 3 replicates, bars indicate the standard deviation. The viability of mock-infected cells treated with BFA or DMSO for the last 22 h of a 24 h incubation period was plotted as a percentage of the mock-infected untreated control. The viability of AHSV-infected cells treated with BFA or DMSO for 22 h from 2 hpi to 24 hpi were plotted as a percentage of the AHSV-infected untreated control. Line indicates the 60% cell viability tolerance threshold.

To determine the effect of BFA on AHSV replication, cells were virus infected (MOI 1), treated with BFA, and virus yield assayed at 24 hpi for BSR cells and 70 hpi for KC cells. Infected BSR cells were treated with BFA for 22 h from 2 to 24 hpi and infected KC cells for 22 h from 48 to 70 hpi. Controls were AHSV-infected cells incubated in medium without BFA. The supernatant and cells were harvested separately, and the released and cell-associated titres determined using $TCID_{50}$ assays (section 2.2.7). Total titres were the released and cell-associated titres combined. Three biological repeats were done in parallel, and the average virus titres of BFA-treated and control samples compared by two-tailed, paired T-tests.

Compared to the controls, a slight increase in total titre (Fig 22 A, B) was observed with BFA treatment in BSR and KC cells. Control total virus titres averaged at 7.4 $\log_{10} TCID_{50}$/ml in BSR cells and 7.2 $\log_{10} TCID_{50}$/ml in KC cells, and 2.5 µg/ml BFA treated samples averaged at 7.7 $\log_{10} TCID_{50}$/ml in BSR cells and 7.5 $\log_{10} TCID_{50}$/ml in KC cells. T-tests indicated no significant difference between the total titres of BFA-treated samples and controls. No significant difference was also found when the total titres were plotted as a relative percentage of the control virus titre (Fig 22 C, D), suggesting that virus production and/or maturation was not affected by BFA inhibition in BSR or KC cells. In untreated BSR cells 37% of the total virus yield was present in the medium at 24 hpi and thus represented released viruses (Fig 22 E), and in control KC cells 31% of the total titre was released at 70 hpi (Fig 22 F). BFA treatment cells significantly (p<0.01) reduced virus release in BSR cells in a dose-dependent fashion, with percentage release being reduced to less than 1% at BFA concentrations of 1 µg/ml or higher. In stark contrast to this, BFA treatment had no significant effect on virus release from KC cells at any of the concentrations tested (Fig 22 E, F).

To confirm that the reduction in virus release was the result of disrupted AHSV trafficking, and not inhibition of AHSV viral protein production, AHSV-4 NS2 expression was analysed by immunoblot (Fig 23). Western blot analysis of NS2 expression showed comparable expression in infected BFA treated and untreated BSR cells (Fig 23 A) and KC cells (Fig 23 B). Cellular actin (β-actin) and promyelocytic leukemia protein (PML) were used as loading controls for BSR and KC samples, respectively. BFA inhibition therefore did not perturb viral protein production or virus titre in BSR and KC cells, and additionally had no effect on virus release in KC cells. Virus release was however significantly inhibited by BFA treatment in BSR cells, indicating that the secretory pathway, probably the ER-Golgi membrane-trafficking pathway is important for AHSV trafficking in BSR cells.

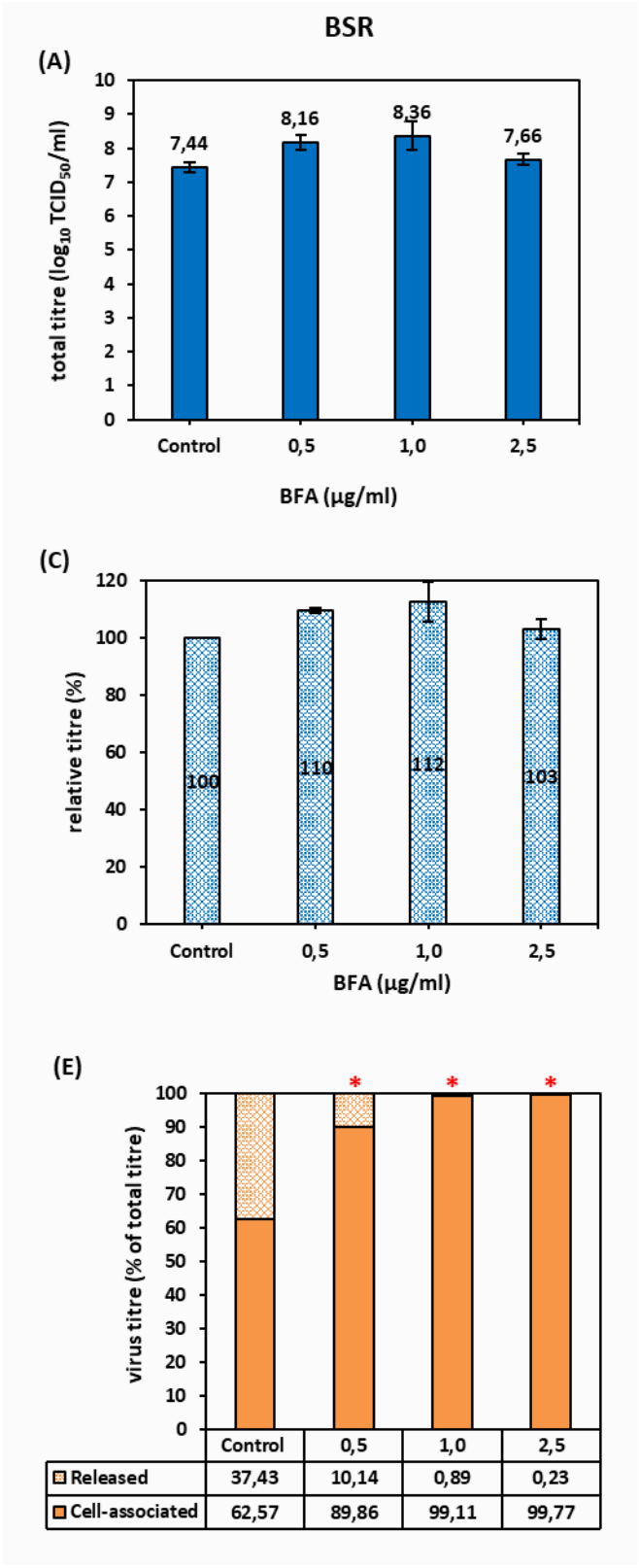

Figure 22. Effect of BFA on AHSV yield. (A-B) Total virus titre (cell-associated and released) in untreated control cells or cells treated with different concentrations of BFA, and (C-D) relative titres (treated/control) following treatment. (E-F) Percentage released and cell-associated virus in control cells or cells treated for 22 h with BFA (E) from 2 hpi to 24 hpi in BSR cells or (F) from 48 hpi to 70 hpi in KC cells. Values represent the average of 3 biological repeats and bars the standard deviation. Asterisks indicate significant difference ($p<0,01$) in percentage cell-associated and released virus of treated cells compared to control cells determined by paired T-test.

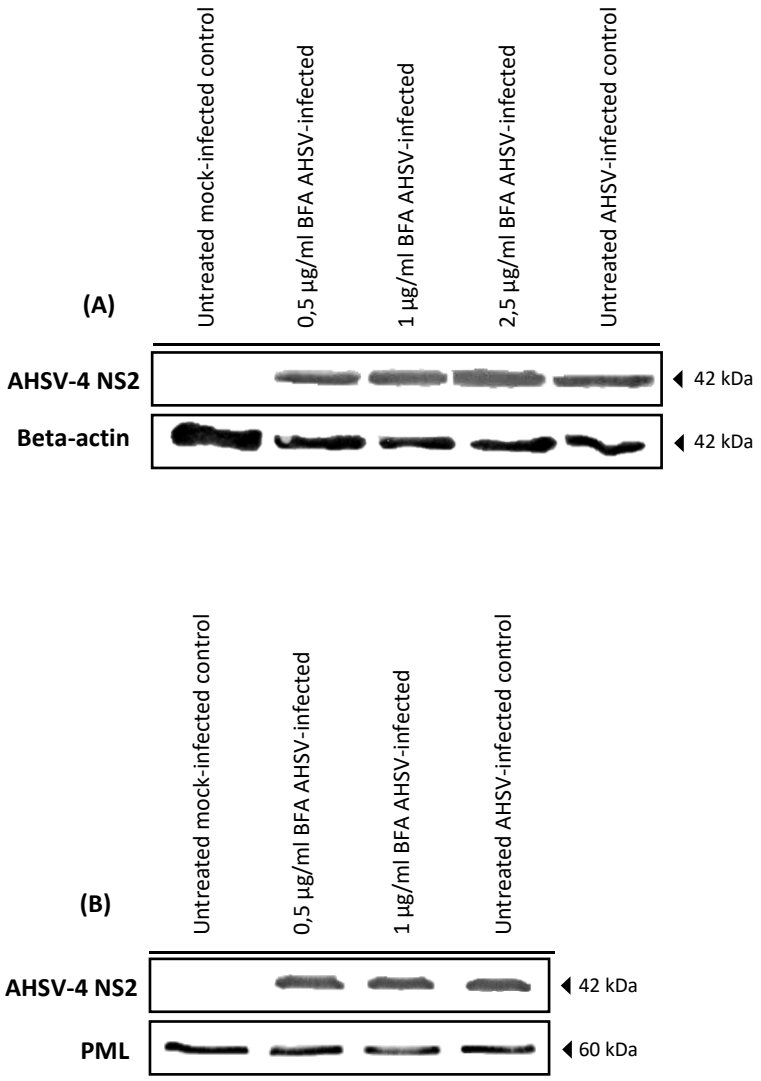

Figure 23. Western blot analysis of NS2 protein expression in BFA treated cells. (A) Treatment was applied for 22 hours from 2 hpi to 24 hpi in AHSV-infected BSR cells, and (B) for 22 hours from 48 hpi to 70 hpi in AHSV-infected KC cells. Lysates were harvested at 24 hpi for BSR cells and 70 hpi for KC cells. Molecular masses and proteins are indicated on right and left. Beta-actin and promyelocytic leukemia protein (PML) were the loading control in BSR cells and KC cells, respectively.

Ubiquitin-proteasome system

MG-132 (carbobenzoxyl-leucinyl-leucinyl-leucinal), a peptide aldehyde inhibitor of the proteasome, was used to investigate the role of the ubiquitin-proteasome system in AHSV replication. Applied to cells, MG-132 primarily blocks the chymotrypsin-like activity of the 26S proteasome responsible for the degradation of ubiquitinated cytosolic proteins (ROCK *et al.* 1994; LEE AND GOLDBERG 1996). This reduces the pool of free amino acids for protein synthesis (VABULAS AND HARTL 2005) and depletes free unconjugated ubiquitin in the cytoplasm (MIMNAUGH *et al.* 1997; LÓPEZ *et al.* 2011; BHATTACHARYA *et al.* 2015). Such ubiquitin molecules are used as sorting signals in the endosomal pathway.

Ubiquitin modification regulates sorting in the *trans*-Golgi network (HELLIWELL *et al.* 2001), entry into vesicular compartments such as MVBs (KATZMANN *et al.* 2001; REGGIORI AND PELHAM 2001; DEMIROV AND FREED 2004) and targets proteins to lysosomes (CIECHANOVER 2005; CLAGUE AND URBÉ 2010; LI *et al.* 2015). A previous study showed an interaction between AHSV NS3 and ubiquitin (BEYLEVELD 2007). Given the role of NS3 in trafficking, the ubiquitin-proteasome system may play a role in AHSV trafficking.

MTT cell viability assays were performed to evaluate the cytotoxicity of the inhibitor MG-132 on AHSV-infected BSR and KC cells. MG-132 is a highly potent inhibitor, its IC_{50} is a few micromolar for the inhibition of proteolysis in cells (LEE AND GOLDBERG 1998). Final concentrations of 0.5 µM, 1.0 µM, 5.0 µM, and 10 µM of MG-132 (PROSCH *et al.* 2003; OKUMURA *et al.* 2008; BHATTACHARYA *et al.* 2015) were applied to cells to determine tolerance. The length of time it takes for the pharmacological effect of the drug to decrease cell viability below the 60% threshold was tested with exposure periods of 6 h, 18 h and 24 h. Previous reports indicated that cell viability and growth are generally not affected for 10 - 11 h after treatment (ROCK *et al.* 1994).

Our previous results with BFA treatment showed that final DMSO concentrations above 1% (v/v) in BSR and KC cells significantly decreased the percentage of viable cells. Similar findings have previously been reported in BSR cells (CHE *et al.* 2009) and other cell lines (GALVAO *et al.* 2014). MG-132 was therefore reconstituted in DMSO to a stock concentration that could be diluted to the desired final MG-132 concentrations, and final DMSO concentrations at or below 1% (v/v). Cells were incubated in media containing only DMSO at final concentrations of 0.5% (v/v) and 1% (v/v) to determine the effect of these concentrations on cell viability. To determine the tolerance of AHSV-infected cells to MG-132 treatment mock-infected and virus-infected cells were treated for 6 h from 1 hpi to 7 hpi and the MTT assays performed as done previously. Controls were monolayers of untreated mock-infected or AHSV-infected (MOI 1) cells incubated for 7 h. The percentage viable cells from treated samples were plotted as percentages of the control. The data from 6 h MG-132 exposure is summarised in Fig 24.

An equivalent reduction in cell viability was observed in BSR cells and KC cells at different MG-132 concentrations (Fig 24 A, B). Treated mock-infected BSR cells showed high variability (Fig 24 A), and only treated AHSV-infected BSR cell viability data was used to evaluate MG-132 tolerance in BSR cells. The viability of all treated samples was above the 60% threshold in both cell lines. The percentage of viable cells for treated AHSV-infected samples were comparable to respective 0.5% and 1% DMSO only samples, indicating that DMSO concentration mostly affected cell viability and not MG-132 concentration. Consistently, the viability of cells incubated in media containing only 0.5% (v/v) DMSO and cells containing 0.5% (v/v) DMSO and 5 µM MG-132 was the highest compared to other concentrations in both BSR and KC cells. The viability of BSR cell and KC cells treated for 18 h or 24 h periods with 0.5 µM, 1 µM and 10 µM were generally below the viability threshold (results not shown). It was decided to use the three concentrations of MG-132 that showed the highest percentage viable cells, i.e. 0.5 µM, 5 µM and 10 µM (Fig 24), with a 6 h exposure period in downstream experiments.

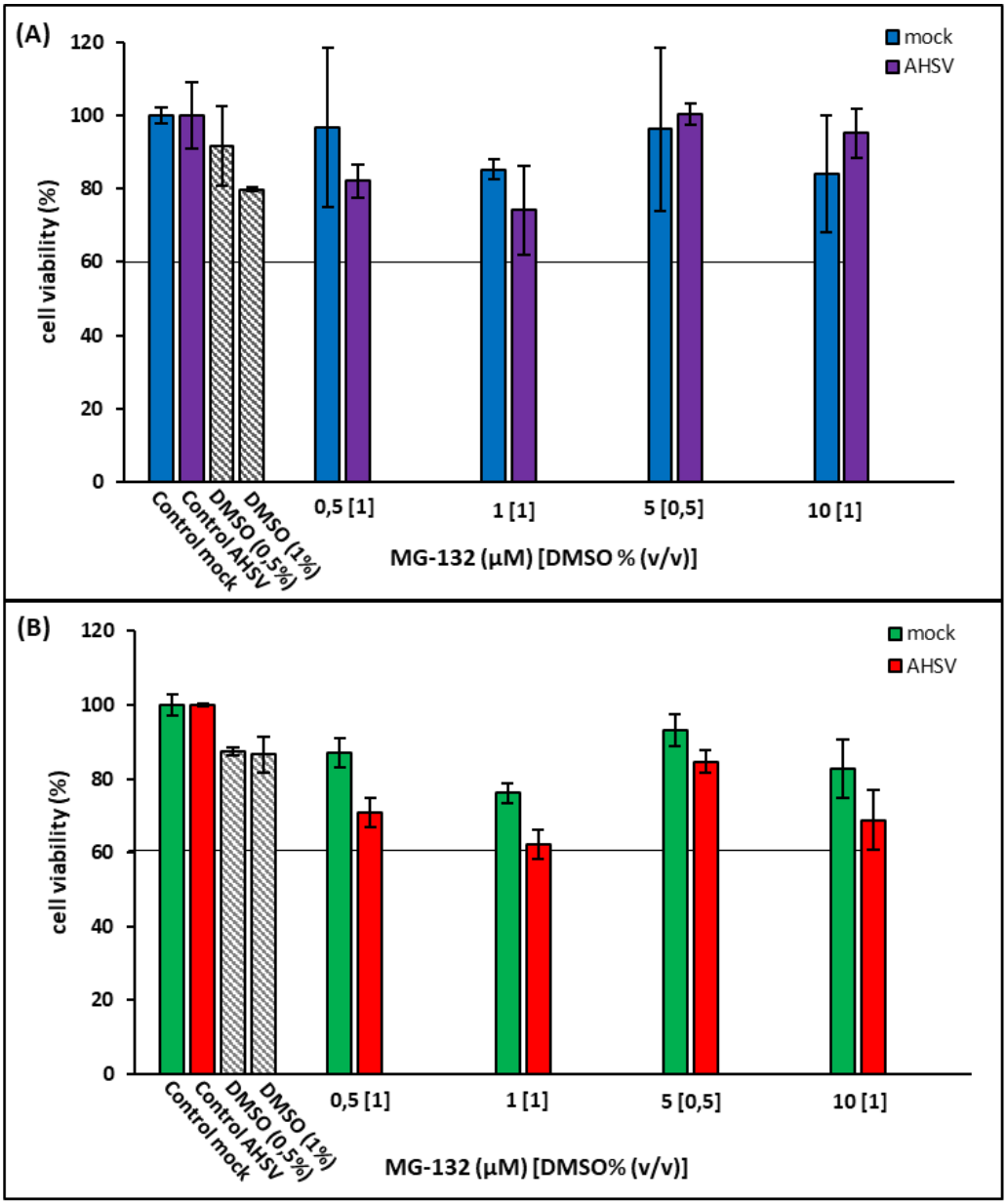

Figure 24. Evaluation of MG-132 tolerance. (A) BSR cells and (B) KC cells were incubated in media containing different concentrations of MG-132. The inhibitor was reconstituted in DMSO, and final DMSO concentrations at 0,5% (v/v) and 1% (v/v) were used. Controls were confluent monolayers of mock- or AHSV-infected (MOI 1) cells incubated in media only. Each value represents the average of 3 replicates, bars indicate the standard deviation. The viability of mock-infected cells and AHSV-infected cells treated with MG-132 for 6 h from 1 hpi to 7 hpi were plotted as percentages of the corresponding untreated controls. Line indicates the 60% cell viability tolerance threshold.

To determine the effect of MG-132 on AHSV replication, cells were infected (MOI 1), treated with MG-132 and assayed at 24 hpi in BSR cells and 46 hpi in KC cells. Treatment was applied for 6 h, from 18 hpi to 24 hpi and from 40 hpi to 46 hpi, in BSR cells and KC cells respectively. Titres of treated samples were compared to control samples, which were AHSV-infected cells incubated in MG-132 free medium. Total virus titres and percentages of virus release were determined and compared as done previously.

With the application of MG-132, total titres decreased relative to the controls in both BSR and KC cells (Fig 25 A, B). The average virus titre in untreated controls was 8.0 $\log_{10}$ $TCID_{50}$/ml in BSR cells and 7.8 $\log_{10}$ $TCID_{50}$/ml in KC cells. Total titres of treated KC cells decreased by a log-fold and around a 20% drop was found in relative titres of treated KC cells (Fig 25 B, D). No statistically significant differences were however observed between the total titres or even the relative titres of control versus treated KC cells. This was attributed to the variability between repeats. With increasing MG-132 concentrations, the percentage virus release seemed to increase in BSR cells, while it decreased in KC cells (Fig 25 E, F). The difference between percentage virus released from untreated and 10 µM MG-132 treated cells was more pronounced in KC cells than in BSR cells.

The percentage virus release was reduced from 33% to 9% in KC cells upon treatment with 10 µM MG-132, while virus release increased from 15% to 27% in BSR cells. No statistical significant difference was observed as the titres between samples within treatment groups varied. Our virus growth studies (section 2.3.2.1) showed 21% of total virus yields released from BSR cells at 24 hpi, and 32% of total virus yields released from KC cells at 48 hpi. The percentages of virus release reported here for 5 µM and 10 µM MG-132 in BSR cells were comparable to virus release in the virus growth studies, and MG-132 treatment may not affect virus release. In contrast, virus release reported for KC cells treated with 5 µM and 10 µM MG-132 were notably decreased compared to virus release in the virus growth studies. This indicates that MG-132 affects virus release from KC cells and not BSR cells. The observed decrease in virus release from KC cells was however not statistically significant, attributed to the variability between repeats (Fig 25 B).

It is possible that MG-132 may impair cellular translation and could inhibit AHSV replication, which would explain the observed reduction in total virus titres in BSR cells and KC cells. The effect of MG-132 treatment on AHSV protein production was therefore analysed by immunoblot (Fig 26). The same loading controls that were used in the previous experiment were used here. AHSV NS2 expression in AHSV-infected MG-132 treated samples was comparable to untreated AHSV-infected control samples in BSR cells (Fig 26 A) and KC cells (Fig 26 B). Proteasome inhibition did therefore not perturb AHSV NS2 protein expression in these cell lines.

The values obtained for total virus yield and virus release in BSR cells indicated that proteasome inhibition probably does not affect AHSV replication in mammalian cells. In KC cells, only viral protein expression was unaffected by MG-132 treatment, while decreased total virus yields and virus release were observed with

MG-132 treatment. As total virus yields between samples treated at different concentrations of MG-132 was comparable, the concentration-dependent decrease of virus release was therefore not attributed to a decrease in mature AHSV particles. Although our data was not statistically significant, it does seem as if inhibition of an active 26S proteasome might impact on efficient AHSV replication and release in KC cells.

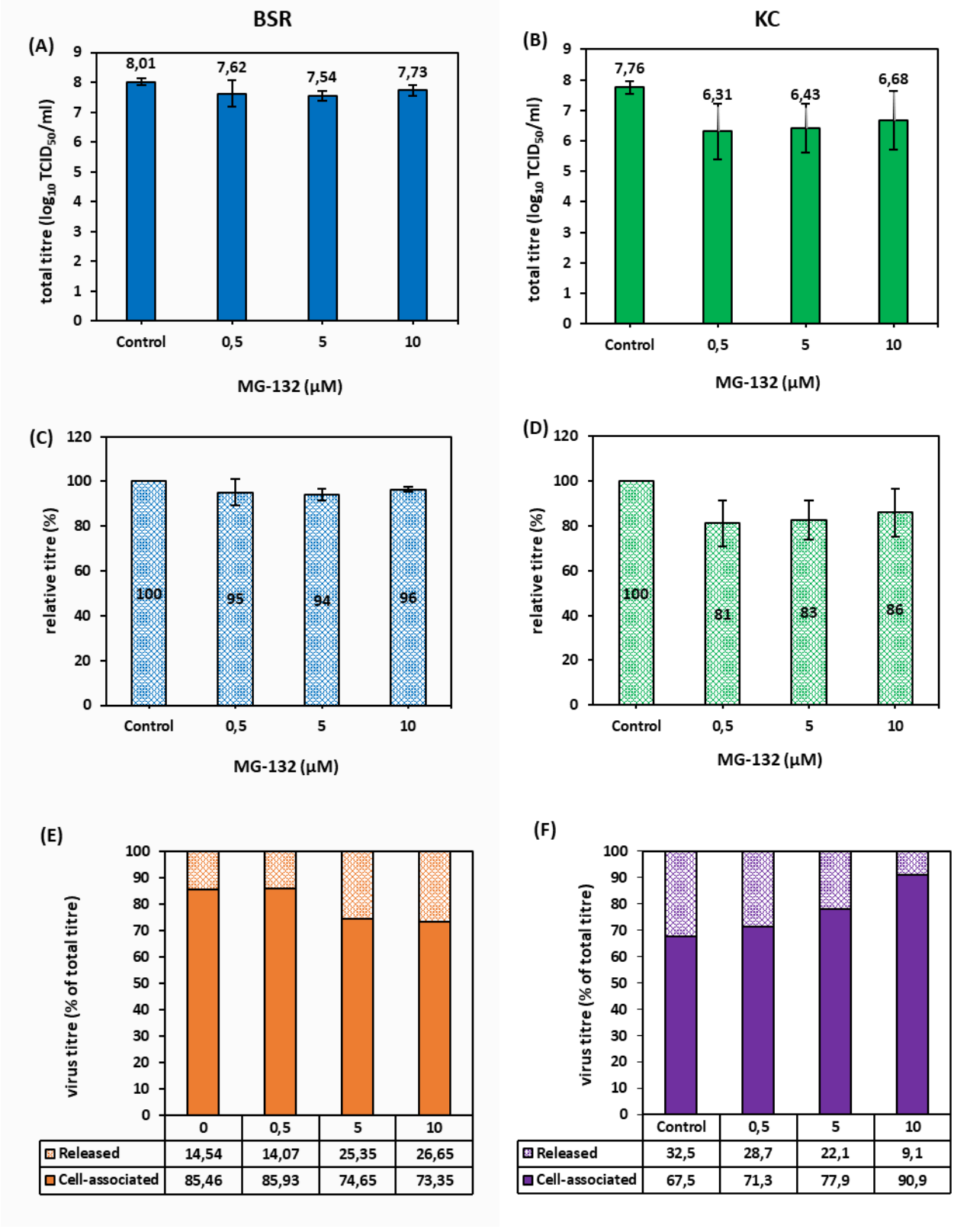

Figure 25. Effect of MG-132 on AHSV yield. (A-B) Total virus titre (cell-associated and released) in untreated control cells or cells treated with different concentrations of MG-132, and (C-D) relative titres (treated/control) following treatment. (E, F) Percentage released and cell-associated virus in control cells or cells treated for 6 h with MG-132 (E) from 18 hpi to 24 hpi in BSR cells or (F) from 40 hpi to 46 hpi in KC cells. Values represent the average of 3 biological repeats and bars the standard deviation. No statistical differences were found between samples.

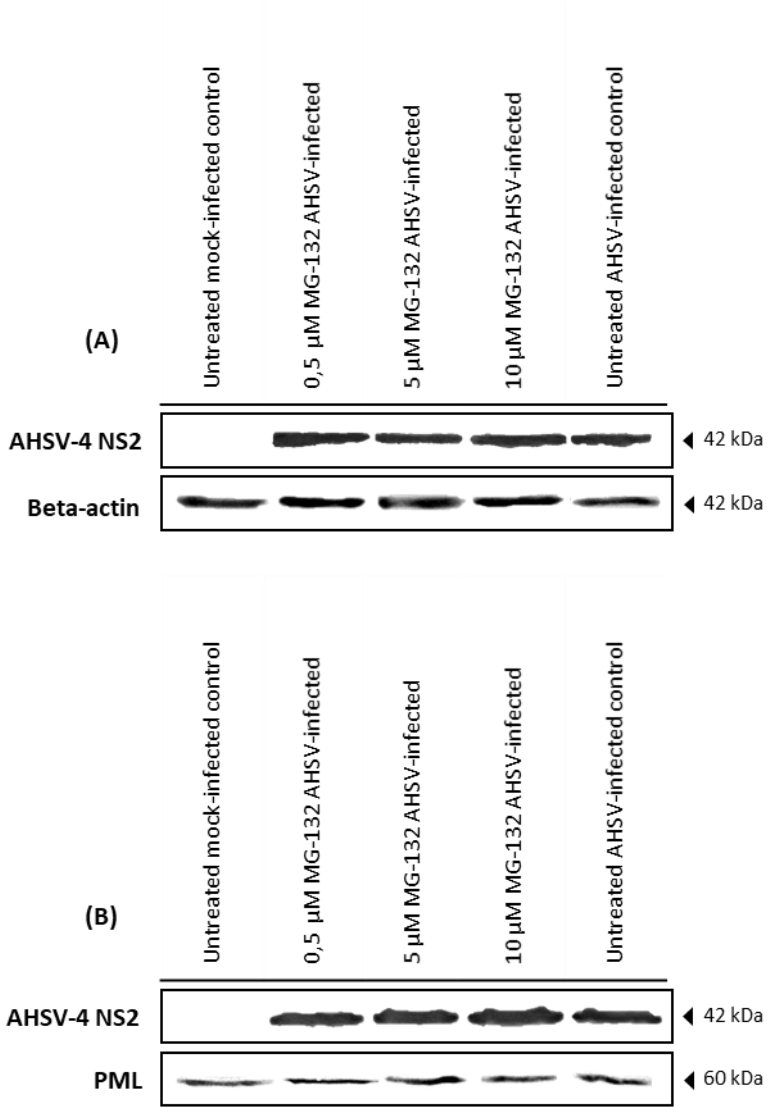

Figure 26. Western blot analysis of NS2 protein expression in MG-132 treated cells. (A) Treatment was applied for 6 hours from 18 hpi to 24 hpi in AHSV-infected BSR cells, and (B) from 40 hpi to 46 hpi in AHSV-infected KC cells. Lysates were harvested at 24 hpi for BSR cells and 46 hpi for KC cells. Molecular masses and proteins are indicated on right and left. Beta-actin and promyelocytic leukemia protein (PML) were the loading control in BSR cells and KC cells, respectively.

Phosphatidylinositol 3-kinase signalling

LY-294002, a bioactive molecule called 2-(4-morpholinyl)-8-phenyl-4H-l-benzopyran-4-one, that specifically and completely inhibits phosphatidylinositol 3-kinase (PI3K) activity (Vlahos *et al.* 1994), was used to investigate the role of PI3K in AHSV replication. PI3Ks are lipid kinases responsible for the phosphorylation of phosphatidylinositol (PI) to produce three lipid products called phosphatidylinositol-3-phosphate (PI3P), phosphatidylinositol-3,4-biphosphate (PI-3,4-P_2) and phosphatidylinositol-3,4,5-trisphosphate (PIP_3). These lipids bind to protein motifs and control the activity and subcellular localisation of a variety of signal transduction molecules (DOWLER *et al.* 2000) essential in membrane trafficking processes such as early endosome fusion (JONES AND CLAGUE 1995), lysosomal protein sorting (BROWN *et al.* 1995), MVB biogenesis (FERNANDEZ-BORJA *et al.* 1999; FUTTER *et al.* 2001) and autophagosome formation (BLOMMAART *et al.* 1997). PI3K activity is required for many cellular processes involving membrane traffic. Our TEM analysis showed AHSV particles inside vesicles, associated with the cytoplasmic face of vesicles and membranous structures. Membrane trafficking pathways may therefore play an important role in the final stages of AHSV replication.

Different concentrations of LY-294002 were applied to BSR and KC cells and the cytotoxicity of the inhibitor evaluated by MTT cell viability assays. The tolerance of cells to LY-294002 was determined at final concentrations of 10 µM, 50 µM, 80 µM, and 100 µM (LEE *et al.* 2005; EHRHARDT *et al.* 2007; ZHANG *et al.* 2010a; BHATTACHARYA *et al.* 2015) with exposure for 8 h and 24 h in uninfected cells, and with exposure for 6h in AHSV-infected cells from 12 hpi to 18 hpi. LY-294002 is highly potent with a IC_{50} of a few micromolar against the phosphorylating activity of many PI3K isoforms (PATEL *et al.* 2004). The data from 24 h exposure in mock-infected cells and 6 h exposure in AHSV-infected cells are summarised in Fig 27. Controls were monolayers of untreated mock-infected cells incubated for appropriate times. LY-294002 was dissolved in DMSO, the different concentrations of the inhibitor were all in 0.07% (v/v) DMSO. The effect of the DMSO was evaluated by incubating mock-infected cells in medium containing only 0.07% (v/v) DMSO.

Cells seemed generally unaffected by a 24 h application of 10 – 100 µM of LY-294002 (Fig 27 A, C). The viability of BSR cells decreased below 85% at 80 µM and 100 µM LY-294002, while the viability of KC cells remained above 90% at these concentrations. Similar results were obtained for the 8 h exposure period (not shown). Based on the study done by Bhattacharya *et al.* (2015) for BTV, we decided to use a 6 h exposure period. Subsequently, the viability of AHSV-infected cells treated with 100 µM LY-294002 for 6 h was determined (Fig 27 C, D) and it equated to the viability of mock-infected treated cells and controls in BSR and KC cells. Seeing as the viability of all treated cells was far above the 60% threshold, it was decided to treat AHSV-infected cells with 10 µM, 50 µM and 100 µM LY-294002 for 6 h to assess the role of PI3Ks in AHSV replication.

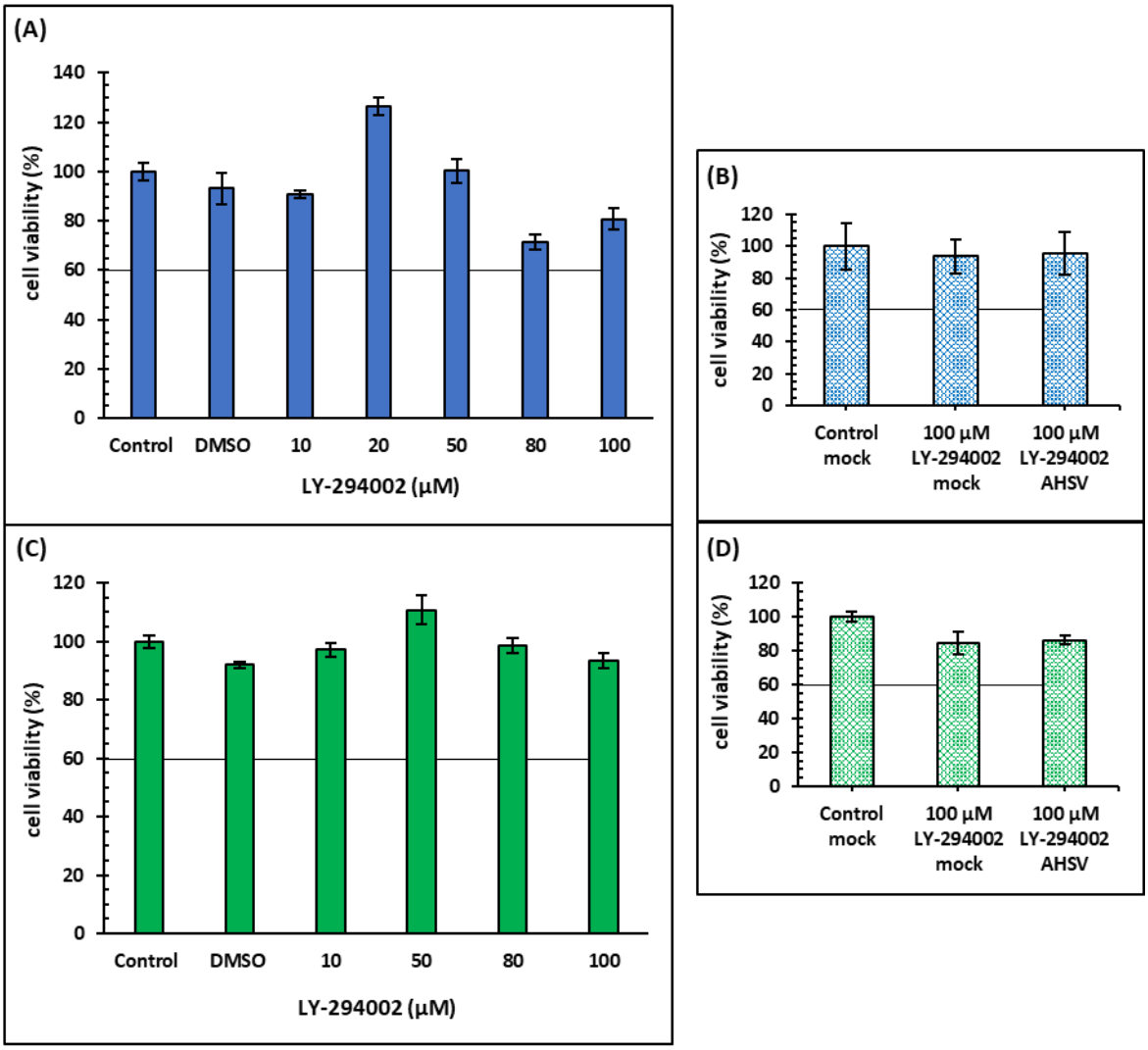

Figure 27. Evaluation of LY-294002 tolerance. (A-B) BSR cells and (C-D) KC cells were incubated in media containing different concentrations of LY-294002 in 0,07% (v/v) DMSO (A, C) The viability of uninfected cells treated with DMSO or LY-294002 for 24 h were plotted as percentages of the untreated cells incubated in media only. (B, D) The viability of mock- or AHSV-infected (MOI of 1) cells treated with 100 µM LY-294002 for 6 h from 12 hpi to 18 hpi were plotted as percentages of the untreated mock-infected control cells incubated in media for 18 hours. Each value represents the average of 3 (A, C) or 4 (B, D) replicates and the bars indicate the standard deviation. Line indicates the 60% cell viability tolerance threshold.

To evaluate AHSV replication in cells with inhibited PI3K activity, cells were infected at an MOI of 1 with AHSV, treated with LY-294002 and subjected to virus yield titration. The total virus titre, relative titre and percentage released virus was calculated from these titration experiments. Since LY-294002 application restricts the entry of some viruses via the PI3K/Akt pathway (SAEED *et al.* 2008), BSR cells were treated from 18 hpi to 24 hpi and KC cells from 40 hpi to 46 hpi at which point the supernatant and cells were harvested separately and the titre determined and compared as was done for previous assays.

Total virus titres in BSR and KC cells decreased in a dose-dependent fashion with increasing LY-294002 concentrations (Fig 28 A, B). In KC cells, a significant reduction ($p<0.001$) in total titre was observed with the application of 100 µM LY-294002 (Fig 28 B). When total titres of treated KC samples were plotted as a percentage of the control, a more significant reduction ($p<0.0001$) in relative titre was observed (Fig 28 D). In BSR cells, relative titres showed no statistically significant differences upon LY-294002 treatment (Fig 28 C). The average percentages virus release in treated and control untreated KC cells were similar across all concentrations (Fig 28 F), indicating that AHSV trafficking and release was not affected. Virus growth studies (section 2.3.2.1) reported that at early times post infection (12 hpi and 18 hpi) approximately 10% - 13% of the total virus yield was released. Virus release observed from BSR samples treated with 10 µM and 50 µM LY-294002 was comparable to these results, whereas 100 µM LY-294002 treated BSR cells showed increased virus release (Fig 28 E).

The decrease in total yield could be the result of an inhibition of AHSV protein synthesis. AHSV-4 NS2 expression was therefore immunoblotted to assess whether this is the case. Western blot analysis of NS2 production in BSR cells (Fig 29 A) showed equivalent expression in treated and untreated cells. Relative to the loading control, NS2 expression in KC cells appear decreased with increasing LY-294002 concentrations (Fig 29 B). The signal strength of the loading control makes the interpretation of the blot difficult, and repeated efforts to increase signal resolution was not successful. Host translation may therefore have been impacted to a certain extent KC cells with the application of LY-294002.

Virus yield and viral protein expression data obtained from experiments in KC cells suggests that PI3K signalling plays a role in AHSV replication, while virus yield and release data from BSR cells suggest that PI3Ks may play a role in the final stages of replication. The data presented here is not sufficient to implicate a role for PI3Ks in AHSV replication in both cell culture systems and further investigation is needed.

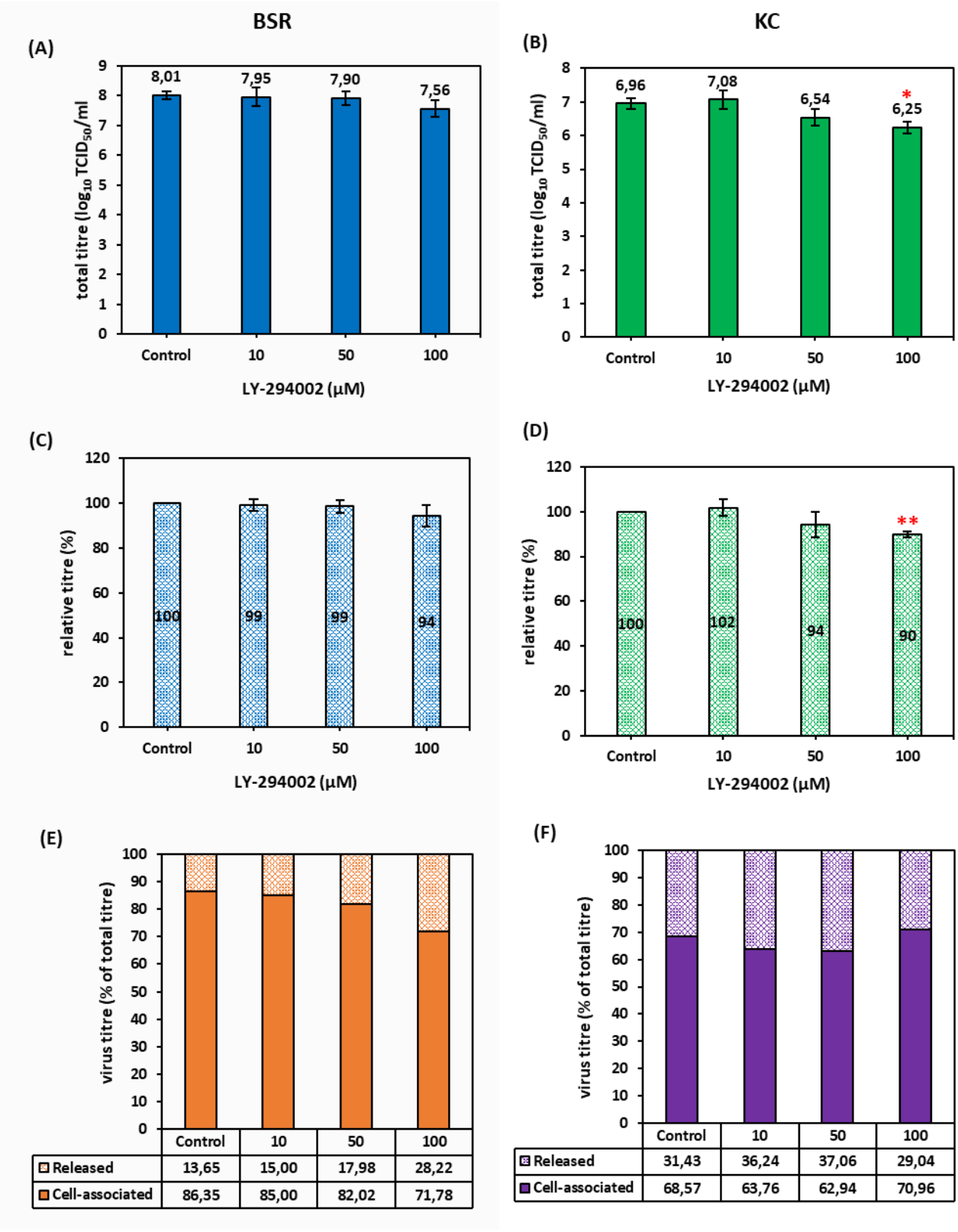

Figure 28. Effect of LY-294002 on AHSV yield. (A-B) Total virus titre (cell-associated and released) in untreated control cells or cells treated with LY-294002, and (C-D) relative titres (treated/control) following treatment. (E-F) Percentage virus release and cell-associated virus in control cells or cells treated for 6 h with LY-294002 from 12 hpi to 18 hpi in BSR cells and in KC cells. Values represent the average of 4 biological repeats and bars the standard deviation. Asterisks indicate significant difference (* p<0,001; ** p<0,0001) between total virus titre and relative titre of treated cells from control cells determined by paired T-test.

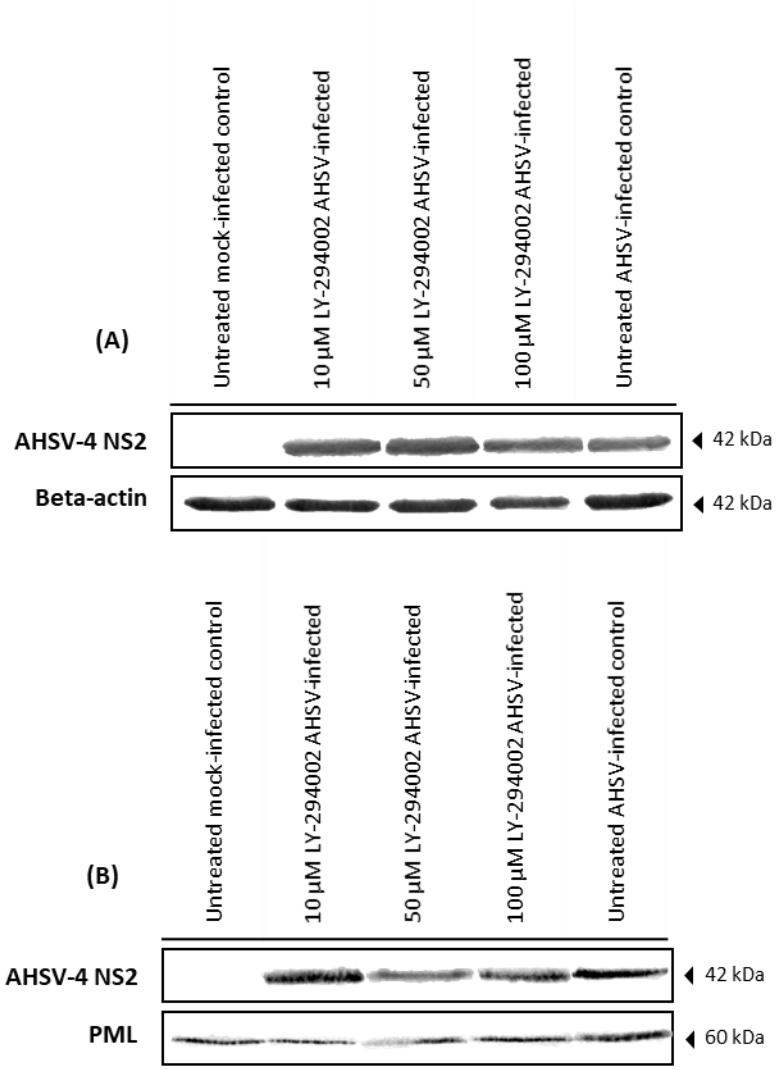

Figure 29. Western blot analysis of NS2 protein expression in LY-294002 treated cells. Treatment was applied for 6 hours from 12 hpi to 18 hpi in (A) AHSV-infected BSR cells and (B) AHSV-infected KC cells. Lysates were harvested at 18 hpi for BSR cells and 18 hpi for KC cells. Molecular masses and proteins are indicated on right and left. Beta-actin and promyelocytic leukemia protein (PML) were the loading control in BSR and KC cells respectively.

2.4. Discussion

The series of events leading to AHSV release from an infected cell is unclear. Previous studies on the final stage of virus replication have focused on virus release by studying BTV replication. These studies concluded that BTV NS3/3A is essential for virus release due to its interaction with cellular factors such as membrane trafficking protein calpactin, members of the MVB pathway i.e. ESCRT complexes, ubiquitin ligases, and outer capsid proteins VP2 and VP5 (BEATON *et al.* 2002; WIRBLICH *et al.* 2006; BHATTACHARYA AND ROY 2008). However, these interactions also implicate a role for NS3 and cellular membrane trafficking pathways in virus transport. When and where the outer capsid proteins VP2 and VP5 are assembled onto core particles is still unclear, but their lack of association with VIBs and characterised host interactions (EATON *et al.* 1987; BHATTACHARYA *et al.* 2007; BHATTACHARYA AND ROY 2008) suggest it to be coupled with trafficking. It has been postulated that the usurpation of specific cellular trafficking pathways for virus transport underlie the mechanism of release i.e. lytic or non-lytic which contribute to the CPE observed in cells (WIRBLICH *et al.* 2006). A detailed understanding of orbivirus trafficking is therefore an important step in understanding virus assembly, release and cellular pathogenicity. For this reason, this study aimed to provide insight into the cellular-related events underlying AHSV trafficking and release in mammalian and insect cells.

Like other members of the *Reoviridae* family, AHSV replicates in the cytoplasm of infected cells. Trafficking of various virus components therefore occur within the cytoplasm of infected cells. This study specifically focused on documenting the localisation of mature AHSV particles. In eukaryotic cells, free diffusion of molecules larger than 500 kDa is restricted due to molecular crowding from organelles, the cytoskeleton and high protein concentrations of up to 300 mg/ml (LUBY-PHELPS 1999; LUKACS *et al.* 2000). Mature AHSV particles are much larger than 500 kDa, thus AHSV trafficking has to occur by active processes such as cellular transport pathways and not diffusion.

This was the first systematic approach to comparatively describe the intracellular location of mature AHSV particles in mammalian (BSR) and insect (KC) cell culture systems over time. Transmission electron microscopic analyses of samples were done at early (12 hpi), intermediate (24 hpi) and late (48 hpi and additionally 72 hpi in KC cells) times post infection. Given the time post infection, observed particles were newly synthesised and in the process of being trafficked to the plasma membrane. AHSV particles were found inside spherical membrane-bound cytoplasmic structures of varying sizes, on the cytoplasmic face of said structures, associated with membranous structures or freely dispersed in the cytoplasm. Observations of viruses inside or associated with similar looking vesicle or membrane structures were made at different intracellular locations in a single cell, in different cells of a population, in different cell populations, and in mammalian and insect cells and at different times post infection. When the intracellular localisation of viruses was recorded and quantified, it was noted that discreet differences occurred over time in each system and between the two different cell culture systems.

In mammalian cells, viruses predominantly distributed into the lumen of vesicles at early times, and to the cytoplasm at later times after infection. In insect cells, viruses predominantly distributed in the cytoplasm throughout the course of infection. Of note, there was twice as many viruses inside vesicles in insect cells at 12 hpi than at any of the later times. This suggests that there may be some important differences in the cellular processes underlying AHSV trafficking between mammalian and insect cells.

AHSV particles have previously been reported inside the lumen of vesicles in Vero (mammalian) cells and KC cells (VENTER *et al.* 2014), but not associated with the cytoplasmic face of vesicles. Other orbiviruses where virions have been reported inside the lumen of vesicles or associated with the cytoplasmic face of vesicles are BTV in mammalian cells (HYATT *et al.* 1991; GOULD AND HYATT 1994; BHATTACHARYA *et al.* 2015) and insect cells (CELMA AND ROY 2011), and Peruvian horse sickness virus in mosquito-derived C6/36 cells (ATTOUI *et al.* 2009). Vesicles containing or associated with AHSV particles were frequently observed in close proximity to the plasma membrane, which alludes to the involvement of vesicles in the trafficking of virus to exit the cell. In support, poliovirus release is mediated by vesicles tethered to microtubules in mammalian cells (TAYLOR *et al.* 2009). The origin of these vesicles, and whether they are virus-induced, is unknown, but implicate the involvement of membrane-related trafficking events in AHSV transport.

Many of the virus-containing vesicles in mammalian cells were small intracellular vesicles, and based on vesicle diameter, membrane-bound morphology (single or double) and the electron density of content, these vesicles looked like secretory vesicles (PIGINO *et al.* 2012). More than one of these vesicles containing virus particles were observed in mammalian cells, especially at early times after infection. The virus-containing vesicles observed in insect cells also resembled secretory vesicles. These vesicles could also easily have been early endosomes or recycling endosomes from the recycling endocytic route. Other virus-containing vesicles in mammalian and insect cells contained free internal vesicles, thereby resembling late endosomes (also known as multivesicular bodies (MVBs) or multivesicular endosomes (MVEs)) (MURK *et al.* 2003). Some of the virus-associated vesicles observed on occasion could also have been lysosomes (CIECHANOVER 2005). Based on content only, the large vesicle-like structures observed in KC cells looked like the autophagic vacuoles observed after hepatitis C infection (AIT-GOUGHOULTE *et al.* 2008). These structures comprise different membrane-trafficking pathways in cells and implicate their potential involvement in AHSV transport. Membrane-trafficking pathways have been linked to viral transport for other non-enveloped viruses such as BTV (BHATTACHARYA *et al.* 2015), rotavirus (JOURDAN *et al.* 1997; CUADRAS AND GREENBERG 2003), and poliovirus (JACKSON *et al.* 2005; TAYLOR *et al.* 2009). Thus, membrane-trafficking pathways involving the most frequently observed vesicle structures, namely secretory vesicles and endosomes, were targeted for inhibition with the application of pharmacological agents.

Brefeldin A (BFA) was used to effectively block the secretory pathway which involves the ER, Golgi complex, secretory vesicles and the plasma membrane. Applied to cells, BFA causes the dissociation of peripheral membrane proteins from the Golgi apparatus (DONALDSON *et al.* 1990) and the redistribution of Golgi

membranes, proteins and contents into the ER lumen which effectively destroys the native function of the Golgi complex (MISUMI *et al.* 1986b; DOMS *et al.* 1989; LIPPINCOTT-SCHWARTZ *et al.* 1989). As a result, BFA affects a wide variety of membrane transformations of endosomes, lysosomes, and the *trans*-Golgi network along with the cytoskeleton organisation of cells that ultimately inhibit membrane traffic from the ER (FUJIWARA *et al.* 1988; HUNZIKER *et al.* 1991; LIPPINCOTT-SCHWARTZ *et al.* 1991; WOOD *et al.* 1991; ALVAREZ AND SZTUL 1999).

At a molecular level, BFA inhibits guanosine exchange activity of the ADP-ribosylation factor (ARF) family (DONALDSON *et al.* 1992b; HELMS AND ROTHMAN 1992). The ARF family comprise a group of small (21 kDa) GTP-binding cytoplasmic proteins that are key regulators of vesicle synthesis (SCHEKMAN AND ORCI 1996). When bound to GTP, ARFs localize to membranes which prompts the recruitment and assembly of a protein coat, either the coatomer or clathrin complexes. This deforms the underlying membrane into a budding vesicle (DONALDSON *et al.* 1992a; STAMNES AND ROTHMAN 1993; WHITNEY *et al.* 1995), which eventually results into the release of a coated vesicle. When hydrolysis of ARF-GTP occurs, the protein coat and ARF-GDP are released into the cytoplasm to be recycled by a guanosine exchange factor, resulting in new ARF-GTP that renew the budding process (TANIGAWA *et al.* 1993). BFA inhibits this exchange step, effectively segregating ARF to the cytosol and preventing vesicle formation.

At the Golgi complex, ARFs are necessary for a component of the coatomer called β-COP to bind to the Golgi membrane (DONALDSON *et al.* 1992a). The coatomer is a cytoplasmic protein complex of seven polypeptide chains that binds to non-clathrin coated structures associated with Golgi membranes and Golgi-derived transport vesicles (SERAFINI *et al.* 1991; WATERS *et al.* 1991), regulating intracellular membrane traffic and organelle structure (KLAUSNER *et al.* 1992). BFA causes rapid redistribution of β-COP into the cytoplasm and the release of the coatomer from membranes (DONALDSON *et al.* 1990) which halts vesicle traffic from the Golgi complex. We used BFA to evaluate whether vesicle-dependent transport from the Golgi complex play a role in the late stages of AHSV replication.

In mammalian cells, we found BFA as a potent inhibitor of AHSV release, but not particle morphogenesis or viral protein translation. Unpublished data by Eaton, Hyatt and Gould cited in (HYATT *et al.* 1993; GOULD AND HYATT 1994) reported similar findings for BTV release with BFA treatment in mammalian cells. They postulated that the observed decrease in BTV release was the result of a decrease in NS3/3A-containing vesicles that originate from the smooth ER. Since under normal conditions NS3/3A becomes incorporated into smooth-surfaced vesicles associated with BTV particles and into the plasma membrane at sites of virus release (HYATT *et al.* 1991). In support, Hyatt *et al.* (1993) suggested the following series of vesicle-dependent events that leads to BTV release. The association of BTV to the cytoskeleton (EATON *et al.* 1987) *via* VP2 and/or VP5 facilitate the interaction of viruses with NS3/3A (HYATT *et al.* 1993) contained in smooth-surfaced vesicles (HYATT *et al.* 1991). BTV-associated vesicles are then transported to the plasma membrane, where they fuse with the plasma membrane causing release.

This finding together with the predominance of viruses within vesicles in mammalian cells at early times post infection and support this model. At later times post infection, the bulk of viruses distributed to the cytoplasm of cells in no proximity to vesicles. These observations do not support the proposed model, and suggest the possibility of more than one mechanism of viral transport in mammalian cells. This could explain why the application of BFA did not effectively block all virus release.

Taken together, AHSV particle transport at early times after infection of mammalian cells probably occurs by a vesicle-dependent mechanism, potentially facilitated by the secretory pathway. Of note, our results do not reveal the mechanism of BFA inhibition of AHSV release, it only implicates a role for GTP-dependent synthesis of transport vesicles in AHSV trafficking and release. The endosomal pathway could thus have played a role and should not be excluded, as BFA application also affects it. Regardless, a report demonstrating that the membrane association of NS3/3A is necessary for AHSV release from mammalian cells (unpublished data, Ferreira-Venter), indicate that BFA may have affected virus release by blocking the formation of NS3/3A-containing vesicles. Whether the formation of such vesicles in mammalian cells occurs at the ER membrane, Golgi membrane or endosomal membrane is unknown.

In insect cells, BFA did not affect AHSV release, particle morphogenesis or protein translation. Studies showing that BTV NS3 is essential for baculovirus-synthesised VLP release from Sf9 (insect) cells (HYATT *et al.* 1993), that high levels of BTV NS3 correlate with non-lytic virus release from insect cells (GUIRAKHOO *et al.* 1995) and the requirements of both NS3/3A for efficient BTV growth in insect cells (CELMA AND ROY 2011) implicate NS3 in virus trafficking and release. Our inhibition data indicated that vesicle-dependent transport is not essential for AHSV release from insect cells, suggesting that ER-Golgi vesicle transport may not be important for AHSV trafficking. Thus, the formation of NS3/3A-containing vesicles may not be required for AHSV transport and release. In support, electron microscopic analyses revealed that the majority of AHSV particles were freely distributed in the cytoplasm throughout the course of infection, including at 48 hpi and 72 hpi when the inhibitor was applied and effect on virus replication assayed. It is known that NS3/3A becomes incorporated in the ER membrane and subsequently into smooth-surfaced vesicles. Since NS3/3A-containing vesicles do not seem to facilitate AHSV transport, NS3 may function in a cell-mediated transport mechanism different to mammalian cells to facilitate trafficking. A recent publication by van Gennip *et al.* (2017) showed that VP2 is required for release from insect cells but not mammalian cells, suggesting the importance of NS3/3A-VP2-mediated processes for virus release from insect cells.

A previous study utilising a yeast two-hybrid interaction assay showed that the AHSV NS3 protein interacts with ubiquitin (BEYLEVELD 2007). Another study showed that BTV particles lacking the PPXY late domain motif in NS3/3A, a domain known to recruit NEDD4-like ubiquitin ligases, affected the intracellular distribution of virus particles in mammalian cells (BHATTACHARYA *et al.* 2015). Unlike wild-type BTV viruses present within vesicles and underlying the plasma membrane, these mutant viruses were found outside vesicles, surrounding them (BHATTACHARYA *et al.* 2015). PPXY mutant viruses also yielded significantly lower virus titres,

especially at early times after infection, indicating the importance of the PPXY domain at early stages of infection in mammalian cells, possibly in the sorting of virus particles into the lumen of vesicles. As such, virus release of mutant viruses were also significantly decreased demonstrating the importance of NS3-NEDD4 family of proteins interactions in virus release (BHATTACHARYA *et al.* 2015). To assess the role of ubiquitin sorting in virus yield and release, the proteasome inhibitor MG-132 was used to reduce the free levels of ubiquitin in infected cells.

Ubiquitin modification in cells either tags proteins for proteolysis by the 26S proteasome (DRISCOLL AND GOLDBERG 1990) or have functional consequences for the targeted protein. It can affect their binding ability (HOELLER *et al.* 2006), intracellular location [reviewed in (HICKE 2001)] and activity (SALGHETTI *et al.* 2001). Ubiquitin modified endosomal cargo initiates entry into MVBs (KATZMANN *et al.* 2001) and lysosomes (CIECHANOVER 2005; CLAGUE AND URBÉ 2010). Membrane traffic, ubiquitin signalling and degradation by the ubiquitin-proteasome are highly integrated pathways. The application of MG-132 to cells effectively blocks the proteolytic activity of the ubiquitin-proteasome system, thereby the degradation of many ubiquitinated proteins which reduces the pool of free amino acids for protein synthesis (VABULAS AND HARTL 2005) and depletes free unconjugated ubiquitin in the cytoplasm (MIMNAUGH *et al.* 1997; LÓPEZ *et al.* 2011; BHATTACHARYA *et al.* 2015). At a molecular level, MG-132, an analogue for the preferred substrates of the chymotrypsin-like active site (ROCK *et al.* 1994; LEE AND GOLDBERG 1996) forms adducts with the threonine residues of the 20S proteasome to attack peptide bonds (LOWE *et al.* 1995; GROLL *et al.* 1997; LEE AND GOLDBERG 1998; VOGES *et al.* 1999).

We found MG-132 inhibition affected AHSV particle morphogenesis and release, but not viral protein translation in insect cells. In mammalian cells, MG-132 did not affect AHSV particle morphogenesis, release or translation. This implicates the proteasome in the final stages of AHSV replication in only insect cells. The levels of free ubiquitin and amino acid availability were not determined, and the reduction of infectious virus progeny and virus release could not be attributed to these factors. In insect cells, different concentrations of MG-132 reduced virus yields equivalently, while virus release decreased in a concentration-dependent manner. Decreased virus yields could not be explained by decreased virus release, suggesting that the ubiquitin-proteasome system may have more than one role in the final stages of AHSV replication.

A study by López *et al.* (2011) reported decreased rotavirus yields and a concentration-dependent reduction in the synthesis of several structural proteins and one non-structural protein after MG-132 treatment. Subsequent investigations showed that amino acid depletion, reduced viral genome replication, as well as redistributed viroplasmic proteins all played a part in decreased rotavirus yields (LÓPEZ *et al.* 2011). Bhattacharya *et al.* (2015) showed a similar result for virus yield and NS2 expression after BTV infection in cells treated with MG-132. In light of these studies, we concluded that our analysis of AHSV protein translation was incomplete. Decreased AHSV yields from insect cells treated with MG-132 may be the result of interrupted translation and/or AHSV genome replication.

Given the integral role of ubiquitin in vesicle-dependent transport, the findings of Bhattacharya *et al.* (2015) with BTV on mammalian cells, and our EM data in mammalian cells it seemed unlikely that MG-132 would not affect AHSV replication in mammalian cells. Decreased rotavirus yields from MG-132 treatment have been reported under conditions where cellular and viral protein translation was severely reduced (LÓPEZ *et al.* 2011). Previous studies have shown that MG-132 induces a translational arrest of cellular proteins and expression of the cellular stress response protein Hsp72 (JIANG AND WEK 2005; MAZROUI *et al.* 2007). We propose using concentrations of MG-132 in mammalian (BSR) cells where cellular protein translation is reduced and the expression of the stress response protein Hsp72 is induced to analyse AHSV replication.

Ubiquitin is well known to be important for the fission of virions from the plasma membrane during viral budding [reviewed in (HICKE 2001)], and depletion of the intracellular levels of ubiquitin reduces the release of retroviruses by directly blocking budding at the plasma membrane (PATNAIK *et al.* 2000). The requirement of ubiquitin for virus budding or non-lytic release might be more general, because many viruses carry PPXY domains, the interaction motif required for the recruitment of ubiquitination enzymes at the site of virus budding (STRACK *et al.* 2000). If this is also the case for orbiviruses, it could explain why increasing concentrations of MG-132 resulted in decreased AHSV release while virus yield remained relatively the same. Whether the PPXY domain of the AHSV NS3 protein or ubiquitin function in AHSV release is unknown. Altogether, our data show that the proteolytic activity of the 26S proteasome i.e. free ubiquitin is required for the final stages of AHSV replication in insect cells. Whether it plays a role in mammalian cells still need to be confirmed.

Of note, peptide aldehyde inhibitors such as MG-132 also inhibit certain cathepsins and calpains. Cathepsins are involved in intralysosomal protein degradation of membrane-associated proteins and extracellular proteins taken up by endocytosis (GLAUMANN AND BALLARD 1987). Calpains are regulatory proteases of important regulators of apoptosis (SATO AND KAWASHIMA 2001; HARWOOD *et al.* 2005) and are responsible for Ca^{2+}-dependent proteolysis in the cytoplasm (PARIAT *et al.* 1997; ONO AND SORIMACHI 2012). Our results need to be followed up by experiments showing that selective inhibitors of lysosomal function or calpains do not have a similar effect on AHSV replication or that AHSV replication is affected in a similar way with other proteasome inhibitors, for example lactacystin, that do not effect these other proteases.

Phospholipid metabolism by a family of lipid kinases called PI3Ks was recently implicated in BTV morphogenesis in mammalian cells (BHATTACHARYA *et al.* 2015). These kinases are responsible for the phosphorylation of the 3'-hydroxyl group of phosphatidylinositol or phosphoinositides (VANHAESEBROECK AND WATERFIELD 1999) which leads to the activation of many intracellular signalling pathways that regulate functions as diverse as cell metabolism, survival, polarity, and vesicle transport [reviewed in (ENGELMAN *et al.* 2006)]. Three classes of PI3Ks (I-III) exist and are divided according to their substrate specificity and sequence homology (VANHAESEBROECK *et al.* 1997; FRUMAN *et al.* 1998; WYMANN AND PIROLA 1998).

Class I PI3Ks are heterodimeric enzymes that consists of a regulatory subunit activated by growth factor tyrosine kinases, G-protein coupled receptors and Ras [reviewed in (KATSO *et al.* 2001)]; and a catalytic subunit that functions to generate phosphatidylinositol-3,4,5-trisphosphate (PIP_3) from phosphatidylinositol-4,5-bisphosphate (PI-4,5-P_2 or PIP_2) (HAWKINS *et al.* 1992; VANHAESEBROECK *et al.* 1997). PIP_3 regulates the activation of many proteins, including protein kinases, guanosine exchange factors and phospholipases (HINCHLIFFE 2001) by binding to their FYVE and pleckstrin homology (PH) domains (DINITTO *et al.* 2003). The protein kinase Akt is a principle target of PIP_3, and plays a central role in in cell metabolism, growth, survival, and protein synthesis [reviewed in (ENGELMAN *et al.* 2006)].

Class II PI3Ks consists of only of a single catalytic subunit that function downstream of growth factor tyrosine kinase, cytokine receptors and integrin receptors (TURNER *et al.* 1998; BROWN *et al.* 1999; ARCARO *et al.* 2000). This catalytic subunit can also utilise Ca^{2+}-ATP for lipid kinase activity (ARCARO *et al.* 1998) to generate phosphatidylinositol-3-phosphate (PI-3-P) and phosphatidylinositol-3,4-biphosphate (PI-3,4-P_2) from PI and phosphatidylinositol-4-phosphate (PI-4-P) [reviewed in (KATSO *et al.* 2001)]. These enzymes bind to clathrin and are predominantly located in the *trans*-Golgi network and clathrin-coated vesicles, indicating a role in the regulation of membrane trafficking and receptor internalization (DOMIN *et al.* 2000; GAIDAROV *et al.* 2001).

Class III PI3Ks consists also of a single catalytic subunit, the homolog of the yeast vesicular-sorting protein Vps34 (SCHU *et al.* 1993; VOLINIA *et al.* 1995) required for intracellular vesicle trafficking from the Golgi (BROWN *et al.* 1995; ODORIZZI *et al.* 2000). Vps34 is recruited to endosomal membranes by Vps15, a serine/threonine protein kinase (HERMAN *et al.* 1991; STACK *et al.* 1995), where it phosphorylates PI to form PI-3-P [reviewed in (KATSO *et al.* 2001)]. PI-3-P regulates the recruitment of cytoplasmic proteins to the endosome by binding to FYVE domains (ODORIZZI *et al.* 2000; DINITTO *et al.* 2003). One such protein is human early endosome autoantigen 1 (EEA1) involved in endosome fusion (SIMONSEN *et al.* 1998). Vsp34 is also involved in the targeting of newly synthesised proteins to lysosomes (BROWN *et al.* 1995) and the formation of intraluminal vesicles in MVBs (FUTTER *et al.* 2001). Recently, Vsp34 has been discovered to mediate mammalian target of rapamycin (mTOR) activation in response to amino acid repletion (NOBUKUNI *et al.* 2005), suggesting its importance in cell growth. The Vps34-Vps15 complex is also essential for autophagosome formation and autophagic sequestration (BLOMMAART *et al.* 1997; KIHARA *et al.* 2001; WURMSER AND EMR 2002),

PI3K activity is thus required for many processes involving membrane traffic. The PI3K activity inhibitor, LY-294002, was used to investigate the role of PI3K-related membrane traffic events such as MVBs in the final stages of AHSV replication. LY-294002 completely inhibits the activity of classes I and III, and to lesser extent the activity of class II (STEIN 2001), *via* competitive inhibition of the ATP-binding site (VLAHOS *et al.* 1994). This inhibitory activity is not exclusive to PI3Ks, LY294002 also binds to PI3K-related kinases (BRUNN *et al.* 1996) and unrelated protein kinases (DAVIES *et al.* 2000; JACOBS *et al.* 2005). LY294002 has also been directly implicated, independently of PI3K inhibition, in the inhibition of Ca^{2+} signalling (TOLLOCZKO *et al.* 2004) and the inhibition of NF-κB activation (KIM *et al.* 2005).

The presence of LY-294002 inhibited AHSV particle morphogenesis in mammalian and insect cells, suggesting that PI3K activity plays a role in virus progeny production, maybe virus assembly. PI3K inhibition disrupts MVB biogenesis, a cell-mediated event crucial in the assembly of enveloped viruses (MORI *et al.* 2008; CALISTRI *et al.* 2009). In support, AHSV NS2 expression was unaffected in mammalian cells indicating that the viral components required for virus assembly were presumably all present. Corresponding results were obtained by Bhattacharya *et al.* (2015) with BTV infection in mammalian cells. A reduction in protein expression was however found in insect cells and could explain decreased virus yields, suggesting that MVB biogenesis is not required for AHSV morphogenesis, possibly assembly. Our EM data showed that newly assembled viruses freely dispersed in the cytoplasm in insect cells instead of associating with vesicles as in mammalian cells at early times after infection.

Decreased protein expression could be the direct result of the inhibitor. LY-294002 suppresses eukaryotic initiation factor 4E (eIF4E) activity required for cap-dependent translation (VANHAESEBROECK *et al.* 2001). BTV mRNA undergoes cap-dependent translation (DECROLY *et al.* 2012; MOHL AND ROY 2014), and AHSV mRNA should contain a similar cap to undergo cap-dependent translation. Inhibition of cap-dependent translation would therefore affect cell and viral protein expression. The report of novel strategies of translation initiation of Dengue virus proteins when cap-dependent translation is inhibited in mammalian cells (EDGIL *et al.* 2006) could explain why protein translation seemed unaffected in mammalian cells. AHSV release was unaffected in LY-294002 treated insect cells, and at low concentrations in mammalian cells. At high concentrations of LY-294002 AHSV release increased in mammalian cells. Because of the integral role of PI3K activity in cell metabolism and survival, high concentrations of LY-294002 in infected mammalian cells could cause CPE at earlier times after infection. Cell lysis at earlier times post infection explains increased virus release at high inhibitor concentrations. For this reason, we suspect that PI3Ks are not actively involved in virus release from mammalian cells and insect cells.

Given the diverse role of PI3Ks and the broad inhibitory profile of LY-294002, the decrease in AHSV particle morphogenesis can also be explained by interrupted PI3K activity of other cell-mediated events underlying the final stages of AHSV replication. For example, rotavirus proteins have been reported to directly interact with and activate cellular PI3Ks to mediate antiapoptotic signals (BAGCHI *et al.* 2012) that support progeny virus synthesis *via* the PI3K/Akt pathway (BAGCHI *et al.* 2010). Similar results has also been reported for Influenza A virus (EHRHARDT *et al.* 2007), Hepatitis C virus (MANNOVÁ AND BERETTA 2005), and Epstein–Barr virus (PORTIS AND LONGNECKER 2004). Studies showing Class III PI3K Vps34 activity known to function in membrane trafficking processes that underlie autophagy is required for Hepatitis C virus replication (SU *et al.* 2011; MOHL *et al.* 2016). LY-294002 inhibits class III Vps34 activity, and could therefore also could explain the decrease in progeny production. No current evidence suggests the involvement of autophagosomes in AHSV replication, but in light of our EM observation of virus particles associated with membranous structures, membrane precursors of the autophagic pathway cannot be excluded.

Our results suggest a role for PI3Ks in AHSV maturation in mammalian cells only, the mechanism is unknown and yet to be defined. The PI3K-mediated events involved in AHSV morphogenesis and protein production in insect cells need to elucidated. Whether membrane trafficking pathways or PI3K/Akt/mTOR pathways play a role in AHSV replication in these systems is unclear. Experiments using inhibitors of PI3K activity and/or downstream effectors of PI3K mediated pathways should be done to build on these results. For example, wortmannin blocks the membrane association EEA1 protein (PATKI *et al.* 1997), an downstream effector of Vsp34 PI3K signalling, required for early endosome fusion *via* Rab5 activity (SIMONSEN *et al.* 1998).

The inhibitors used in this study targeted processes involved in the formation of transport vesicles in the secretory and endocytic route. The targets included budding and membrane fission events, sorting of cargo into vesicles of the secretory and endocytic route, and endosome fusion. All three inhibitors were tested for cell toxicity; at the incubation times and concentrations virus yield and protein production was assayed. The results showed that cell survival was highly dependent on DMSO concentration. A technical improvement on this study would be to keep the DMSO concentration constant at or below 1% (v/v) at different inhibitor concentrations. A cell-type dependent variation in response to DMSO can be expected (ADLER *et al.* 2006; HEBLING *et al.* 2015) and the optimal DMSO concentration should first be established for model cell lines.

This study showed discrete changes in the distribution of AHSV particles over time in mammalian cells. The predominant vesicle distribution of AHSV particles occurred early after infection when non-lytic release has been reported. Subsequent investigation showed the inhibition of vesicle-dependent transport *via* the secretory route to significantly inhibit virus release. From these results, we conclude that AHSV transport early after infection predominantly occurs by vesicles. Entrance into these organelles would allow viruses to be transported to and released from the plasma membrane by conventional secretion, and would provide a mechanism of non-lytic virus release in addition to virus budding.

At later times post infection in mammalian cells, viruses were predominantly freely dispersed in the cytoplasm as single particles, pairs and aggregates. These particles were not in the vicinity of vesicles or VIBs and in close proximity to the plasma membrane, indicating active trafficking. Similar cytoplasmic distributions have been reported for progeny BTV particles (EATON *et al.* 1990a). AHSV particle transport later in infection may perhaps not be vesicle dependent. Further investigation is required. BTV has been shown to bind to vimentin rich, intermediate filamentous networks of the cytoskeleton (EATON *et al.* 1987). This interaction was attributed to the outer capsid proteins, VP2 and VP5, as both proteins are required for a stable BTV-cytoskeleton interaction (HYATT *et al.* 1993). The assembly of these proteins onto the AHSV core is unclear, but the addition of BTV VP2 is thought to occur to upon VIB exit (WALTON AND OSBURN 1992). The role of the cytoskeleton in AHSV replication has not been investigated, and could explain the cytoplasmic distribution of particles. The reorganisation and even destruction of cytoskeleton elements has been reported late in infection for various viruses and is thought to facilitate the diffusion of virus structures to the plasma membrane and virus release after cell death (CUDMORE *et al.* 1997). The change from predominantly vesicle-

bound viruses to freely dispersed viruses over time in mammalian cells was interesting, and implicate more than one mechanism of AHSV transport in mammalian cells. Whether the mechanism of transport underlie the mode of virus release seems probable, but remains to be elucidated.

In insect cells the bulk of viruses distributed freely in the cytoplasm throughout the course of infection. Viruses rarely distributed into vesicles after infection, and the inhibition of vesicle-dependent transport along the secretory route did not affect virus release. Of note, due to experimental constraints virus release was assayed at later times in infection when the vesicle distribution was lower than at early times post infection. Nonetheless, AHSV transport in insect cells seem to be vesicle independent. This is interesting because vesicle-dependent transport was linked to non-lytic virus release mammalian cells implicating an alternative mechanism of non-lytic virus release. Venter *et al.* (2014) reported the incidence of novel vesicle-like structures insect cells that may be exploited by AHSV as a non-lytic release mechanism different from budding.

Inhibition of cellular components comprising vesicle-dependent transport along the secretory and endocytic routes did not affect AHSV release and presumably AHSV transport. Phospholipid metabolism *via* PI3Ks in mammalian cells is involved in AHSV morphogenesis, of which the final stages are believed to occur during AHSV transport to the plasma membrane. From our results, PI3K metabolism also seem to play a role in AHSV replication in insect cells. Furthermore, an active 26S proteasome is required for AHSV morphogenesis in insect cells, potentially by mediating the levels of free ubiquitin. The role of ubiquitin in non-lytic release of enveloped viruses is well documented (DEMIROV AND FREED 2004), and a previous study has implicated it in the events leading to AHSV release from insect cells (BEYLEVELD 2007). From our results, whether an active 26S proteasome is required for events leading to AHSV release in mammalian cells is unclear. Investigations into the cellular transport pathways implicated by these cellular factors could inform the origin of vesicles observed to contain or be associated with AHSV particles, and their role in AHSV replication, and whether membrane-trafficking pathways are essential for AHSV release.

Taken together, our results show that cell-mediated events underlie the final stages of AHSV replication in mammalian and insect cell culture systems. The activity of specific cellular factors affected particle morphogenesis and release differently within and between systems. This suggests that AHSV may be trafficked and released *via* various intracellular routes, maybe to optimize the chances of trafficking and release from infected cells. This study demonstrates that different cell-mediated events underlie the final stages of AHSV replication in mammalian and insect cell systems, and elucidation of these mechanisms will provide valuable insight into virus release and the differences in cellular pathogenicity.

2.5. Concluding Remarks

We set out to investigate the events leading to AHSV release from infected cells. Our study was based on results obtained for BTV, the model orbivirus of the *Reoviridae*, and results from Venter *et al.* (2014) for AHSV in mammalian and insect cells. Like reoviruses, the majority of progeny AHSV particles remain cell-associated. Depending on cell type, a proportion is released by lytic or non-lytic processes. We analysed the distribution of intracellular progeny particles to investigate how particles move to the plasma membrane for release. Particles were found in three distinct intracellular distributions, namely inside the lumen of smooth-surfaced vesicles, associated with the cytoplasmic face of vesicles or freely dispersed in the cytoplasm. The nature of AHSV associated vesicles is obscure, but their observation implicated membrane traffic for AHSV transport to the cell surface.

We subsequently targeted cellular factors involved in membrane traffic, with the hope of providing evidence for the involvement of cell-mediated events in AHSV trafficking and elucidating cellular transport pathways with potential roles in AHSV trafficking and release. We found that vesicle-dependent transport along the secretory route is required for AHSV release from mammalian cells, but not insect cells, and that this mode of trafficking may underlie non-lytic release observed early after infection in mammalian cells. The 26S proteasome was demonstrated to influence AHSV morphogenesis in insect cells, but not mammalian cells, and PI3K metabolism is involved in AHSV replication in mammalian and insect cells.

Thus, cell-mediated events are involved in the final stages of AHSV replication. The cellular factors targeted in this study function in different membrane-trafficking pathways or at different levels of the same pathway, and inhibition of these factors affected AHSV replication differently in mammalian and insect cells. This could be because AHSV trafficking occurs by several cellular transport pathways, and depending on the host factors present certain pathways are usurped for trafficking. This might explain the limitation of AHSV infection in insect vectors to specific tissues, and the systemic AHSV spread in mammalian hosts, and might also provide new therapeutic strategies to reduce viral load or the spread of viral infection within the host. We propose that AHSV trafficking occurs by different highly ordered cell-mediated processes in mammalian and insect cells that lead to release from the infected cell.

RESEARCH OUTPUTS

Poster presentations

A. Oosthuizen, E. Venter and V. van Staden. (2017) *In vitro* analysis of newly synthesised African horse sickness virus particle morphogenesis and trafficking. 55th Annual Congress of the Microscopy Society of South Africa (MSSA 2017), Bela-Bela, South Africa, 4-7 December 2017.

A. Oosthuizen and V. van Staden. (2018) The cytosolic conveyance of newly synthesised mature African horse sickness particles. 13th International dsRNA Virus Symposium, Houffalize, Belgium, 24-28 September 2018.

LIST OF ABBRE*VIA*TIONS

µg	micrograms
µl	microliter
µm	micrometre
aa	amino acid
AHS	African horse sickness
AHSV	African horse sickness virus
arbovirus	arthropod-borne virus
BHK	baby hamster kidney
bp	base pairs
BTV	bluetongue virus
°C	degrees Celsius
CLP	core-like particle
cm	centimetre
cm^2	centimetre squared
CPE	cytopathic effect
Da	Dalton
DMEM	Dulbecco's Modified Eagle's medium
DNA	deoxyribonucleic acid
dpi	days post infection
ds	double-stranded
e.g.	*exempli gratia*; for example
EHDV	epizootic haemorrhagic disease virus
EM	electron microscope
ER	endoplasmic reticulum
ESCRT	endosomal sorting complexes required for transport

et al.	et alia; and others
FCS	foetal calf serum
Fig.	figure
FS	freeze-substitution
G	gauge
g	gravitational force
h	hour/s
HIV	human immunodeficiency virus
HPF	high-pressure freezing
HPF-FS	high-pressure freezing and freeze-substitution
hpi	hours post infection
Hz	hertz
i.e.	*id est*; that is
IU	international units
kDa	kilodalton
kHz	kilohertz
M	molar
mA	milliampere
MBCD	methyl-β-cyclodextrin
MDCK	Madin-Darby canine kidney
MEM	Eagle's Minimal Essential medium
min	minute/s
mL	millilitre
mM	millimolar
mm	millimetre
MOI	multiplicity of infection

mRNA	messenger RNA
ms	milliseconds
mTOR	mammalian target of Rapamycin
MVB	multivesicular body
nm	nanometre
NS	non-structural
NSP	non-structural protein
O/N	overnight
OIE	Office International des Epizooties
ORF	open reading frame
OVI	Onderstepoort Veterinary Institute
PAGE	polyacrylamide gel electrophoresis
PBS	phosphate buffered saline
PCA	paracrystalline array
pfu	plaque-forming unit
p.i.	post infection
PSB	protein solvent buffer
RDV	rice dwarf virus
RER	rough endoplasmic reticulum
RNA	ribonucleic acid
rpm	revolutions per minute
RT	room temperature
Seg-1 – Seg-10	orbivirus genome segments 1 – 10
SD	standard deviation
SDS	sodium dodecyl sulphate
ss	single-stranded

TEM	transmission electron microscope
TEMED	N,N,N’,N’-tetramethylethylene diamine
Tris	Tris hydroxymethyl aminomethane
TX-100	Triton-X 100
UA	uranyl acetate
UV	ultraviolet
V	volts
VIB	viral inclusion body
VLP	virus-like particle
VP	virus protein
W	watt
WNV	West Nile virus

LIST OF BUFFERS

RIPA lysis buffer	0.15 M NaCl
	1% Triton-X
	0.5% $C_{24}H_{39}NaO_4$
	0.1% SDS
	0.05 M Tris-HCl [pH 8.0]
PBS (1x)	0.137 M NaCl
[pH 7.4]	0.0027 M KCl
	0.0043 M $Na_2HPO_4.7H_2O$
	0.0014 M KH_2PO_4
PSB (6x)	15% 2-Mercaptoethanol
[pH 6.6]	40% Glycerol
	12% SDS
	0.375 M Tris-HCl
	0.005% Bromophenol blue
TGS (1x)	0.025 M Tris-HCl
[pH 8.5]	0.192 M Glycine
	0.1% SDS
Towbin's transfer buffer	0.025 M Tris-HCl
[pH 8.3]	0.192 M Glycine
	20% Methanol
Wash Buffer	0.05% [v/v] Tween-20 in PBS

LIST OF FIGURES

Figure 1. Overall organization of AHSV virion. 13
Figure 2. Schematic representation of the functional domains of AHSV NS3 protein 20
Figure 3. Schematic representation of membrane-trafficking pathways facilitating secretion at the cell surface 25
Figure 4. TEM micrographs of AHSV-infected BSR cells at 12 hpi 41
Figure 5. TEM micrographs of AHSV-infected BSR cells at 24 hpi 42
Figure 6. TEM micrographs of AHSV-infected BSR cells at 48 hpi 43
Figure 7. TEM micrographs depicting AHSV particles at the plasma membrane of virus-infected BSR cells 44
Figure 8. Quantification of intra-vesicular viruses 45
Figure 9. Quantification of membrane-associated viruses 47
Figure 10. Quantification of cytoplasmic viruses 47
Figure 11. Summary of the AHSV distribution profile in BSR cells over time 51
Figure 12. TEM micrographs of AHSV-infected KC cells at 12 hpi 56
Figure 13. TEM micrographs of AHSV-infected KC cells at 24 hpi 57
Figure 14. TEM micrographs of virus localisations in KC cells at 24 hpi 58
Figure 15. TEM micrographs of vesicles containing cellular-derived material in KC cells at 24 hpi 59
Figure 16. TEM micrographs of vesicles containing cellular-derived material in KC cells at 24 hpi 60
Figure 17. TEM micrographs illustrating virus localisations in KC cells at 48 hpi 61
Figure 18. TEM micrographs of AHSV-infected KC cells at 7 dpi 62
Figure 19. Summary of the AHSV distribution profile in KC cells over time 67
Figure 20. Virus growth after AHSV infection of mammalian and insect cells 69
Figure 21. Evaluation of BFA and DMSO tolerance 72
Figure 22. Effect of BFA on AHSV yield 74
Figure 23. Western blot analysis of NS2 protein expression in BFA treated cells 75
Figure 24. Evaluation of MG-132 tolerance. 78
Figure 25. Effect of MG-132 on AHSV yield. 81
Figure 26. Western blot analysis of NS2 protein expression in MG-132 treated cells 82
Figure 27. Evaluation of LY-294002 tolerance 84
Figure 28. Effect of LY-294002 on AHSV yield. 86
Figure 29. Western blot analysis of NS2 protein expression in LY-294002 treated cells 87

LIST OF REFERENCES

Adler, S., C. Pellizzer, M. Paparella, T. Hartung and S. Bremer, 2006 The effects of solvents on embryonic stem cell differentiation. Toxicolin vitro 20**:** 265-271.

AHS Trust, 2019 African Horse Sickness Trust, http://www.africanhorsesickness.co.za/.

Ait-Goughoulte, M., T. Kanda, K. Meyer, J. S. Ryerse, R. B. Ray *et al.*, 2008 Hepatitis C Virus Genotype 1a Growth and Induction of Autophagy. J Virol 82**:** 2241-2249.

Alberts, B., A. Johnson and J. Lewis, 2002 The Endoplasmic Reticulum in *Molecular Biology of the Cell*. Garland Science, New York.

Alenquer, M., and M. J. Amorim, 2015 Exosome biogenesis, regulation, and function in viral infection. Viruses 7**:** 5066-5083.

Alexander, K. A., P. W. Kat, J. House, C. House, S. J. O'Brien *et al.*, 1995 African horse sickness and African carnivores. Vet Microbiol 47**:** 133-140.

Allan, V. J., and T. A. Schroert, 1999 Membrane motors. Curr Opin Cell Biol11**:** 476-482.

Alvarez, C., and E. S. Sztul, 1999 Brefeldin A (BFA) disrupts the organization of the microtubule and the actin cytoskeletons. Eur J Cell Biol78**:** 1-14.

Anwar, M., and M. Qureshi, 1972 Control and eradication of African horse sickenss in Pakistan in *Central Treaty Organization. CENTO Seminar on the Control and Eradication of Viral Diseases*.

Arcaro, A., S. Volinia, M. J. Zvelebil, R. Stein, S. J. Watton *et al.*, 1998 Human phosphoinositide 3-kinase C2β, the role of calcium and the C2 domain in enzyme activity. J Biol Chem 273**:** 33082-33090.

Arcaro, A., M. J. Zvelebil, C. Wallasch, A. Ullrich, M. D. Waterfield *et al.*, 2000 Class II phosphoinositide 3-kinases are downstream targets of activated polypeptide growth factor receptors. Mol Cell Biol 20**:** 3817-3830.

Attoui, H., M. R. Mendez-Lopez, S. Rao, A. Hurtado-Alendes, F. Lizaraso-Caparo *et al.*, 2009 Peruvian horse sickness virus and Yunnan orbivirus, isolated from vertebrates and mosquitoes in Peru and Australia. Virology 394**:** 298-310.

Awad, F., M. Amin, S. Salama and M. Aly, 1981 Incidence of African horse sickness antibodies in animals of various species in Egypt. Bulletin of animal health and production in Africa Bulletin des sante et production animales en Afrique.

Babst, M., G. Odorizzi, E. J. Estepa and S. D. Emr, 2000 Mammalian tumor susceptibility gene 101 (TSG101) and the yeast homologue, Vps23p, both function in late endosomal trafficking. Traffic 1**:** 248-258.

Bagchi, P., D. Dutta, S. Chattopadhyay, A. Mukherjee, U. C. Halder *et al.*, 2010 Rotavirus Nonstructural Protein 1 Suppresses Virus-Induced Cellular Apoptosis To Facilitate Viral Growth by Activating the Cell Survival Pathways during Early Stages of Infection. J Virol 84**:** 6834-6845.

Bagchi, P., S. Nandi, M. K. Nayak and M. Chawla-Sarkar, 2012 Molecular Mechanism behind Rotavirus NSP1 Mediated PI3Kinase Activation: Interaction between NSP1 and p85 Subunit of PI3K. J Virol JVI.02479-02412.

Bansal, O. B., A. Stokes, A. Bansal, D. Bishop and P. Roy, 1998 Membrane organization of bluetongue virus nonstructural glycoprotein NS3. J Virol 72**:** 3362-3369.

Barnard, B. J., 1998 Epidemiology of African horse sickness and the role of the zebra in South Africa. Arch Virol Suppl 14**:** 13-19.

Barratt-Boyes, S. M., and N. J. MacLachlan, 1994 Dynamics of viral spread in bluetongue virus infected calves. Vet Microbiol 40**:** 361-371.

Basak, A. K., J. M. Grimes, P. Gouet, P. Roy and D. I. Stuart, 1997 Structures of orbivirus VP7: implications for the role of this protein in the viral life cycle. Structure 5**:** 871-883.

Basak, A. K., D. I. Stuart and P. Roy, 1992 Preliminary crystallographic study of bluetongue virus capsid protein, VP7. J Mol Biol 228**:** 687-689.

Bayer, N., D. Schober, E. Prchla, R. F. Murphy, D. Blaas *et al.*, 1998 Effect of bafilomycin A1 and nocodazole on endocytic transport in HeLa cells: implications for viral uncoating and infection. J Virol 72**:** 9645-9655.

Bearer, E., X. Breakefield, D. Schuback, T. Reese and J. LaVail, 2000 Retrograde axonal transport of herpes simplex virus: evidence for a single mechanism and a role for tegument. Proc Natl Acad Sci 97**:** 8146-8150.

Beaton, A. R., J. Rodriguez, Y. K. Reddy and P. Roy, 2002 The membrane trafficking protein calpactin forms a complex with bluetongue virus protein NS3 and mediates virus release. Proc Natl Acad Sci U S A 99**:** 13154-13159.

Bekker, S., H. Huismans and V. van Staden, 2014 Factors that affect the intracellular localization and trafficking of African horse sickness virus core protein, VP7. Virology 456-457**:** 279-291.

Belhouchet, M., F. Mohd Jaafar, A. E. Firth, J. M. Grimes, P. P. Mertens *et al.*, 2011 Detection of a fourth orbivirus non-structural protein. Plos One 6**:** e25697.

Belov, G. A., N. Altan-Bonnet, G. Kovtunovych, C. L. Jackson, J. Lippincott-Schwartz *et al.*, 2007 Hijacking Components of the Cellular Secretory Pathway for Replication of Poliovirus RNA. J Virol 81**:** 558-567.

Beyleveld, M., 2007 Interaction of nonstructural protein NS3 of African horsesickness virus with viral and cellular proteins. University of Pretoria.

Bhattacharya, B., C. C. Celma and P. Roy, 2015 Influence of cellular trafficking pathway on bluetongue virus infection in ovine cells. Viruses 7**:** 2378-2403.

Bhattacharya, B., R. J. Noad and P. Roy, 2007 Interaction between Bluetongue virus outer capsid protein VP2 and vimentin is necessary for virus egress. Virol J 4**:** 7.

Bhattacharya, B., and P. Roy, 2008 Bluetongue virus outer capsid protein VP5 interacts with membrane lipid rafts via a SNARE domain. J Virol 82**:** 10600-10612.

Bhattacharya, B., and P. Roy, 2010 Role of Lipids on Entry and Exit of Bluetongue Virus, a Complex Non-Enveloped Virus. Viruses 2**:** 1218-1235.

Binepal, V. S., B. N. Wariru, F. G. Davies, R. Soi and R. Olubayo, 1992 An attempt to define the host range for African horse sickness virus (Orbivirus, reoviridae) in East Africa, by a serological survey in some equidae, camelidae, loxodontidae and carnivore. Vet Microbiol 31**:** 19-23.

Blommaart, E. F., U. Krause, J. P. Schellens, H. Vreeling-Sindelárová and A. J. Meijer, 1997 The phosphatidylinositol 3-kinase inhibitors wortmannin and LY294002 inhibit autophagy in isolated rat hepatocytes. Eur J Biochem 243**:** 240-246.

Bonifacino, J. S., and A. M. Weissman, 1998 Ubiquitin and the control of protein fate in the secretory and endocytic pathways. Ann Rev Cell Develop Biol14**:** 19-57.

Borden, E., R. Shope and F. Murphy, 1971 Physicochemical and morphological relationships of some arthropod-borne viruses to bluetongue virus—a new taxonomic group. Physicochemical and serological studies. J Gen Virol 13**:** 261-271.

Boyce, M., C. C. Celma and P. Roy, 2012 Bluetongue virus non-structural protein 1 is a positive regulator of viral protein synthesis. Virol J 9**:** 178.

Boyce, M., J. Wehrfritz, R. Noad and P. Roy, 2004 Purified recombinant bluetongue virus VP1 exhibits RNA replicase activity. J Virol 78**:** 3994-4002.

Braverman, Y., and J. Boorman, 1978 Rates of infection in, and transmission of, African horse-sickness virus by Aedes aegypti mosquitoes. Acta virologica 22**:** 329-332.

Bremer, C. W., 1976 A gel electrophoretic study of the protein and nucleic acid components of African horsesickness virus. Onderstepoort J Vet Res 43**:** 193-199.

Bremer, C. W., H. Huismans and A. A. Van Dijk, 1990 Characterization and cloning of the African horsesickness virus genome. J Gen Virol 71 (Pt 4)**:** 793-799.

Brookes, S. M., A. D. Hyatt and B. T. Eaton, 1993 Characterization of virus inclusion bodies in bluetongue virus-infected cells. J Gen Virol 74 (Pt 3)**:** 525-530.

Brown, R. A., J. Domin, A. Arcaro, M. D. Waterfield and P. R. Shepherd, 1999 Insulin activates the α isoform of class II phosphoinositide 3-kinase. J Biol Chem 274**:** 14529-14532.

Brown, W. J., D. B. DeWald, S. D. Emr, H. Plutner and W. E. Balch, 1995 Role for phosphatidylinositol 3-kinase in the sorting and transport of newly synthesized lysosomal enzymes in mammalian cells. J Cell Biol 130**:** 781-796.

Bruce, E. A., A. Stuart, M. W. McCaffrey and P. Digard, 2012 Role of the Rab11 pathway in negative-strand virus assembly. Biochem Soc Trans 40**:** 1409-1415.

Brunn, G. J., J. Williams, C. Sabers, G. Wiederrecht, J. Lawrence Jr *et al.*, 1996 Direct inhibition of the signaling functions of the mammalian target of rapamycin by the phosphoinositide 3-kinase inhibitors, wortmannin and LY294002. Embo J 15**:** 5256-5267.

Buchholz, U. J., S. Finke and K. K. Conzelmann, 1999 Generation of bovine respiratory syncytial virus (BRSV) from cDNA: BRSV NS2 is not essential for virus replication in tissue culture, and the human RSV leader region acts as a functional BRSV genome promoter. J Virol 73**:** 251-259.

Burkhardt, C., P.-Y. Sung, C. C. Celma and P. Roy, 2014 Structural constraints in the packaging of bluetongue virus genomic segments. J Gen Virol 95**:** 2240-2250.

Burrage, T. G., R. Trevejo, M. Stone-Marschat and W. W. Laegreid, 1993 Neutralizing epitopes of African horsesickness virus serotype 4 are located on VP2. Virology 196**:** 799-803.

Burroughs, J. N., R. S. O'Hara, C. J. Smale, C. Hamblin, A. Walton *et al.*, 1994 Purification and properties of virus particles, infectious subviral particles, cores and VP7 crystals of African horsesickness virus serotype 9. J Gen Virol 75 (Pt 8)**:** 1849-1857.

Butan, C., and P. Tucker, 2010 Insights into the role of the non-structural protein 2 (NS2) in Bluetongue virus morphogenesis. Virus Res 151**:** 109-117.

Calder, P. C., and P. Yaqoob, 2007 Lipid rafts--composition, characterization, and controversies. J Nutr 137**:** 545-547.

Calisher, C. H., and P. P. Mertens, 1998 Taxonomy of African horse sickness viruses. Arch Virol Suppl 14**:** 3-11.

Calistri, A., C. Salata, C. Parolin and G. Palu, 2009 Role of multivesicular bodies and their components in the egress of enveloped RNA viruses. Rev Med Virol 19**:** 31-45.

Carpenter, S., P. Mellor and S. Torr, 2008 Control techniques for Culicoides biting midges and their application in the UK and northwestern Palaearctic. Med Vet Entomol 22**:** 175-187.

Carpenter, S., P. S. Mellor, A. G. Fall, C. Garros and G. J. Venter, 2017 African horse sickness virus: history, transmission, and current status. Ann Rev Entomol 62**:** 343-358.

Carpp, L. N., R. Galler and M. C. Bonaldo, 2011 Interaction between the yellow fever virus nonstructural protein NS3 and the host protein Alix contributes to the release of infectious particles. Microbes Infect 13**:** 85-95.

Celma, C. C., and P. Roy, 2009 A viral nonstructural protein regulates bluetongue virus trafficking and release. J Virol 83**:** 6806-6816.

Celma, C. C. P., and P. Roy, 2011 Interaction of Calpactin Light Chain (S100A10/p11) and a Viral NS Protein Is Essential for Intracellular Trafficking of Nonenveloped Bluetongue Virus. J Virol 85**:** 4783-4791.

Chavrier, P., R. G. Parton, H. P. Hauri, K. Simons and M. Zerial, 1990 Localization of low molecular weight GTP binding proteins to exocytic and endocytic compartments. Cell 62**:** 317-329.

Che, P., L. Wang and Q. Li, 2009 The development, optimization and validation of an assay for high throughput antiviral drug screening against Dengue virus. Int J Clin Exp Med 2**:** 363-373.

Ciechanover, A., 2005 Proteolysis: from the lysosome to ubiquitin and the proteasome. Nat Rev Mol Cell Biol 6**:** 79.

Clague, M. J., and S. Urbé, 2010 Ubiquitin: same molecule, different degradation pathways. Cell 143**:** 682-685.

Clift, S. J., and M. L. Penrith, 2010 Tissue and cell tropism of African horse sickness virus demonstrated by immunoperoxidase labeling in natural and experimental infection in horses in South Africa. Vet Pathol 47**:** 690-697.

Coetzer, J. A. W., and B. J. Erasmus, 1994 African horsesickness. In: Infectious Diseases Of Livestock With Special Reference To Southern Africa. J.A.W. Coetzer, G.R. Thomson, R.C. Tustin (Ed); N.P.J. Kriek (Ass Ed). Oxford University Press, Cape Town, pp 460-75.

Coetzer, J. A. W., and A. J. Guthrie, 2004 African horse sickness in *Infectious Diseases of Livestock, 2nd*, edited by J. A. W. Coetzer and R. C. Tustin. Oxford University Press, Southern Africa.

Cole, N. B., and J. Lippincott-Schwartz, 1995 Organization of organelles and membrane traffic by microtubules. Curr Opin Cell Biol 7**:** 55-64.

Cuadras, M. A., and H. B. Greenberg, 2003 Rotavirus infectious particles use lipid rafts during replication for transport to the cell surface in vitro and in vivo. Virology 313**:** 308-321.

Cuconati, A., A. Molla and E. Wimmer, 1998 Brefeldin A inhibits cell-free, de novo synthesis of poliovirus. J Virol 72**:** 6456-6464.

Cudmore, S., I. Reckmann and M. Way, 1997 Viral manipulations of the actin cytoskeleton. Trends Microbiol 5**:** 142-148.

Cybinski, D. H., and T. D. St George, 1982 Preliminary Characterization of D'Aguilar Virus and Three Palyam Group Viruses New to Australia. Aus J Biol Sci 35**:** 343-352.

Darpel, K. E., K. F. Langner, M. Nimtz, S. J. Anthony, J. Brownlie *et al.*, 2011 Saliva proteins of vector Culicoides modify structure and infectivity of bluetongue virus particles. Plos one 6**:** e17545.

Davidson, M., 1995 Endosomes and Endocytosis, pp. in *Cells and Virus Structure*. Molecular Expressions, Florida State University.

Davies, S. P., H. Reddy, M. Caivano and P. Cohen, 2000 Specificity and mechanism of action of some commonly used protein kinase inhibitors. Biochem J 351**:** 95-105.

de Waal, P. J., and H. Huismans, 2005 Characterization of the nucleic acid binding activity of inner core protein VP6 of African horse sickness virus. Arch Virol 150**:** 2037-2050.

Decroly, E., F. Ferron, J. Lescar and B. Canard, 2012 Conventional and unconventional mechanisms for capping viral mRNA. Nat Rev Microbiol10**:** 51.

Demirov, D. G., and E. O. Freed, 2004 Retrovirus budding. Virus Res 106**:** 87-102.

DiNitto, J. P., T. C. Cronin and D. G. Lambright, 2003 Membrane recognition and targeting by lipid-binding domains. Sci. Stke 2003**:** re16-re16.

Diouf, N. D., E. Etter, M. M. Lo, M. Lo and A. J. Akakpo, 2012 Outbreaks of African horse sickness in Senegal, and methods of control of the 2007 epidemic. Vet Rec**:** vr.101083.

Diprose, J. M., J. N. Burroughs, G. C. Sutton, A. Goldsmith, P. Gouet *et al.*, 2001 Translocation portals for the substrates and products of a viral transcription complex: the bluetongue virus core. Embo J 20**:** 7229-7239.

Diprose, J. M., J. M. Grimes, G. C. Sutton, J. N. Burroughs, A. Meyer *et al.*, 2002 The core of bluetongue virus binds double-stranded RNA. J Virol 76**:** 9533-9536.

Domin, J., I. Gaidarov, M. E. Smith, J. H. Keen and M. D. Waterfield, 2000 The class II phosphoinositide 3-kinase PI3K-C2α is concentrated in the trans-Golgi network and present in clathrin-coated vesicles. J Biol Chem 275**:** 11943-11950.

Domitrovic, T., N. Movahed, B. Bothner, T. Matsui, Q. Wang *et al.*, 2013 Virus assembly and maturation: auto-regulation through allosteric molecular switches. J Mol Biol 425**:** 1488-1496.

Doms, R. W., G. Russ and J. W. Yewdell, 1989 Brefeldin A redistributes resident and itinerant Golgi proteins to the endoplasmic reticulum. J Cell Biol109**:** 61-72.

Donaldson, J. G., D. Cassel, R. A. Kahn and R. D. Klausner, 1992a ADP-ribosylation factor, a small GTP-binding protein, is required for binding of the coatomer protein beta-COP to Golgi membranes. Proc Natl Acad Sci89**:** 6408-6412.

Donaldson, J. G., D. Finazzi and R. D. Klausner, 1992b Brefeldin A inhibits Golgi membrane-catalysed exchange of guanine nucleotide onto ARF protein. Nature 360**:** 350.

Donaldson, J. G., J. Lippincott-Schwartz, G. S. Bloom, T. E. Kreis and R. D. Klausner, 1990 Dissociation of a 110-kD peripheral membrane protein from the Golgi apparatus is an early event in brefeldin A action. J Cell Biol111**:** 2295-2306.

Dowler, S., R. A. Currie, D. G. Campbell, M. Deak, G. Kular *et al.*, 2000 Identification of pleckstrin-homology-domain-containing proteins with novel phosphoinositide-binding specificities. Biochem J 351**:** 19-31.

Driscoll, J., and A. L. Goldberg, 1990 The proteasome (multicatalytic protease) is a component of the 1500-kDa proteolytic complex which degrades ubiquitin-conjugated proteins. J Biol Chem 265**:** 4789-4792.

Du Toit, R., 1944 The transmission of bluetongue and horse-sickness by Culicoides. Onderstepoort J Vet Sci Anim Indust 19**:** 7-16.

Dubourget, P., J. Preaud, F. Detraz, F. Lacoste, A. Fabry *et al.*, 1992 Development, production and quality control of an industrial inactivated vaccine against African horse sickness virus serotype 4. Bluetongue, African horse sickness and related orbiviruses, CRC Press, Boca Raton**:** 874-886.

Eaton, B., A. Hyatt and S. Brookes, 1990a The replication of bluetongue virus, pp. 89-118 in *Bluetongue Viruses*. Springer.

Eaton, B. T., A. D. Hyatt and S. M. Brookes, 1990b The replication of bluetongue virus. Curr Top Microbiol Immunol 162**:** 89-118.

Eaton, B. T., A. D. Hyatt and J. R. White, 1987 Association of bluetongue virus with the cytoskeleton. Virology 157**:** 107-116.

Edgil, D., C. Polacek and E. Harris, 2006 Dengue Virus Utilizes a Novel Strategy for Translation Initiation When Cap-Dependent Translation Is Inhibited. J Virol 80**:** 2976-2986.

Ehrhardt, C., T. Wolff, S. Pleschka, O. Planz, W. Beermann *et al.*, 2007 Influenza A Virus NS1 Protein Activates the PI3K/Akt Pathway To Mediate Antiapoptotic Signaling Responses. J Virol 81**:** 3058-3067.

Engelman, J. A., J. Luo and L. C. Cantley, 2006 The evolution of phosphatidylinositol 3-kinases as regulators of growth and metabolism. Nat Rev Gen 7**:** 606.

Erasmus, B., 1973 Pathogenesis of African horsesickness, pp. in *Proceedings International Conference on Equine Infectious Diseases*.

Erasmus, B. J., 1972 The Pathogenesis of African Horsesickness. Proc 3rd Int Conf Equine Inf Dis, Paris, pp1-11.

Fang, Y., N. Wu, X. Gan, W. Yan, J. C. Morrell *et al.*, 2007 Higher-order oligomerization targets plasma membrane proteins and HIV gag to exosomes. Plos Biol 5**:** e158.

Feenstra, F., R. G. van Gennip, M. Maris-Veldhuis, E. Verheij and P. A. van Rijn, 2014 Bluetongue virus without NS3/NS3a expression is not virulent and protects against virulent bluetongue virus challenge. J Gen Virol 95**:** 2019-2029.

Fernandez-Borja, M., R. Wubbolts, J. Calafat, H. Janssen, N. Divecha *et al.*, 1999 Multivesicular body morphogenesis requires phosphatidyl-inositol 3-kinase activity. Curr Biol 9**:** 55-58.

Forzan, M., M. Marsh and P. Roy, 2007 Bluetongue virus entry into cells. J Virol 81**:** 4819-4827.

Forzan, M., C. Wirblich and P. Roy, 2004 A capsid protein of nonenveloped Bluetongue virus exhibits membrane fusion activity. Proc Natl Acad Sci U S A 101**:** 2100-2105.

French, T. J., S. Inumaru and P. Roy, 1989 Expression of two related nonstructural proteins of bluetongue virus (BTV) type 10 in insect cells by a recombinant baculovirus: production of polyclonal ascitic fluid and characterization of the gene product in BTV-infected BHK cells. J Virol 63**:** 3270-3278.

French, T. J., and P. Roy, 1990 Synthesis of bluetongue virus (BTV) corelike particles by a recombinant baculovirus expressing the two major structural core proteins of BTV. J Virol 64**:** 1530-1536.

Fruman, D. A., R. E. Meyers and L. C. Cantley, 1998 Phosphoinositide kinases, pp. Ann Rev 4139 El Camino Way, PO Box 10139, Palo Alto, CA 94303-0139, USA.

Fujiwara, T., K. Oda, S. Yokota, A. Takatsuki and Y. Ikehara, 1988 Brefeldin A causes disassembly of the Golgi complex and accumulation of secretory proteins in the endoplasmic reticulum. J Biol Chem 263**:** 18545-18552.

Fukuda, M., J. E. Moreira, V. Liu, M. Sugimori, K. Mikoshiba *et al.*, 2000 Role of the conserved WHXL motif in the C terminus of synaptotagmin in synaptic vesicle docking. Proc Natl Acad Sci USA 97**:** 14715-14719.

Futter, C., L. Collinson, J. Backer and C. Hopkins, 2001 Human VPS34 is required for internal vesicle formation within multivesicular endosomes. J Cell Biol 155**:** 1251-1264.

Gaidarov, I., M. E. Smith, J. Domin and J. H. Keen, 2001 The class II phosphoinositide 3-kinase C2α is activated by clathrin and regulates clathrin-mediated membrane trafficking. Mol Cell 7**:** 443-449.

Galvao, J., B. Davis, M. Tilley, E. Normando, M. R. Duchen *et al.*, 2014 Unexpected low-dose toxicity of the universal solvent DMSO. Faseb J 28**:** 1317-1330.

Glaumann, H., and F. J. Ballard, 1987 *Lysosomes: their role in protein breakdown*. Academic Pr.

Gosling, J. P., A. Hart, D. C. Mouat, M. Sabirovic, S. Scanlan *et al.*, 2012 Quantifying experts' uncertainty about the future cost of exotic diseases. Risk Anal 32**:** 881-893.

Gottlieb, T. A., I. E. Ivanov, M. Adesnik and D. D. Sabatini, 1993 Actin microfilaments play a critical role in endocytosis at the apical but not the basolateral surface of polarized epithelial cells. J Cell Biol 120**:** 695-710.

Gouet, P., J. M. Diprose, J. M. Grimes, R. Malby, J. N. Burroughs *et al.*, 1999 The highly ordered double-stranded RNA genome of bluetongue virus revealed by crystallography. Cell 97**:** 481-490.

Gould, A. R., and A. D. Hyatt, 1994 The orbivirus genus. Diversity, structure, replication and phylogenetic relationships. Comp Immun Microbiol Infect Dis 17**:** 163-188.

Gould, A. R., A. D. Hyatt and B. T. Eaton, 1988 Morphogenesis of a bluetongue virus variant with an amino acid alteration at a neutralization site in the outer coat protein, VP2. Virology 165**:** 23-32.

Griffiths, G., and P. Rottier, 1992 Cell biology of viruses that assemble along the biosynthetic pathway. Semin Cell Biol 3**:** 367-381.

Grimes, J. M., J. N. Burroughs, P. Gouet, J. M. Diprose, R. Malby *et al.*, 1998 The atomic structure of the bluetongue virus core. Nature 395**:** 470-478.

Groll, M., L. Ditzel, J. Löwe, D. Stock, M. Bochtler *et al.*, 1997 Structure of 20S proteasome from yeast at 2.4 Å resolution. Nature 386**:** 463.

Guirakhoo, F., J. A. Catalan and T. P. Monath, 1995 Adaptation of bluetongue virus in mosquito cells results in overexpression of NS3 proteins and release of virus particles. Arch Virol 140**:** 967-974.

Guthrie, A. J., N. J. Maclachlan, C. Joone, C. W. Lourens, C. T. Weyer *et al.*, 2013 Diagnostic accuracy of a duplex real-time reverse transcription quantitative PCR assay for detection of African horse sickness virus. J Virol Methods.

Guthrie, A. J., M. Quan, C. W. Lourens, J. C. Audonnet, J. M. Minke *et al.*, 2009 Protective immunization of horses with a recombinant canarypox virus vectored vaccine co-expressing genes encoding the outer capsid proteins of African horse sickness virus. Vaccine 27**:** 4434-4438.

Han, Z., and R. N. Harty, 2004 The NS3 protein of bluetongue virus exhibits viroporin-like properties. J Biol Chem 279**:** 43092-43097.

Harding, C., J. Heuser and P. Stahl, 1983 Receptor-mediated endocytosis of transferrin and recycling of the transferrin receptor in rat reticulocytes. J Cell Biol 97**:** 329-339.

Härri, E., W. Loeffler, H. Sigg, H. Stähelin and C. Tamm, 1963 Über die Isolierung neuer Stoffwechselprodukte aus Penicillium brefeldianum DODGE. Helvetica Chimica Acta 46**:** 1235-1243.

Harwood, S. M., M. M. Yaqoob and D. A. Allen, 2005 Caspase and calpain function in cell death: bridging the gap between apoptosis and necrosis. Ann Clin Biochem 42**:** 415-431.

Hassan, S. H., C. Wirblich, M. Forzan and P. Roy, 2001 Expression and Functional Characterization of Bluetongue Virus VP5 Protein: Role in Cellular Permeabilization. J Virol 75**:** 8356-8367.

Hawkins, P., T. Jackson and L. Stephens, 1992 Platelet-derived growth factor stimulates synthesis of Ptdlns (3, 4, 5) P3 by activating a Ptdlns (4, 5) P2 3-OH kinase. Nature 358**:** 157.

Hebling, J., L. Bianchi, F. G. Basso, D. L. Scheffel, D. G. Soares *et al.*, 2015 Cytotoxicity of dimethyl sulfoxide (DMSO) in direct contact with odontoblast-like cells. Acad Dent Material 31**:** 399-405.

Helenius, A., J. Kartenbeck, K. Simons and E. Fries, 1980 On the entry of Semliki forest virus into BHK-21 cells. J Cell Biol 84**:** 404-420.

Helliwell, S. B., S. Losko and C. A. Kaiser, 2001 Components of a ubiquitin ligase complex specify polyubiquitination and intracellular trafficking of the general amino acid permease. J Cell Biol 153**:** 649-662.

Helms, J. B., and J. E. Rothman, 1992 Inhibition by brefeldin A of a Golgi membrane enzyme that catalyses exchange of guanine nucleotide bound to ARF. Nature 360**:** 352.

Helms, J. B., and C. Zurzolo, 2004 Lipids as targeting signals: lipid rafts and intracellular trafficking. Traffic 5**:** 247-254.

Henne, W. M., N. J. Buchkovich and S. D. Emr, 2011 The ESCRT pathway. Developmental cell 21**:** 77-91.

Henning, M. W., 1956 *African Horsesickness, Perdesiekte, Pestis Equorum*. Central News Agency Ltd, South Africa.

Herman, P. K., J. H. Stack, J. A. DeModena and S. D. Emr, 1991 A novel protein kinase homolog essential for protein sorting to the yeast lysosome-like vacuole. Cell 64**:** 425-437.

Hershko, A., and A. Ciechanover, 1998 The ubiquitin system, pp. Annual Reviews 4139 El Camino Way, PO Box 10139, Palo Alto, CA 94303-0139, USA.

Hicke, L., 2001 Ubiquitin and proteasomes: protein regulation by monoubiquitin. Nat Rev Mol Cell Biol 2**:** 195.

Hicke, L., and H. Riezman, 1996 Ubiquitination of a yeast plasma membrane receptor signals its ligand-stimulated endocytosis. Cell 84**:** 277-287.

Hinchliffe, K. A., 2001 Cellular signalling: Stressing the importance of PIP3. Current Biology 11**:** R371-R373.

Hoeller, D., N. Crosetto, B. Blagoev, C. Raiborg, R. Tikkanen *et al.*, 2006 Regulation of ubiquitin-binding proteins by monoubiquitination. Nat Cell Biol 8**:** 163-169.

Howell, 1963 observations on the occurrence of african horsesickness amongst immunised horses. Onderstepoort J Vet Res 30**:** 3-10.

Howell, P. G., 1962 The isolation and identification of further antigenic types of african horsesickness virus. Onderstepoort J Vet Res 29**:** 139-149.

Hsu, N.-Y., O. Ilnytska, G. Belov, M. Santiana, Y.-H. Chen *et al.*, 2010 Viral reorganization of the secretory pathway generates distinct organelles for RNA replication. Cell 141**:** 799-811.

Huismans, H., 1979 Protein synthesis in bluetongue virus-infected cells. Virology 92**:** 385-396.

Huismans, H., and H. J. Els, 1979 Characterization of the tubules associated with the replication of three different orbiviruses. Virology 92**:** 397-406.

Huismans, H., A. A. van Dijk and A. R. Bauskin, 1987a In vitro phosphorylation and purification of a nonstructural protein of bluetongue virus with affinity for single-stranded RNA. J Virol 61**:** 3589-3595.
Huismans, H., A. A. van Dijk and H. J. Els, 1987b Uncoating of parental bluetongue virus to core and subcore particles in infected L cells. Virology 157**:** 180-188.
Huismans, H., N. T. Vanderwalt, M. Cloete and B. J. Erasmus, 1987c Isolation of a Capsid Protein of Bluetongue Virus That Induces a Protective Immune-Response in Sheep. Virology 157**:** 172-179.
Huismans, H. V., V. Van Staden, W. C. Fick and M. M. van Niekerk, 2004 A comparison of different orbivirus proteins that could affect virulence and pathogenesis. Vet Ital 40**:** 417-425.
Hunziker, W., J. A. Whitney and I. Mellman, 1991 Selective inhibition of transcytosis by brefeldin A in MDCK cells. Cell 67**:** 617-627.
Hwang, G., Y. Yang, J. Chiou and J. K. Li, 1992 Sequence conservation among the cognate nonstructural NS3/3A protein genes of six bluetongue viruses. Virus Res 23**:** 151-161.
Hyatt, A. D., and B. T. Eaton, 1988 Ultrastructural distribution of the major capsid proteins within bluetongue virus and infected cells. J Gen Virol 69 (Pt 4)**:** 805-815.
Hyatt, A. D., B. T. Eaton and S. M. Brookes, 1989 The release of bluetongue virus from infected cells and their superinfection by progeny virus. Virology 173**:** 21-34.
Hyatt, A. D., A. R. Gould, B. Coupar and B. T. Eaton, 1991 Localization of the non-structural protein NS3 in bluetongue virus-infected cells. J Gen Virol 72 (Pt 9)**:** 2263-2267.
Hyatt, A. D., Y. Zhao and P. Roy, 1993 Release of bluetongue virus-like particles from insect cells is mediated by BTV nonstructural protein NS3/NS3A. Virology 193**:** 592-603.
Jackson, W. T., T. H. Giddings, Jr., M. P. Taylor, S. Mulinyawe, M. Rabinovitch *et al.*, 2005 Subversion of cellular autophagosomal machinery by RNA viruses. Plos Biol 3**:** e156.
Jacobs, M. D., J. Black, O. Futer, L. Swenson, B. Hare *et al.*, 2005 Pim-1 ligand-bound structures reveal the mechanism of serine/threonine kinase inhibition by LY294002. J Biol Chem 280**:** 13728-13734.
James, D. J., C. Khodthong, J. A. Kowalchyk and T. F. Martin, 2008 Phosphatidylinositol 4, 5-bisphosphate regulates SNARE-dependent membrane fusion. Journal Cell Biol 182**:** 355-366.
Janowicz, A., M. Caporale, A. Shaw, S. Gulletta, L. Di Gialleonardo *et al.*, 2015 Multiple genome segments determine virulence of bluetongue virus serotype 8. J Virol 89**:** 5238-5249.
Jiang, H.-Y., and R. C. Wek, 2005 Phosphorylation of eIF2α reduces protein synthesis and enhances apoptosis in response to proteasome inhibition. J Biol Chem.
Jones, A. T., and M. J. Clague, 1995 Phosphatidylinositol 3-kinase activity is required for early endosome fusion. Biochem J 311**:** 31-34.
Jones, R. H., 1957 The Laboratory Colonization of Culicoides variipennis (Coq.). J Econom Entomol 50**:** 107-108.
Jourdan, N., M. Maurice, D. Delautier, A. M. Quero, A. L. Servin *et al.*, 1997 Rotavirus is released from the apical surface of cultured human intestinal cells through nonconventional vesicular transport that bypasses the Golgi apparatus. J Virol71**:** 8268-8278.
Kar, A. K., B. Bhattacharya and P. Roy, 2007 Bluetongue virus RNA binding protein NS2 is a modulator of viral replication and assembly. BMC Mol Biol 8**:** 4.
Katso, R., K. Okkenhaug, K. Ahmadi, S. White, J. Timms *et al.*, 2001 Cellular function of phosphoinositide 3-kinases: implications for development, immunity, homeostasis, and cancer. Ann Rev Cell Develop Biol 17**:** 615-675.
Katzmann, D. J., M. Babst and S. D. Emr, 2001 Ubiquitin-dependent sorting into the multivesicular body pathway requires the function of a conserved endosomal protein sorting complex, ESCRT-I. Cell 106**:** 145-155.
Kihara, A., T. Noda, N. Ishihara and Y. Ohsumi, 2001 Two Distinct Vps34 Phosphatidylinositol 3–Kinase complexes function in autophagy and carboxypeptidase Y Sorting inSaccharomyces cerevisiae. J Cell Biol 152**:** 519-530.
Kim, Y. H., K.-H. Choi, J.-W. Park and T. K. Kwon, 2005 LY294002 inhibits LPS-induced NO production through a inhibition of NF-κB activation: independent mechanism of phosphatidylinositol 3-kinase. Immunol Let 99**:** 45-50.
Klausner, R. D., J. G. Donaldson and J. Lippincott-Schwartz, 1992 Brefeldin A: insights into the control of membrane traffic and organelle structure. J Cell Biol 116**:** 1071-1080.

Kundu, A., R. Avalos, C. Sanderson and D. Nayak, 1996 Transmembrane domain of influenza virus neuraminidase, a type II protein, possesses an apical sorting signal in polarized MDCK cells. J Virol 70**:** 6508-6515.

Laegreid, W. W., T. G. Burrage, M. Stone-Marschat and A. Skowronek, 1992 Electron microscopic evidence for endothelial infection by African horsesickness virus. Vet Pathol 29**:** 554-556.

Laegreid, W. W., A. Skowronek, M. Stone-Marschat and T. Burrage, 1993 Characterization of virulence variants of African horsesickness virus. Virology 195**:** 836-839.

Lee, C.-J., C.-L. Liao and Y.-L. Lin, 2005 Flavivirus activates phosphatidylinositol 3-kinase signaling to block caspase-dependent apoptotic cell death at the early stage of virus infection. J Virol 79**:** 8388-8399.

Lee, D. H., and A. L. Goldberg, 1996 Selective inhibitors of the proteasome-dependent and vacuolar pathways of protein degradation in Saccharomyces cerevisiae. J Biol Chem 271**:** 27280-27284.

Lee, D. H., and A. L. Goldberg, 1998 Proteasome inhibitors: valuable new tools for cell biologists. Trends Cell Biol 8**:** 397-403.

Lee, J. W., and P. Roy, 1986 Nucleotide Sequence of a cDNA Clone of RNA Segment 10 of Bluetongue Virus (Serotype 10). J Gen Virol 67**:** 2833-2837.

Leopold, P. L., G. Kreitzer, N. Miyazawa, S. Rempel, K. K. Pfister *et al.*, 2000 Dynein-and microtubule-mediated translocation of adenovirus serotype 5 occurs after endosomal lysis. Hum Gene Ther11**:** 151-165.

Li, M., Y. Rong, Y. S. Chuang, D. Peng and S. D. Emr, 2015 Ubiquitin-dependent lysosomal membrane protein sorting and degradation. Mol Cell 57**:** 467-478.

Limn, C.-K., N. Staeuber, K. Monastyrskaya, P. Gouet and P. Roy, 2000 Functional Dissection of the Major Structural Protein of Bluetongue Virus: Identification of Key Residues within VP7 Essential for Capsid Assembly. J Virol 74**:** 8658-8669.

Lippincott-Schwartz, J., T. H. Roberts and K. Hirschberg, 2000 Secretory protein trafficking and organelle dynamics in living cells. Annu Rev Cell Dev Biol 16**:** 557-589.

Lippincott-Schwartz, J., L. Yuan, C. Tipper, M. Amherdt, L. Orci *et al.*, 1991 Brefeldin A's effects on endosomes, lysosomes, and the TGN suggest a general mechanism for regulating organelle structure and membrane traffic. Cell 67**:** 601-616.

Lippincott-Schwartz, J., L. C. Yuan, J. S. Bonifacino and R. D. Klausner, 1989 Rapid redistribution of Golgi proteins into the ER in cells treated with brefeldin A: evidence for membrane cycling from Golgi to ER. Cell 56**:** 801-813.

Lodish, H. F., A. Berk and S. L. Zipursky, 2000a Insertion of Membrane Proteins into the ER Membrane in *Molecular Cell Biology*, edited by W. H. Freeman. https://www.ncbi.nlm.nih.gov/books/NBK21731/, New York.

Lodish, H. F., A. Berk and S. L. Zipursky, 2000b Overview of the Secretory Pathway in *Molecular Cell BIology*, edited by W. H. Freeman, New York.

López, T., D. Silva-Ayala, S. López and C. F. Arias, 2011 Rotavirus genome replication requires an active ubiquitin-proteasome system. J Virol**:** JVI. 05286-05211.

Loudon, P. T., and P. Roy, 1991 Assembly of five bluetongue virus proteins expressed by recombinant baculoviruses: inclusion of the largest protein VP1 in the core and virus-like proteins. Virology 180**:** 798-802.

Lourenco, S., and P. Roy, 2011 In vitro reconstitution of Bluetongue virus infectious cores. Proc Natl Acad Sci USA 108**:** 13746-13751.

Lowe, J., D. Stock, B. Jap, P. Zwickl, W. Baumeister *et al.*, 1995 Crystal structure of the 20S proteasome from the archaeon T. acidophilum at 3.4 A resolution. Science 268**:** 533-539.

Luby-Phelps, K., 1999 Cytoarchitecture and physical properties of cytoplasm: volume, viscosity, diffusion, intracellular surface area, pp. 189-221 in *International review of cytology*. Elsevier.

Lukacs, G. L., P. Haggie, O. Seksek, D. Lechardeur, N. Freedman *et al.*, 2000 Size-dependent DNA mobility in cytoplasm and nucleus. J Biol Chem 275**:** 1625-1629.

Lymperopoulos, K., C. Wirblich, I. Brierley and P. Roy, 2003 Sequence Specificity in the Interaction of Bluetongue Virus Non-structural Protein 2 (NS2) with Viral RNA. J. Biol. Chem. 278**:** 31722-31730.

Macias, M. J., S. Wiesner and M. Sudol, 2002 WW and SH3 domains, two different scaffolds to recognize proline-rich ligands. Febs Lett 513**:** 30-37.

Maclachlan, N. J., 2010 Global implications of the recent emergence of bluetongue virus in europe. Vet Clin North Am Food Anim Pract 26**:** 163-171, table of contents.

MacLachlan, N. J., and A. J. Guthrie, 2010 Re-emergence of bluetongue, African horse sickness, and other orbivirus diseases. Vet Res 41.

Mannová, P., and L. Beretta, 2005 Activation of the N-Ras–PI3K–Akt-mTOR Pathway by Hepatitis C Virus: Control of Cell Survival and Viral Replication. J Virol 79**:** 8742-8749.

Manole, V., P. Laurinmaki, W. Van Wyngaardt, C. A. Potgieter, I. M. Wright *et al.*, 2012 Structural Insight into African Horsesickness Virus Infection. J Virol 86**:** 7858-7866.

Maree, F. F., and H. Huismans, 1997 Characterization of tubular structures composed of nonstructural protein NS1 of African horsesickness virus expressed in insect cells. J Gen Virol 78 (Pt 5)**:** 1077-1082.

Martin, S. A., and H. J. Zweerink, 1972 Isolation and characterization of two types of bluetongue virus particles. Virology 50**:** 495-506.

Martinez-Costas, J., G. Sutton, N. Ramadevi and P. Roy, 1998 Guanylyltransferase and RNA 5'-triphosphatase activities of the purified expressed VP4 protein of bluetongue virus. J Mol Biol 280**:** 859-866.

Matsuo, E., and P. Roy, 2013 Minimum Requirements for Bluetongue Virus Primary Replication. J Virol 87**:** 882-889.

Maurer, F. D., 1963 African Horse-Sickness - With Emphasis on Pathology. Am J Vet Res 24**:** 235-266.

Maxfield, F. R., and T. E. McGraw, 2004 Endocytic recycling. Nat Rev Mol Cell Biol 5**:** 121.

Mazroui, R., S. Di Marco, R. J. Kaufman and I.-E. Gallouzi, 2007 Inhibition of the ubiquitin-proteasome system induces stress granule formation. Mol Biol Cell 18**:** 2603-2618.

McCracken, A., and J. Brodsky, 2006 Recognition and delivery of ERAD substrates to the proteasome and alternative paths for cell survival, pp. 17-40 in *Dislocation and Degradation of Proteins from the Endoplasmic Reticulum*. Springer.

McIntosh, B. M., 1958 Immunological types of horsesickness virus and their significance in immunization. Onderstepoort J Vet Res 27**:** 466-538.

Meiring, T. L., H. Huismans and V. van Staden, 2009 Genome segment reassortment identifies non-structural protein NS3 as a key protein in African horsesickness virus release and alteration of membrane permeability. Arch Virol 154**:** 263-271.

Meiswinkel, R., E. M. Nevill and G. J. Venter, 1994 Vectors: Culicoides spp. in *Infectious Diseases of Livestock*, edited by J. A. W. C. e. al. Oxford University Press.

Mellor, P. S., 1993 African horse sickness: transmission and epidemiology. Vet Res 24**:** 199-212.

Mellor, P. S., 1994 Epizootiology and vectors of African horse sickness virus. Comp Immunol Microbiol Infect Dis 17**:** 287-296.

Mellor, P. S., J. Boned, C. Hamblin and S. Graham, 1990 Isolations of African horse sickness virus from vector insects made during the 1988 epizootic in Spain. Epidemiol Infect 105**:** 447-454.

Mellor, P. S., J. Boorman and M. Baylis, 2000 Culicoides biting midges: their role as arbovirus vectors. Ann Rev Entomol 45**:** 307-340.

Mellor, P. S., S. Carpenter, D. M. White, P. Mellor, M. Baylis *et al.*, 2009 Bluetongue virus in the insect host. Biology of Animal Infections: Bluetongue**:** 295-320.

Mellor, P. S., and C. Hamblin, 2004 African horse sickness. Vet Res 35**:** 445-466.

Mertens, P. P., F. Brown and D. V. Sangar, 1984 Assignment of the genome segments of bluetongue virus type 1 to the proteins which they encode. Virology 135**:** 207-217.

Mertens, P. P., J. N. Burroughs, A. Walton, M. P. Wellby, H. Fu *et al.*, 1996 Enhanced infectivity of modified bluetongue virus particles for two insect cell lines and for two Culicoides vector species. Virology 217**:** 582-593.

Mertens, P. P., and J. Diprose, 2004 The bluetongue virus core: a nano-scale transcription machine. Virus Res 101**:** 29-43.

Mimnaugh, E. G., H. Y. Chen, J. R. Davie, J. E. Celis and L. Neckers, 1997 Rapid deubiquitination of nucleosomal histones in human tumor cells caused by proteasome inhibitors and stress response inducers: effects on replication, transcription, translation, and the cellular stress response. Biochem 36**:** 14418-14429.

Mirchamsy, H., and H. Taslimi, 1964 Immunization against African Horse Sickness with Tissue-Culture-Adapted Neurotropic Viruses. Brit Vet J 120**:** 481-&.

Misumi, Y., K. Miki, A. Takatsuki, G. Tamura and Y. Ikehara, 1986a Novel blockade by brefeldin A of intracellular transport of secretory proteins in cultured rat hepatocytes. J Biol Chem 261**:** 11398-11403.

Misumi, Y., K. Miki, A. Takatsuki, G. Tamura and Y. Ikehara, 1986b Novel blockade by brefeldin A of intracellular transport of secretory proteins in cultured rat hepatocytes. J Biol Chem 261**:** 11398-11403.

Modrof, J., K. Lymperopoulos and P. Roy, 2005 Phosphorylation of bluetongue virus nonstructural protein 2 is essential for formation of viral inclusion bodies. J Virol 79**:** 10023-10031.

Mohl, B.-P., C. Bartlett, J. Mankouri and M. Harris, 2016 Early events in the generation of autophagosomes are required for the formation of membrane structures involved in hepatitis C virus genome replication. J Gen Virol97**:** 680-693.

Mohl, B. P., and P. Roy, 2014 Bluetongue virus capsid assembly and maturation. Viruses 6**:** 3250-3270.

Moor, H., and U. Riehle, 1968 Snap-freezing under high pressure: A new fixation technique for freeze-etching. Proc. Fourth Eur Reg Conf Elect Microsc 2**:** 33-34.

Mori, Y., M. Koike, E. Moriishi, A. Kawabata, H. Tang *et al.*, 2008 Human herpesvirus-6 induces MVB formation, and virus egress occurs by an exosomal release pathway. Traffic 9**:** 1728-1742.

Mortola, E., R. Noad and P. Roy, 2004 Bluetongue virus outer capsid proteins are sufficient to trigger apoptosis in mammalian cells. J Virol 78**:** 2875-2883.

Mosmann, T., 1983 Rapid colorimetric assay for cellular growth and survival: application to proliferation and cytotoxicity assays. J Immunol Methods 65**:** 55-63.

Moule, L., 1896 Histoire de la Médecine Vétérinaire, pp. 38. Maulde, Paris.

Mroczkiewicz, M., K. Winkler, D. Nowis, G. Placha, J. Golab *et al.*, 2010 Studies of the synthesis of all stereoisomers of MG-132 proteasome inhibitors in the tumor targeting approach. J Med Chem 53**:** 1509-1518.

Murk, J. L. A. N., B. M. Humbel, U. Ziese, J. M. Griffith, G. Posthuma *et al.*, 2003 Endosomal compartmentalization in three dimensions: Implications for membrane fusion. Proc Natl Acad Sci 100**:** 13332-13337.

Nagaleekar, V. K., A. K. Tiwari, R. S. Kataria, M. V. Bais, P. V. Ravindra *et al.*, 2007 Bluetongue virus induces apoptosis in cultured mammalian cells by both caspase-dependent extrinsic and intrinsic apoptotic pathways. Arch Virol 152**:** 1751-1756.

Nason, E. L., R. Rothagel, S. K. Mukherjee, A. K. Kar, M. Forzan *et al.*, 2004 Interactions between the inner and outer capsids of bluetongue virus. J Virol 78**:** 8059-8067.

Nevill, E. M., and D. Anderson, 1972 Host preferences of Culicoides midges (Diptera: Ceratopogonidae) in South Africa as determined by precipitin tests and light trap catches. Onderstepoort J Vet Res 39.

Nickerson, D. P., M. R. Russell and G. Odorizzi, 2007 A concentric circle model of multivesicular body cargo sorting. Embo reports 8**:** 644-650.

Nieva, J. L., V. Madan and L. Carrasco, 2012 Viroporins: structure and biological functions. Nat Rev Micro 10**:** 563-574.

Nobukuni, T., M. Joaquin, M. Roccio, S. G. Dann, S. Y. Kim *et al.*, 2005 Amino acids mediate mTOR/raptor signaling through activation of class 3 phosphatidylinositol 3OH-kinase. Proc Natl Acad Sci 102**:** 14238-14243.

Nydegger, S., M. Foti, A. Derdowski, P. Spearman and M. Thali, 2003 HIV-1 egress is gated through late endosomal membranes. Traffic 4**:** 902-910.

O'Dell, N., L. Arnot, C. E. Janisch and J. C. Steyl, 2018 Clinical presentation and pathology of suspected vector transmitted African horse sickness in South African domestic dogs from 2006 to 2017. Vet Rec 182**:** 715-715.

Odorizzi, G., M. Babst and S. D. Emr, 1998 Fab1p PtdIns (3) P 5-kinase function essential for protein sorting in the multivesicular body. Cell 95**:** 847-858.

Odorizzi, G., M. Babst and S. D. Emr, 2000 Phosphoinositide signaling and the regulation of membrane trafficking in yeast. Trends Biol Sci 25**:** 229-235.

Oellermann, R. A., H. J. Els and B. J. Erasmus, 1970 Characterization of African horsesickness virus. Arch Gesamte Virusforsch 29**:** 163-174.

OIE, 2019 OIE-Listed diseases, infections and infestations in force in 2019, pp. World Organisation for Animal Health, http://www.oie.int/en/animal-health-in-the-world/oie-listed-diseases-2019/.

Okumura, A., T. Alce, B. Lubyova, H. Ezelle, K. Strebel *et al.*, 2008 HIV-1 accessory proteins VPR and Vif modulate antiviral response by targeting IRF-3 for degradation. Virology 373**:** 85-97.

Ono, Y., and H. Sorimachi, 2012 Calpains — An elaborate proteolytic system. Biochimica et Biophysica Acta (BBA) - Proteins and Proteomics 1824**:** 224-236.

Owens, R. J., C. Limn and P. Roy, 2004 Role of an arbovirus nonstructural protein in cellular pathogenesis and virus release. J Virol 78**:** 6649-6656.

Ozawa, Y., and G. Nakata, 1965 Experimental transmission of African horse-sickness by means of mosquitoes. Am J Vet Res26**:** 744-748.

Pan, B.-T., and R. M. Johnstone, 1983 Fate of the transferrin receptor during maturation of sheep reticulocytes in vitro: selective externalization of the receptor. Cell 33**:** 967-978.

Pan, B.-T., K. Teng, C. Wu, M. Adam and R. M. Johnstone, 1985 Electron microscopic evidence for externalization of the transferrin receptor in vesicular form in sheep reticulocytes. J Cell Biol 101**:** 942-948.

Pariat, M., S. Carillo, M. Molinari, C. Salvat, L. Debüssche *et al.*, 1997 Proteolysis by calpains: a possible contribution to degradation of p53. Mol Cell Biol 17**:** 2806-2815.

Patel, A., and P. Roy, 2014 The molecular biology of Bluetongue virus replication. Virus Research 182**:** 5-20.

Patel, K. M., M. L. Watson and S. G. Ward, 2004 Differential sensitivity of class II phosphoinositide 3- kinase (PI3K) isoforms to broad spectrum PI3K inhibitors, pp. 1. University of Bath, Claverton Down.

Patki, V., J. Virbasius, W. S. Lane, B.-H. Toh, H. S. Shpetner *et al.*, 1997 Identification of an early endosomal protein regulated by phosphatidylinositol 3-kinase. Proc Natl Acad Sci 94**:** 7326-7330.

Patnaik, A., V. Chau and J. W. Wills, 2000 Ubiquitin is part of the retrovirus budding machinery. Proc Natl Acad Sci 97**:** 13069-13074.

Pickart, C. M., and M. J. Eddins, 2004 Ubiquitin: structures, functions, mechanisms. Biochimica et Biophysica Acta (BBA). Mol Cell Res 1695**:** 55-72.

Pigino, G., G. A. Morfini and S. T. Brady, 2012 Chapter 7 - Intracellular Trafficking, pp. 119-145 in *Basic Neurochemistry (Eighth Edition)*, edited by S. T. Brady, G. J. Siegel, R. W. Albers and D. L. Price. Academic Press, New York.

Portis, T., and R. Longnecker, 2004 Epstein–Barr virus (EBV) LMP2A mediates B-lymphocyte survival through constitutive activation of the Ras/PI3K/Akt pathway. Oncogene 23**:** 8619.

Prosch, S., C. Priemer, C. Hoflich, C. Liebenthaf, N. Babel *et al.*, 2003 Proteasome inhibitors: a novel tool to suppress human cytomegalovirus replication and virus-induced immune modulation. Antivir Ther 8**:** 555-568.

Purse, B. V., and D. J. Rogers, 2009 Bluetongue virus and climate change, pp. 343-364 in *Bluetongue* edited by R. Noad and P. Roy, Amsterdam.

Ramadevi, N., N. J. Burroughs, P. P. C. Mertens, I. M. Jones and P. Roy, 1998 Capping and methylation of mRNA by purified recombinant VP4 protein of bluetongue virus. PNAS 95**:** 13537-13542.

Raposo, G., H. W. Nijman, W. Stoorvogel, R. Liejendekker, C. V. Harding *et al.*, 1996 B lymphocytes secrete antigen-presenting vesicles. J Exp Med183**:** 1161-1172.

Ratinier, M., M. Caporale, M. Golder, G. Franzoni, K. Allan *et al.*, 2011 Identification and characterization of a novel non-structural protein of bluetongue virus. Plos pathog 7**:** e1002477.

Ratinier, M., A. E. Shaw, G. Barry, Q. Gu, L. Di Gialleonardo *et al.*, 2016 Bluetongue virus NS4 protein is an interferon antagonist and a determinant of virus virulence. J Virol.

Reaves, B., and G. Banting, 1992 Perturbation of the morphology of the trans-Golgi network following Brefeldin A treatment: redistribution of a TGN-specific integral membrane protein, TGN38. J Cell Biol 116**:** 85-94.

Reed, L. J., and H. Muench, 1938 A simple method of estimating fifty per cent endpoints. Am J Epidemiol 27**:** 493-497.

Reggiori, F., and H. R. Pelham, 2001 Sorting of proteins into multivesicular bodies: ubiquitin-dependent and-independent targeting. Embo J 20**:** 5176-5186.

Reynolds, E. S., 1963 The use of lead citrate at high pH as an electron-opaque stain in electron microscopy. J Cell Biol 17**:** 208.

Robinson, S. M., G. Tsueng, J. Sin, V. Mangale, S. Rahawi *et al.*, 2014 Coxsackievirus B exits the host cell in shed microvesicles displaying autophagosomal markers. Plos Pathog 10**:** e1004045.

Rock, K. L., C. Gramm, L. Rothstein, K. Clark, R. Stein *et al.*, 1994 Inhibitors of the proteasome block the degradation of most cell proteins and the generation of peptides presented on MHC class I molecules. Cell 78**:** 761-771.

Roy, P., 1989 Bluetongue virus genetics and genome structure. Virus Res 13**:** 179-206.

Roy, P., 2005 Bluetongue virus proteins and particles and their role in virus entry, assembly, and release. Adv Virus Res 64**:** 69-123.

Roy, P., 2008 Functional mapping of bluetongue virus proteins and their interactions with host proteins during virus replication. Cell Biochem Biophys 50**:** 143-157.

Roy, P., A. Adachi, T. Urakawa, T. F. Booth and C. P. Thomas, 1990 Identification of bluetongue virus VP6 protein as a nucleic acid-binding protein and the localization of VP6 in virus-infected vertebrate cells. J Virol 64**:** 1-8.

Roy, P., T. Hirasawa, M. Fernandez, V. M. Blinov and J. M. Sanchez-Vixcain Rodrique, 1991 The complete sequence of the group-specific antigen, VP7, of African horsesickness disease virus serotype 4 reveals a close relationship to bluetongue virus. J Gen Virol 72 (Pt 6)**:** 1237-1241.

Roy, P., P. P.C. Mertens and I. Casal, 1994 African horse sickness virus structure. Comp Immunol Microbiol Infect Dis 17**:** 243-273.

Ruthel, G., G. L. Demmin, G. Kallstrom, M. P. Javid, S. S. Badie *et al.*, 2005 Association of ebola virus matrix protein VP40 with microtubules. J Virol 79**:** 4709-4719.

Sachs, A. B., P. Sarnow and M. W. Hentze, 1997 Starting at the beginning, middle, and end: translation initiation in eukaryotes. Cell 89**:** 831-838.

Saeed, M. F., A. A. Kolokoltsov, A. N. Freiberg, M. R. Holbrook and R. A. Davey, 2008 Phosphoinositide-3 kinase-Akt pathway controls cellular entry of Ebola virus. Plos Pathog 4**:** e1000141.

Sailleau, C., C. Hamblin, J. T. Paweska and S. Zientara, 2000 Identification and differentiation of the nine African horse sickness virus serotypes by RT-PCR amplification of the serotype-specific genome segment 2. J Gen Virol 81**:** 831-837.

Salghetti, S. E., A. A. Caudy, J. G. Chenoweth and W. P. Tansey, 2001 Regulation of transcriptional activation domain function by ubiquitin. Science 293**:** 1651-1653.

Sangar, D., and P. Mertens, 1983 Comparison of type 1 bluetongue virus protein synthesis in vivo and in vitro, pp. 183-191 in *Double-stranded RNA viruses*. Elsevier New York.

Sasaki, T., S. Takasuga, J. Sasaki, S. Kofuji, S. Eguchi *et al.*, 2009 Mammalian phosphoinositide kinases and phosphatases. Prog Lipid Res 48**:** 307-343.

Sato, K., and S. Kawashima, 2001 Calpain function in the modulation of signal transduction molecules. Biol Chem 382**:** 743-751.

Schekman, R., and L. Orci, 1996 Coat proteins and vesicle budding. Science 271**:** 1526-1533.

Schorey, J. S., Y. Cheng, P. P. Singh and V. L. Smith, 2015 Exosomes and other extracellular vesicles in host–pathogen interactions. Embo reports 16**:** 24-43.

Schroer, T. A., 2000 Motors, clutches and brakes for membrane traffic: a commemorative review in honor of Thomas Kreis. Traffic 1**:** 3-10.

Schu, P. V., K. Takegawa, M. J. Fry, J. H. Stack, M. D. Waterfield *et al.*, 1993 Phosphatidylinositol 3-kinase encoded by yeast VPS34 gene essential for protein sorting. Science 260**:** 88-91.

Serafini, T., L. Orci, M. Amherdt, M. Brunner, R. A. Kahn *et al.*, 1991 ADP-ribosylation factor is a subunit of the coat of Golgi-derived COP-coated vesicles: a novel role for a GTP-binding protein. Cell 67**:** 239-253.

Shaw, A. E., A. Bruning-Richardson, E. E. Morrison, J. Bond, J. Simpson *et al.*, 2013 Bluetongue virus infection induces aberrant mitosis in mammalian cells. Virol J 10**:** 319.

Shrivastava, S., P. Devhare, N. Sujijantarat, R. Steele, Y.-C. Kwon *et al.*, 2016 Knockdown of Autophagy Inhibits Infectious Hepatitis C Virus Release by the Exosomal Pathway. J Virol 90**:** 1387-1396.

Simons, K., and E. Ikonen, 1997 Functional rafts in cell membranes. Nature 387**:** 569-572.

Simonsen, A., R. Lippe, S. Christoforidis, J.-M. Gaullier, A. Brech *et al.*, 1998 EEA1 links PI (3) K function to Rab5 regulation of endosome fusion. Nature 394**:** 494.

Sodeik, B., 2000 Mechanisms of viral transport in the cytoplasm. Trends Microbiol 8**:** 465-472.

Sodeik, B., M. W. Ebersold and A. Helenius, 1997 Microtubule-mediated transport of incoming herpes simplex virus 1 capsids to the nucleus. J Cell Biol 136**:** 1007-1021.

Sotelo, J. R., and K. R. Porter, 1959 An electron microscope study of the rat ovum. J Biophys Biochem Cy 5**:** 327-342.

Spence, R. P., N. F. Moore and P. A. Nuttall, 1984 The biochemistry of orbiviruses. Brief review. Arch Virol 82**:** 1-18.

Stack, J. H., D. B. DeWald, K. Takegawa and S. D. Emr, 1995 Vesicle-mediated protein transport: regulatory interactions between the Vps15 protein kinase and the Vps34 PtdIns 3-kinase essential for protein sorting to the vacuole in yeast. J Cell Biol 129**:** 321-334.

Stamnes, M. A., and J. E. Rothman, 1993 The binding of AP-1 clathrin adaptor particles to Golgi membranes requires ADP-ribosylation factor, a small GTP-binding protein. Cell 73**:** 999-1005.

Stassen, L., H. Huismans and J. Theron, 2011 Membrane permeabilization of the African horse sickness virus VP5 protein is mediated by two N-terminal amphipathic alpha-helices. Arch Virol 156**:** 711-715.

Stassen, L., H. Huismans and J. Theron, 2012 African horse sickness virus induces apoptosis in cultured mammalian cells. Virus Res 163**:** 385-389.

Stäuber, N., J. Martinez-Costas, G. Sutton, K. Monastyrskaya and P. Roy, 1997 Bluetongue virus VP6 protein binds ATP and exhibits an RNA-dependent ATPase function and a helicase activity that catalyze the unwinding of double-stranded RNA substrates. J Virol 71**:** 7220-7226.

Stein, R., 2001 Prospects for phosphoinositide 3-kinase inhibition as a cancer treatment. Endocrine-related cancer 8**:** 237-248.

Stewart, M. E., and P. Roy, 2010 Role of cellular caspases, nuclear factor-kappa B and interferon regulatory factors in Bluetongue virus infection and cell fate. Virol J 7**:** 362.

Stoltz, M. A., C. F. van der Merwe, J. Coetzee and H. Huismans, 1996 Subcellular localization of the nonstructural protein NS3 of African horsesickness virus. Onderstepoort J Vet Res 63**:** 57-61.

Strack, B., A. Calistri, M. A. Accola, G. Palù and H. G. Göttlinger, 2000 A role for ubiquitin ligase recruitment in retrovirus release. Proc Natl Acad Sci 97**:** 13063-13068.

Studer, D., W. Graber, A. Al-Amoudi and P. Eggli, 2001 A new approach for cryofixation by high-pressure freezing. Journal Microsc 203**:** 285-294.

Stuffers, S., C. Sem Wegner, H. Stenmark and A. Brech, 2009 Multivesicular endosome biogenesis in the absence of ESCRTs. Traffic 10**:** 925-937.

Su, W.-C., T.-C. Chao, Y.-L. Huang, S.-C. Weng, K.-S. Jeng *et al.*, 2011 Rab5 and Class III Phosphoinositide 3-Kinase Vps34 Are Involved in Hepatitis C Virus NS4B-Induced Autophagy. J Virol 85**:** 10561-10571.

Sung, P.-Y., and P. Roy, 2014 Sequential packaging of RNA genomic segments during the assembly of Bluetongue virus. Nucleic Acids Res 42**:** 13824-13838.

Suomalainen, M., M. Y. Nakano, S. Keller, K. Boucke, R. P. Stidwill *et al.*, 1999 Microtubule-dependent plus- and minus end–directed motilities are competing processes for nuclear targeting of adenovirus. J Cell Biol 144**:** 657-672.

Tan, B. H., E. Nason, N. Staeuber, W. Jiang, K. Monastryrskaya *et al.*, 2001 RGD tripeptide of bluetongue virus VP7 protein is responsible for core attachment to Culicoides cells. J Virol 75**:** 3937-3947.

Tanigawa, G., L. Orci, M. Amherdt, M. Ravazzola, J. B. Helms *et al.*, 1993 Hydrolysis of bound GTP by ARF protein triggers uncoating of Golgi-derived COP-coated vesicles. J Cell Biol 123**:** 1365-1371.

Taraporewala, Z. F., D. Chen and J. T. Patton, 2001 Multimers of the Bluetongue Virus Nonstructural Protein, NS2, Possess Nucleotidyl Phosphatase Activity: Similarities between NS2 and Rotavirus NSP2. Virology 280**:** 221-231.

Taylor, M. P., T. B. Burgon, K. Kirkegaard and W. T. Jackson, 2009 Role of microtubules in extracellular release of poliovirus. J Virol 83**:** 6599-6609.

Theal, G. M., 1900 *Records of South-Eastern Africa: collected in various libraries and archive departments in Europe*. Government of the Cape Colony.

Theiler, A., 1902 Equine malaria. J Comp Pathol Ther15**:** 40-54.

Theiler, A., 1921 African Horse Sickness (Pestiis equorum). Union S. Africa Dept. Agric., Pretoria, Sci. Bull.

Theron, J., J. M. Uitenweerde, H. Huismans and L. H. Nel, 1994 Comparison of the expression and phosphorylation of the non-structural protein NS2 of three different orbiviruses: evidence for the involvement of an ubiquitous cellular kinase. J Gen Virol 75 (Pt 12)**:** 3401-3411.

Thomas, C., T. Booth and P. Roy, 1990 Synthesis of bluetongue virus-encoded phosphoprotein and formation of inclusion bodies by recombinant baculovirus in insect cells: it binds the single-stranded RNA species. J Gen Virol 71**:** 2073-2083.

Thompson, G. M., S. Jess and A. K. Murchie, 2012 A review of African horse sickness and its implications for Ireland. Irish Vet J 65**:** 9-9.

Tokarev, A. A., A. Alfonso and N. Segev, 2009 Overview of Intracellular Compartments and Trafficking Pathways, pp. 2000-2013. Landes Bioscience, Madame Curie Bioscience Database.

Tolloczko, B., P. Turkewitsch, M. Al-Chalabi and J. G. Martin, 2004 LY-294002 [2-(4-morpholinyl)-8-phenyl-4H-1-benzopyran-4-one] affects calcium signaling in airway smooth muscle cells independently of phosphoinositide 3-kinase inhibition. J Pharmacol Exp Ther311**:** 787-793.

Tomova, C., 2013 Brief Introduction to High-Pressure Freezing, pp. Leica Microsystems, Science Lab.

Turner, S. J., J. Domin, M. D. Waterfield, S. G. Ward and J. Westwick, 1998 The CC chemokine monocyte chemotactic peptide-1 activates both the class I p85/p110 phosphatidylinositol 3-kinase and the class II PI3K-C2α. J Biol Chem 273**:** 25987-25995.

Uitenweerde, J. M., J. Theron, M. A. Stoltz and H. Huismans, 1995 The Multimeric Nonstructural NS2 Proteins of Bluetongue Virus, African Horsesickness Virus, and Epizootic Hemorrhagic Disease Virus Differ in Their Single-Stranded RNA-Binding Ability. Virology 209**:** 624-632.

Umeshappa, C. S., K. P. Singh, R. H. Nanjundappa and A. B. Pandey, 2010 Apoptosis and immuno-suppression in sheep infected with bluetongue virus serotype-23. Vet Microbiol 144**:** 310-318.

Urakawa, T., D. G. Ritter and P. Roy, 1989 Expression of largest RNA segment and synthesis of VP1 protein of bluetongue virus in insect cells by recombinant baculovirus: association of VP1 protein with RNA polymerase activity. Nucleic Acids Res 17**:** 7395-7401.

Urbano, P., and F. G. Urbano, 1994 The Reoviridae family. Comp Immunol Microbiol Infect Dis 17**:** 151-161.

Vabulas, R. M., and F. U. Hartl, 2005 Protein synthesis upon acute nutrient restriction relies on proteasome function. Science 310**:** 1960-1963.

van de Water, S. G., R. G. van Gennip, C. A. Potgieter, I. M. Wright and P. A. van Rijn, 2015 VP2 Exchange and NS3/NS3a Deletion in African Horse Sickness Virus (AHSV) in Development of Disabled Infectious Single Animal Vaccine Candidates for AHSV. J Virol 89**:** 8764-8772.

Van der Merwe, C., and J. Coetzee, 1992 Quetol 651 for general use: a revised formulation. Proc Elec Microsc Soc SA 22**:** 31-32.

Van Dijk, A. A., and H. Huismans, 1980 The in vitro activation and further characterization of the bluetongue virus-associated transcriptase. Virology 104**:** 347-356.

van Gennip, R. G., S. G. van de Water and P. A. van Rijn, 2014 Bluetongue virus nonstructural protein NS3/NS3a is not essential for virus replication. Plos One 9**:** e85788.

van Gennip, R. G. P., S. G. P. van de Water, C. A. Potgieter and P. A. van Rijn, 2017 Structural Protein VP2 of African Horse Sickness Virus Is Not Essential for Virus Replication. J Virol 91.

van Niekerk, M., C. C. Smit, W. C. Fick, V. van Staden and H. Huismans, 2001 Membrane association of African horsesickness virus nonstructural protein NS3 determines its cytotoxicity. Virology 279**:** 499-508.

Van Rensberg, I., J. De Clerk, H. Groenewald and W. Botha, 1981 An outbreak of African horsesickness in dogs. J SA Vet Ass 52**:** 323-325.

Van Sittert, S. J., T. M. Drew, J. L. Kotze, T. Strydom, C. T. Weyer *et al.*, 2013 Occurrence of African horse sickness in a domestic dog without apparent ingestion of horse meat. J SA Vet Ass 84**:** 1-5.

van Staden, V., and H. Huismans, 1991 A comparison of the genes which encode non-structural protein NS3 of different orbiviruses. J Gen Virol 72 (Pt 5)**:** 1073-1079.

van Staden, V., C. C. Smit, M. A. Stoltz, F. F. Maree and H. Huismans, 1998 Characterization of two African horse sickness virus nonstructural proteins, NS1 and NS3. Arch Virol Suppl 14**:** 251-258.

van Staden, V., M. A. Stoltz and H. Huismans, 1995 Expression of nonstructural protein NS3 of African horsesickness virus (AHSV): evidence for a cytotoxic effect of NS3 in insect cells, and characterization of the gene products in AHSV infected Vero cells. Arch Virol 140**:** 289-306.

van Staden, V., J. Theron, B. J. Greyling, H. Huismans and L. H. Nel, 1991 A comparison of the nucleotide sequences of cognate NS2 genes of three different orbiviruses. Virology 185**:** 500-504.

Vanhaesebroeck, B., S. J. Leevers, K. Ahmadi, J. Timms, R. Katso *et al.*, 2001 Synthesis and function of 3-phosphorylated inositol lipids. Ann Rev Biochem 70**:** 535-602.

Vanhaesebroeck, B., S. J. Leevers, G. Panayotou and M. D. Waterfield, 1997 Phosphoinositide 3-kinases: a conserved family of signal transducers. Trends Biol Sci 22**:** 267-272.

Vanhaesebroeck, B., and M. Waterfield, 1999 Signaling by distinct classes of phosphoinositide 3-kinases. Exp Cell Res 253**:** 239-254.

Venter, E., C. F. van der Merwe, A. V. Buys, H. Huismans and V. van Staden, 2014 Comparative ultrastructural characterization of African horse sickness virus-infected mammalian and insect cells reveals a novel potential virus release mechanism from insect cells. J Gen Virol 95**:** 642-651.

Vermaak, E., A. M. Conradie, F. F. Maree and J. Theron, 2016 African horse sickness virus infects BSR cells through macropinocytosis. Virology 497**:** 217-232.

Vermaak, E., and J. Theron, 2015 Virus uncoating is required for apoptosis induction in cultured mammalian cells infected with African horse sickness virus. J Gen Virol 96**:** 1811-1820.

Verwoerd, D. W., H. J. Els, E. M. De Villiers and H. Huismans, 1972 Structure of the bluetongue virus capsid. J Virol 10**:** 783-794.

Verwoerd, D. W., and H. Huismans, 1969 On the relationship between bluetongue, African horsesickness and reoviruses: hybridization studies. Onderstepoort J Vet Res 36**:** 175-179.

Vidal, M., J. Sainte-Marie, J. R. Philippot and A. Bienvenue, 1989 Asymmetric distribution of phospholipids in the membrane of vesicles released during in vitro maturation of guinea pig reticulocytes: evidence precluding a role for “aminophospholipid translocase”. J Cell Physiol 140**:** 455-462.

Vlahos, C. J., W. F. Matter, K. Y. Hui and R. F. Brown, 1994 A specific inhibitor of phosphatidylinositol 3-kinase, 2-(4-morpholinyl)-8-phenyl-4H-1-benzopyran-4-one (LY294002). J Biol Chem 269**:** 5241-5248.

Voges, D., P. Zwickl and W. Baumeister, 1999 The 26S proteasome: a molecular machine designed for controlled proteolysis. Ann Rev Biochem 68**:** 1015-1068.

Volinia, S., R. Dhand, B. Vanhaesebroeck, L. MacDougall, R. Stein *et al.*, 1995 A human phosphatidylinositol 3-kinase complex related to the yeast Vps34p-Vps15p protein sorting system. Embo J 14**:** 3339-3348.

Votteler, J., and W. I. Sundquist, 2013 Virus budding and the ESCRT pathway. Cell Host Microbe14**:** 232-241.

Vreede, F. T., and H. Huismans, 1994 Cloning, characterization and expression of the gene that encodes the major neutralization-specific antigen of African horsesickness virus serotype 3. J Gen Virol 75 (Pt 12)**:** 3629-3633.

Walton, T. E., and B. I. Osburn, 1992 *Bluetongue, African Horse Sickness, and Related Orbiviruses: Proceedings of the Second International Symposium*. CRC Press.

Waters, M. G., T. Serafini and J. E. Rothman, 1991 'Coatomer': a cytosolic protein complex containing subunits of non-clathrin-coated Golgi transport vesicles. Nature 349**:** 248.

Wechsler, S. J., and L. E. McHolland, 1988 Susceptibilities of 14 cell lines to bluetongue virus infection. J Clin Microbiol 26**:** 2324-2327.

Wei, T., H. Hibino and T. Omura, 2008 Rice dwarf virus is engulfed into and released via vesicular compartments in cultured insect vector cells. J Gen Virol 89**:** 2915-2920.

Whitney, J. A., M. Gomez, D. Sheff, T. E. Kreis and I. Mellman, 1995 Cytoplasmic coat proteins involved in endosome function. Cell 83**:** 703-713.

Williams, R. L., and S. Urbe, 2007 The emerging shape of the ESCRT machinery. Nat Rev Mol Cell Biol 8**:** 355-368.

Wilson, A., P. S. Mellor, C. Szmaragd and P. P. Mertens, 2009 Adaptive strategies of African horse sickness virus to facilitate vector transmission. Vet Res 40**:** 16.

Wirblich, C., B. Bhattacharya and P. Roy, 2006 Nonstructural protein 3 of bluetongue virus assists virus release by recruiting ESCRT-I protein Tsg101. J Virol 80**:** 460-473.

Wohlsein, P., J. F. Pohlenz, F. L. Davidson, J. S. Salt and C. Hamblin, 1997 Immunohistochemical demonstration of African horse sickness viral antigen in formalin-fixed equine tissues. Vet Pathol 34**:** 568-574.

Wood, S. A., J. E. Park and W. J. Brown, 1991 Brefeldin A causes a microtubule-mediated fusion of the trans-Golgi network and early endosomes. Cell 67**:** 591-600.

Wu, X., S. Y. Chen, H. Iwata, R. W. Compans and P. Roy, 1992 Multiple glycoproteins synthesized by the smallest RNA segment (S10) of bluetongue virus. J Virol 66**:** 7104-7112.

Wurmser, A. E., and S. D. Emr, 1998 Phosphoinositide signaling and turnover: PtdIns (3) P, a regulator of membrane traffic, is transported to the vacuole and degraded by a process that requires lumenal vacuolar hydrolase activities. Embo J 17**:** 4930-4942.

Wurmser, A. E., and S. D. Emr, 2002 Novel PtdIns (3) P-binding protein Etf1 functions as an effector of the Vps34 PtdIns 3-kinase in autophagy. J Cell Biol 158**:** 761-772.

Wymann, M. P., and L. Pirola, 1998 Structure and function of phosphoinositide 3-kinases. Biochimica et Biophysica Acta (BBA). Mol Cell Biol Lipid 1436**:** 127-150.

Xu, G., W. Wilson, J. Mecham, K. Murphy, E. Zhou *et al.*, 1997 VP7: an attachment protein of bluetongue virus for cellular receptors in Culicoides variipennis. Journal of general virology 78**:** 1617-1623.

Zhang, D.-g., W.-z. Li, G.-f. Wang, Y. Su, J. Zeng *et al.*, 2010a Heterologous SH3-p85β inhibits influenza A virus replication. Virol J 7**:** 170.

Zhang, X., M. Boyce, B. Bhattacharya, X. Zhang, S. Schein *et al.*, 2010b Bluetongue virus coat protein VP2 contains sialic acid-binding domains, and VP5 resembles enveloped virus fusion proteins. Proc Natl Acad Sci 107**:** 6292-6297.

Zhi, Y., A. Mayhew, N. Seng and G. B. Takle, 2010 Validation of a PCR method for the detection of mycoplasmas according to European Pharmacopoeia section 2.6. 7. Biologicals 38**:** 232-237.

Zientara, S., and S. Lecollinet, 2015 African horse sickness.

Zwart, L., C. A. Potgieter, S. J. Clift and V. Van Staden, 2015 Characterising non-structural protein NS4 of African horse sickness virus. Plos one 10**:** e0124281.